Dissertations

Fall 12-2009

Reactor R&D: Synthesis and Optimization of Metallic Nitride Fullerenes and the Introduction of Two New Classes of Endohedral Metallofullerenes, Metallic Nitride Azafullerenes and Oxo-metallic Fullerenes

Curtis Earl Coumbe
University of Southern Mississippi

The University of Southern Mississippi

REACTOR R&D: SYNTHESIS AND OPTIMIZATION OF METALLIC NITRIDE

FULLERENES AND THE INTRODUCTION OF TWO NEW CLASSES OF

ENDOHEDRAL METALLOFULLERENES, METALLIC NITRIDE

AZAFULLERENES AND OXO-METALLIC FULLERENES

by

Curtis Earl Coumbe

A Dissertation
Submitted to the Graduate School
of The University of Southern Mississippi
in Partial Fulfillment of the Requirements
for the Degree of Doctor of Philosophy

Approved:

December 2009

The University of Southern Mississippi

REACTOR R&D: SYNTHESIS AND OPTIMIZATION OF METALLIC NITRIDE FULLERENES AND THE INTRODUCTION OF TWO NEW CLASSES OF ENDOHEDRAL METALLOFULLERENES, METALLIC NITRIDE AZAFULLERENES AND OXO-METALLIC FULLERENES

by

Curtis Earl Coumbe

Abstract of a Dissertation
Submitted to the Graduate School
of The University of Southern Mississippi
in Partial Fulfillment of the Requirements
for the Degree of Doctor of Philosophy

December 2009

ABSTRACT

REACTOR R&D: SYNTHESIS AND OPTIMIZATION OF METALLIC NITRIDE

FULLERENES AND THE INTRODUCTION OF TWO NEW CLASSES OF

ENDOHEDRAL METALLOFULLERENES, METALLIC NITRIDE

AZAFULLERENES AND OXO-METALLIC FULLERENES

by Curtis Earl Coumbe

December 2009

Metallic nitride fullerenes (MNFs) were discovered in 1999. This class of
endohedral fullerenes show promise in a new diverse range of useful applications. Since
then, focus has shifted to the selective synthesis of these molecules with yields that would
accommodate adequate sample distribution. Using the electric arc method, the traditional
yield of these molecules has been very low (i.e. < 5 mg), and only a small percentage of
the fullerene products (i.e. < 5%). This dissertation introduces the novel CAPTEAR
(Chemically Adjusting Plasma Temperature, Energy, And Reactivity) method that allows
the targeted synthesis of MNFs in high purity and yield. This method utilizes a
nontraditional oxidizing method for fullerene synthesis that has not only provided
optimization of MNFs, but also resulted in the discovery of two new classes of fullerenes:
metallic nitride azafullerenes (MNAFs) and oxo-metallic fullerenes (OMFs). Evidence
suggests that the nitrogen of the MNAF cage provides stability for the trimetallic nitride
clusters, while the OMFs are the first fullerenes to encapsulate oxygen and incorporate a
seven atom cluster inside a C_{80} cage.

Other efforts to increase yields resulted from scaling up production of fullerenes
by using larger quantities of starting materials. These larger quantities required energy

(electrical current) beyond the capacity of the traditional electric arc generator. Therefore, a new electric arc generator was designed and fabricated to accommodate these demands. This scale-up process resulted in yield increases by an average of 400%. However, to reduce the waste of scaling up as well as costs, our lab developed a recycling method for the expensive metal oxide starting materials. This method has greatly improved cost effectiveness and waste reduction.

DEDICATION

I would like to dedicate this work to my wife Courtney Coumbe and my son Maddox

Coumbe. Both of you have been my greatest inspiration on this journey. Thank you for

your patience. I love you always.

Curt

ACKNOWLEDGEMENTS

I would like to thank

1. My PhD. Advisor, Dr. Steven Stevenson, who always pushed me further than I thought I could go.

2. My committee members

    Dr. Janice Phillips

    Dr. Karl Wallace

    Dr. Yong Zhang

    Dr. Randy Buchanan

3. The University of Southern Mississippi, Department of Chemistry and Biochemistry

4. Dr. Robert Bateman, for being a good listener and chairman

4. The Stevenson Research group, past and present

5. The Phillips Research group, past and present

6. GAANN Fellowship (GRO2619), for funding

7. NSF Career Grant (GRO2538), for funding

8. Friends and family for support

9. A special thanks to

    My Family and Friends, for all the support and encouragement

    Louie Coumbe, my brother, friend, and a previous member of our research group who helped improve our R&D of fullerene science greatly

    Corey Thompson, for a physics point of view and always an ear to turn to when I couldn't solve a problem in the lab

    M.A. Mackey, my co-graduate student and friend, for so much assistance, and a

TABLE OF CONTENTS

LIST OF TABLES

LIST OF ILLUSTRATIONS

Figure

CHAPTER I

EXECUTIVE SUMMARY

Significance of Research

Worldwide, several groups have focused on the synthesis, purification, characterization, and reactivity of metallic nitride fullerenes (MNFs).[1-28] MNFs are fullerenes (spherical carbon cages, usually ≥ 60 sp^2 hybridized carbons) that include an entrapped (or endohedral) trimetallic nitride cluster, in which all three metals are bonded to a nitrogen to form a trigonal planar or pyramidalized, internal complex. MNFs have the generic formula $M_3N@C_n$, where "M" is any metal from group IIIB or 4f-block metal and "n" refers to the number of carbons in the cage. The smallest "n" value for MNFs, thus far, is 68.[8] The structure of a MNF is shown in Figure 1.
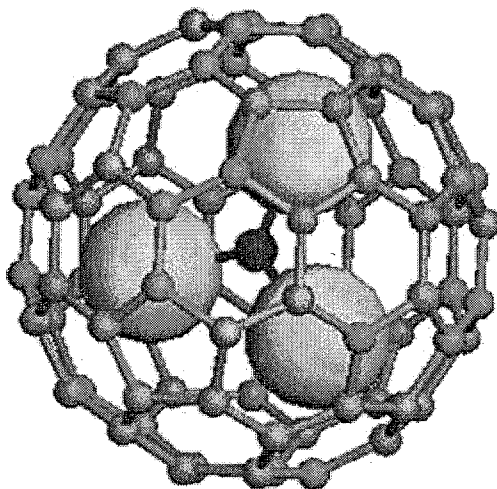
Figure 1. Example of a MNF molecule

MNF research has been hindered greatly by their typical low yields of only a few milligrams per day.[29, 30] This dissertation offers a paradigm shift in the synthesis of MNFs, insight into the discovery of new endohedral fullerenes, and contributions to

green chemistry and recycling of waste material.[15, 18, 31-34] Yield optimization and selective synthesis are very important aspects of this research. This dissertation focuses on four major research thrusts as follows:

1. *Introduction of additives to the plasma environment for yield optimization and selectivity* – This research includes metal and nonmetal additives to the packing material (i.e. in cored graphite rods) for the plasma generator.

2. *Synthesis and optimization of new endohedral fullerenes* – This research includes changing the identity of the endohedral cluster as well as the composition of the carbon cage.

3. *Design, construction, and evaluation of a new reactor capable of using higher quantities of reactants* – This research overcomes limitations of traditional arc reactors for synthesis of larger quantities of desired materials.

4. *Reduction of nanomaterial waste by recycling of spent reactor soot (i.e. post fullerene extraction)* – Scale-up and use of larger quantities of expensive starting materials generates larger amounts of waste and cost. Therefore, recycling of waste materials via chemical transformation to recovered metal oxides has become a necessary tool for this research to be cost effective.

The MNF class of nanomaterials is expected to possess diverse applications such as MRI contrast agents,[35-37] X-ray contrast agents,[38] biocidal activity (via singlet oxygen generation from fullerene coated polymer films),[39] and fluorescent or radioactive tagging.[1] Magnetic resonance imaging (MRI) and X-ray contrast agents improve the resolution/contrast of diagnostic images. Medical applications depend on which cluster is encapsulated within the carbon cage. Gadolinium MNFs have already proven useful as

MRI contrast agents.[37] Lutetium MNFs may be used an X-ray contrast agent (which is attributed to the large cross section of the lutetium atoms),[38] whereas mixed Ho-metal MNFs such as holmium/lutetium and holmium/gadolinium should provide (pending further studies) new radiopharmaceuticals based on the irradiation of ^{165}Ho metallofullerenes under various neutron flux conditions and its use in nuclear medicine.[40] The attraction to MNFs is due to their structural and physical properties. For instance, the trimetallic cluster is capable of optical emission or absorption, as well as magnetism. For example, the Er_3N cluster may be used for optical applications[41] (fluorescent coatings), having emission decay lifetimes of 1.1 – 1.6 sec. and quantum efficiency for emission at $\sim 10^{-4}$, while the Gd_3N cluster functions better as a magnetic agent. However, since these clusters are encapsulated inside the carbon cage, this entrapment provides protection from enzymatic degradation and toxic release of the metals (e.g. gadolinium) inside the body. In fact, *in vivo* studies were performed on rat brains using $Gd_3N@C_{80}$-[DiPEG5000(OH)$_x$], which was found to be effective as MRI contrast agents. No toxicity of the gadolinium or the functionalized cage was reported. [37] Although this dissertation does not focus on MNF applications, an outcome of this research would be improved sample availability for researchers who pursue those goals.

Electric Arc Synthesis: Research and Design

The electric arc synthesis of fullerenes is the typical method for fullerene researchers. Of the four known methods for fullerene production, the electric arc process is the only known approach to synthesize MNFs.[42-45] This method utilizes an electrical current to vaporize graphite rods impregnated with a metal of choice. The electrical current (i.e. resistive heating and rod vaporization) creates a plasma between the packed

rod and another solid graphite rod. Only a small percentage (i.e. typically < 5%) of the materials packed in the cored graphite rod are transformed into fullerene products.

Poor MNF yields hamper the R&D from a lack of sample distribution. MNF production costs are extremely high for milligram quantities and as such, MNFs are not commercially available. The expense varies within the MNF family and is dependent on the cost of feedstock material (e.g. Sc_2O_3 is ~$3000/kg)[46] and separation method (e.g. HPLC fraction collection or SAFA).[12] These constraints demonstrate the importance of our goals for new reactor R&D.

Broad Impact

Our results will show a significant impact to fullerene science including the following – (1) significant increases in yield and purity, (2) new classes of molecules, and (3) a new green chemistry process for fullerene science.[15, 18, 31-34, 47] Fullerenes have traditionally been synthesized using inert or reducing atmospheres (i.e. helium, nitrogen, and ammonia).[48] Our lab has accomplished fullerene production with targeted selectivity (i.e. extracts of highly purified MNF without significant loss of yield) under an oxidizing atmosphere![33] Our new method has led to the discovery of new endohedral fullerenes that are synthesized as a result of this shift to oxidizing atmospheres.[18, 47] Also, scale up of milligram yield was believed to be futile until the introduction of our new reactor design. Our scale up has resulted in a 400% average increase in fullerene yield. However, our scale up has resulted in (1) cost increases from increased quantities of starting materials and (2) a larger production of waste material. Our lab has remedied these issues by developing a novel recycling method that enables the reuse of waste materials for

subsequent reactions.[31, 32] Overall, our research has yielded success in several areas and

continues to benefit the scientific community.

CHAPTER II

LITERATURE REVIEW

Buckminster Fullerene (C_{60})

Discovered in 1985 by Kroto, the late Smalley, and Curl, C_{60}[49] is the most abundant fullerene. It was produced in macroscopic amounts in 1990 via resistive heating of graphite.[44] This electric-arc fullerene method produced sufficient quantities of C_{60} to be isolated. The subsequent availability of purified C_{60} generated excitement to research this new molecule and characterize its chemical and its physical properties.

Fullerene C_{60} exhibits I_h symmetry and contains all sp^2 hybridized carbons. It is a quasi-spherical structure that consists of 20 hexagons and 12 pentagons. This molecule does not follow Huckel's rule, and is not planar, and therefore is not considered aromatic. The structure obeys the isolated pentagon rule (IPR), which contributes to its stability as no two pentagons are adjacent to each other, but surrounded by hexagons. Figure 2 shows an example of C_{60}, in which each hexagon is surrounded by pentagons, thus demonstrating the IPR. The rule makes C_{60} the smallest stable fullerene obeying the IPR, and is related to its prominent abundance. Smaller fullerenes, C_{20}[50] and C_{36},[51] have been produced but do not follow the IPR. Therefore, these molecules are highly unstable and thus have a very low abundance.
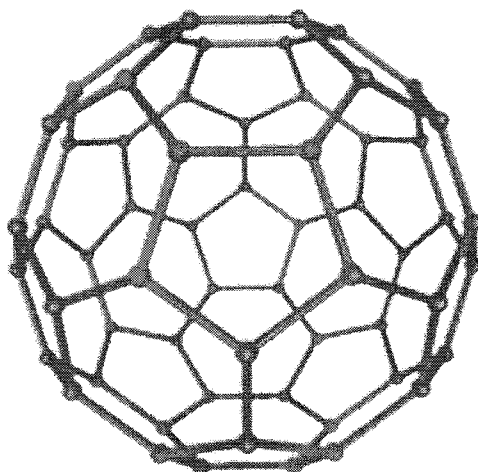
Figure 2. Fullerene C_{60}

The electrons in the hexagons of C_{60} do not delocalize over the entire molecule and thus do not exhibit superaromaticity. This electronic structure contributes to an increase in cage reactivity and ability to attach functional groups to its surface. Fullerene C_{60} has an open shell electronic structure which is consistent with its reactivity.[44]

Higher Order Fullerenes (C_{2n})

Higher order fullerenes (C_{2n}) are less abundant than the C_{60} molecule (i.e. usually, an HPLC trace of an empty cage fullerene extract is comprised of 50% or more of the C_{60} molecule and less than 50% of all other higher order fullerenes such as C_{70}, C_{76}, and C_{84}) but are comparable in stability and reactivity. The low abundance of higher order fullerenes in soot extract and proclivity toward structural isomers contribute to their difficulty in isolation. Some examples of higher order fullerenes include C_{70}, C_{76}, C_{78}, and C_{80}. The C_{116}[52] fullerene has been isolated but theoretical calculations suggest even larger cage sizes. C_{70} is currently the most stable higher order fullerene.

Endohedral Fullerenes- Metallofullerenes and Metallic Nitride Fullerenes

Shortly after the discovery of C_{60}, it was proposed that the fullerene cage could encapsulate atoms to produce endohedral structures,[53] with entrapped metals and/or nonmetals. These new endohedral fullerenes have electronic and optical properties that their empty cage counterparts lack. Yields of endohedral metallofullerenes are traditionally much lower than those of empty cage fullerenes. Metallofullerenes typically represent yields less than 0.1% of the arc reactor soot. Distribution of metallofullerene samples has been limited due to their low yields and difficulty in separation.

Non-Metallic Doped Fullerenes

Several non-metallic endohedral fullerenes have been isolated. He, Ne, Ar, Kr, and Xe have been encapsulated inside the C_{60} cage. This requires exposing C_{60} to 3 bar of each respective noble gas.[54-56] These endohedral fullerenes occurred in ~1 out of 650,000 C_{60} cages. Also isolated were encapsulated $N@C_{60}$, $N@C_{70}$, and $P@C_{60}$, using an ion implantation method in which a thin film of C_{60}, slowly deposited by an effusion cell on a cooled target, was bombarded with N^+ (or P^+) ions from an ion source in a high vacuum chamber.[57] This method results in ~0.001 – 0.01% nitrogen or phosphorous encapsulation by the C_{60} molecules. The endohedral atoms are neutral, centered inside the cage, and have properties that resemble electromagnetic traps.

Classical Metallofullerenes $M_x@C_y$

Metal-doped fullerenes are synthesized via laser evaporation or arc plasma methods.[58] Encapsulated metals include alkaline earth metals, alkali metals, transition and inner transition metals, and trivalent metals (uranium, zirconium, and hafnium).[58] Carbon cage sizes can range from 60 to 90. Application development of classical

metallofullerenes has been hampered due to their low stability in air, multiple cage isomers, and difficulty in purification.

La@C_{60} was the first metallofullerene to be reported as having metallic properties.[58] These metallic properties were found to be the result of a charge transfer from the La to the C_{60} cage. This transfer is believed to be a metal – ligand charge transfer.[59, 60] The ionic formula would actually be written as [La]$^{3+}$@[C_{60}].$^{3-}$ Er@C_{60} was also among the first of rare earth metallofullerenes to be isolated.[61] In contrast, bimetallic fullerenes have shown more stability than the mono-complexes.[58] Sc_2@C_{66} has been isolated, and the X-ray crystal structure has been determined.[62] The C_{66} cage does not follow the IPR but is stabilized by the cage's interaction with the two encapsulated Sc atoms. In fact, the cage housing range from C_{66} to C_{90} includes many unstable, empty cage fullerenes that do not follow the IPR, but are stabilized by the endohedral complexes (e.g. La_2@C_{72}).[63]

Metallic Nitride Fullerenes M_3N@C_x

Sc_3N@C_{80} (I_h cage symmetry). Sc_3N@C_{80} was the first MNF to be discovered.[1] It was prepared in a Krätschmer-Huffman plasma generator[44] using Sc_2O_3, graphite, and FeN at 300 torr in a helium atmosphere. The nitrogen source used was N_2. The mass spectrum showed a [M]$^+$ peak at 1109 m/z. The identity of this mystery peak was believed by others to be Sc@$C_{86}O_2$. Subsequently, the identity was confirmed when Stevenson and Dorn isolated the compound via HPLC. X-ray crystallography was used to determine the structure. This discovery led to a new research field in fullerene chemistry and has since then provided the necessary means to produce an array of MNFs with unique properties that are useful in many industrial and medical applications.[37, 38, 64-70]

Figure 3 shows the structure of $Sc_3N@C_{80}$ cage. X-ray crystallographic studies have reported I_h symmetry for the C_{80} carbon cage.[1, 9, 71-73]
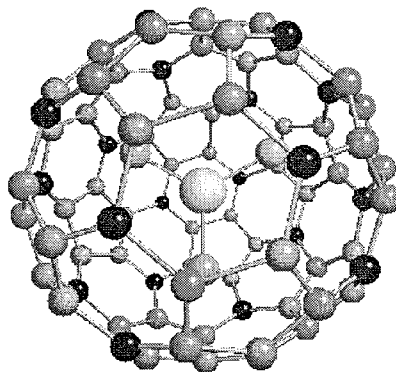
Figure 3. Example of $Sc_3N@C_{80}$

MNFs have unique metallic properties compared to classical metallofullerenes due to the increased stability and charge transfer (6 electrons) from the MNF cluster to the cage. In the case of $Sc_3N@C_{80}$, each Sc atom donates one electron to the nitrogen atom and two electrons to the C_{80} cage. The ionic formula can be written as $[Sc_3N]^{6+}@[C_{80}]^{6-}$. Although MNFs have also been produced using rare earth metals, $Sc_3N@C_{80}$ is the highest yielding MNF.[15]

There are two types of carbons in the I_h $Sc_3N@C_{80}$ cage.[1] The first carbon type consists of 60 carbons that are located at the vertices of two hexagons and one pentagon. The other 20 carbons are located at the center of three hexagons. Therefore, the ^{13}C NMR has two signals (144.57 and 137.24 ppm). The presence of only two carbon peaks also indicates that the Sc_3N cluster is in dynamic equilibrium on the NMR time scale and does not chemically bond to any specific site on the cage.[1] This result is also supported by ^{45}Sc NMR, which gives a single signal, and thus suggests that all of the Sc atoms are equivalent. The UV-Vis spectrum of $Sc_3N@C_{80}$ shows two distinct peaks at 900 and

1140 nm with high absorbance values below 1000 nm.[1] Density functional theory (DFT) calculations have been used to determine the most stable isomeric conformation of the Sc_3N cluster inside the C_{80} cage.[5] The energy difference between the I_h cage (major isomer) and D_{5h} cage (minor) is only about 2 kcal/mol.

Other examples of MNFs are provided below with specific MNFs structures varying by cage size and cluster.

$Sc_3N@C_{68}$. The isolation and characterization of $Sc_3N@C_{68}$[8] (Figure 4) resulted in the first MNF that violates the IPR. Figure 5 shows eleven different isomers for the C_{68} cage, each with two different orientations. The C_{68} cage is an unstable cage, and there is no known evidence of it being isolated without the cluster. The interaction of the metallic nitride cluster stabilizes the otherwise unstable C_{68} cage.
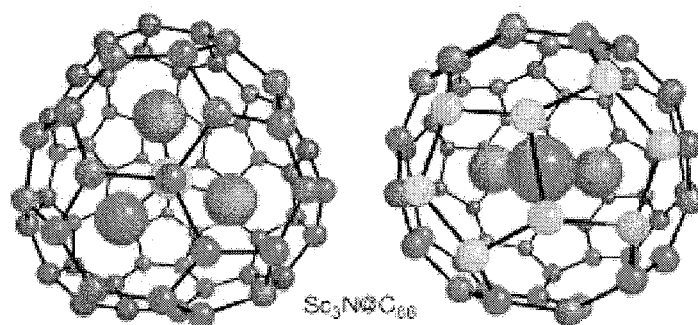
Figure 4. Structure of $Sc_3N@C_{68}$[8]
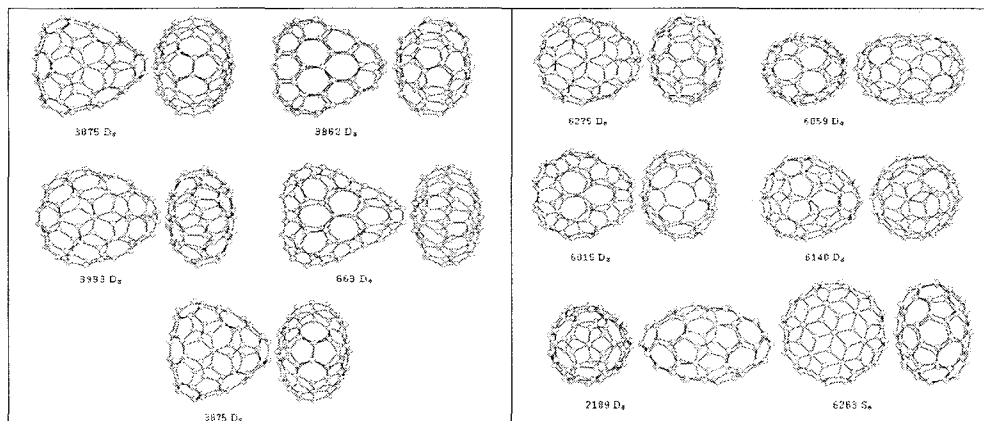
Figure 5. Eleven isomers of the C_{68} cage[8]

$Sc_3N@C_{68}$ is produced in much smaller extract yields (~10%) in relation to the

C_{80} MNF.[8] The numbers in Figure 5 refer to the spiral algorithm[74] that calculates 6,332

possible C_{68} fullerenes with pentagons and hexagons. The eleven structures above are the

only feasible structures that are consistent with the single symmetric peak in the ^{45}Sc

NMR and the 12 singlet peaks in the ^{13}C NMR. From these structures, number 6140 is

the most stable cage isomer due to the three sets of fused pentagons. These fused

pentagons are aligned with the positions of each Sc ion and are stabilized by electronic

interactions.[8] The metal interaction with the fused pentagons hinders the rotation of the

metal-nitride cluster as described earlier.

$Sc_3N@C_{78}$. Olmstead *et al.* reported the isolation and characterization of

$Sc_3N@C_{78}$.[4] With an abundance of ~10% of the $Sc_3N@C_{80}$, $Sc_3N@C_{78}$ has a retention

time similar to $Sc_3N@C_{80}$. The mass spectrum shows an $[M]^+$ peak of 1085 amu. The

crystal structure of $Sc_3N@C_{78}$ follows the isolated pentagon rule (IPR), but its spherical

geometry, in relation to the I_h C_{80} cage, is somewhat disrupted. Since the IPR is followed

in this case, the C_{78} cage is generally more stable than the C_{68} cage and thus allows some

rotation of the metal-nitride cluster inside the C_{78} cage.

Lu₃N@C₈₀. The isolation and characterization of $Lu_3N@C_{80}$ was performed by Stevenson *et al.*[7] The Lu MNF structure proved to be similar to the $Sc_3N@C_{80}$ MNF. The geometries of the metallic nitride clusters are subjected to the same constraints and therefore experience similar degrees of cluster rotation. Both clusters have planar geometries, and the bond distances of the metal-nitrogen bond are similar (e.g. Lu-N bond length is ~2.05 Å for experimental and ~2.04 Å for theoretical; Sc-N bond length is ~2.03 Å for experimental and ~2.03 Å for theoretical).[7] It was determined that the cage size is not distorted despite an increase in the Lu_3N cluster size.

Sc₃N@C₈₀ (D₅ₕ). In 2003, Duchamp *et al.* discovered, isolated and characterized a D_{5h} isomer of $Sc_3N@C_{80}$.[75] This isomer is similar to the I_h isomer. If the top half and bottom half of the C_{80} cage is divided into hemispheres, the D_{5h} isomer is obtained by rotation of the top hemisphere of the I_h isomer by 36°.[75] The lower energy of the I_h isomer (versus D_{5h} isomer) is consistent with the relative abundance of the two species. Using HPLC, the elution time is almost identical for each isomer and elutes as an asymmetric tail of the I_h chromatographic peak. This D_{5h} isomer has also been found for other MNFs.[76]

Gd₃N@C₈₀. The synthesis of $Gd_3N@C_{80}$ represents an important discovery[77] due to the medical applications of Gd as an MRI contrast agent.[78] Unfortunately, this MNF is the lowest yielding MNF.[79] In contrast to the planar geometry of the Sc and Lu nitride clusters, the bulky Gd_3N moiety has a pyramidal geometry inside the C_{80} cage.[77] This geometry is believed to be a contributing factor in its poor yield. The focus on $Gd_3N@C_{80}$ is to optimize the yield and formulate water soluble derivatives that will

enable MRI contrast agent development. The Gd MNF also possesses a minor D_{5h} isomer.[30]

Hetero-Metallic Nitride Fullerenes $M_{3-n}X_n@C_{80}$, n = 1-2

Introduction. This generic formula represents MNFs having two different metals in the cluster. There have been several reports discussing hetero-metallic MNFs, their structural data and chemical characterization. Synthesis of these compounds differs only by addition of two different metals of choice to the packing material, rather than one.

The first hetero-metallic MNF was reported by Stevenson *et al.*[80] in which a mixture of Sc_2O_3 and Er_2O_3 in the packing material yielded the following product distribution: $Sc_3N@C_{80}$, $Er_3N@C_{80}$, $Sc_2ErN@C_{80}$, and $ScEr_2N@C_{80}$.

ScYErN@C$_{80}$. Chen *et al.*[81] first isolated and characterized the tri-hetero-metallic MNF, $ScYErN@C_{80}$. This molecule was characterized by HPLC, laser desorption time-of-flight (LD-TOF) mass spectroscopy, cyclic voltammetry, Fourier transform infrared (FTIR) spectroscopy, and visible-near infrared (Vis-NIR) absorption spectroscopy. Six electrons are transferred to the cage. Similar to the Sc_3N analog, this ScYEr cluster rotates freely. The molecule has a closed-shell electronic structure, and is thus very stable.

Gd/Sc MNF. Yang *et al.* recently reported[29] the synthesis of $GdSc_2N@C_{80}$ and $Gd_2ScN@C_{80}$. These MNFs had yields 30 times that of typical $Gd_3N@C_{80}$ and 2 times higher than typical $Sc_3N@C_{80}$. Both are stable MNFs with large optical band gaps.

Figure 6 shows the periodic table with encapsulated MNF metals highlighted. Despite the ability to make a rich array of MNFs, applications are still hindered by low

yields and poor sample availability. Yield optimization is one of the most important

factors of this research.

1 H																	1 H	2 He
3 Li	4 Be												5 B	6 C	7 N	8 O	9 F	10 Ne
11 Na	12 Mg												13 Al	14 Si	15 P	16 S	17 Cl	18 Ar
19 K	20 Ca	Sc	22 Ti	23 V	24 Cr	25 Mn	26 Fe	27 Co	28 Ni	29 Cu	30 Zn	31 Ga	32 Ge	33 As	34 Se	35 Br	36 Kr
37 Rb	38 Sr	Y	40 Zr	41 Nb	42 Mo	43 Tc	44 Ru	45 Rh	46 Pd	47 Ag	48 Cd	49 In	50 Sn	51 Sb	52 Te	53 I	54 Xe
55 Cs	56 Ba	57 La	72 Hf	73 Ta	74 W	75 Re	76 Os	77 Ir	78 Pt	79 Au	80 Hg	81 Tl	82 Pb	83 Bi	84 Po	85 At	86 Rn
87 Fr	88 Ra	89 Ac	104 Rf	105 Db	106 Sg	107 Bh	108 Hs	109 Mt	110	111	112		114		116		118

58 Ce	59 Pr	60 Nd	61 Pm	62 Sm	63 Eu	Gd	Tb	Dy	Ho	Er	Tm	70 Yb	Lu
90 Th	91 Pa	92 U	93 Np	94 Pu	95 Am	96 Cm	97 Bk	98 Cf	99 Es	100 Fm	101 Md	102 No	103 Lr

$M_3N@C_{80}$

$M_xSc_{3-x}N@C_{80}$ Mixed Metals

Figure 6. Periodic Table of MNFs and mixed metal MNFs

Synthetic Methods for Fullerenes

Introduction

Currently, there are several methods for synthesizing empty-cage fullerenes.

Methods include laser ablation,[45] electric arc,[44] solar process,[43] and hydrocarbon

pyrolysis.[42] Yields are determined as a ratio of fullerene extract to soot mass. The average

percentage fullerene yields for each method is as follows: 40% (laser ablation), 10-15%

(electric arc), 15% (solar process), and 10-40% (solar process).

Laser Ablation

Although this method is the highest yielding method for empty-cage fullerenes,

this approach has the lowest productivity (in grams/hour). This is also the most expensive

method due to high power requirements and low scale-up feasibility. Laser ablation

employs the use of a high power laser on a targeted graphite source to vaporize the carbon, which produces fullerenes, nanotubes, and amorphous carbon.[42] To our knowledge, this method has not been explored for producing MNFs.

Electric Arc

The electric arc synthesis method involves a DC arc welder to create an arc between two graphite electrodes. Fullerene formation occurs in the resultant arc plasma as electrical discharge occurs. This is currently the most popular method for fullerene production and is our lab's current method of synthesis for MNFs. It is also the only known method to produce MNFs. This technique has been explored extensively for empty-cage and endohedral fullerenes. Although it is the lowest yielding method in percentage fullerenes/gram soot, the larger amount of extract produced compensates for this disadvantage. The arc process is also the most inexpensive method for overall fullerene production. Our current electric arc reactor has productivity rates for Sc MNFs as high as 60 mg/hr.[79]

Solar Process

The solar process utilizes a solar furnace to sublime graphite samples and produce fullerenes in a "dark" zone,[82] in which product formation is unhindered by photochemical destruction. This process was introduced in 1993 as a solution to the proposed photochemical destruction of fullerenes in the electric arc process.[83] However, after several studies, the solar process has been shown to be more expensive and less productive than the electric arc process.

Hydrocarbon Pyrolysis

Hydrocarbons have been used to produce fullerenes with typical hydrocarbons being 2-5 carbons in length.[42] This method has the second highest yield, but the productivity is typically lower than the electric arc process. However, Scott *et al.*[84] have reported a selective synthesis of C_{60} using chlorine-substituted aromatic hydrocarbons. Formation of C_{60} occurred after the hydrocarbons were subjected to flash vacuum pyrolysis at 1100 °C. MNFs have not been reported using this method.

Plasma Analysis in Electric Arc Fullerene Production

Introduction

Plasma analysis is an ongoing research aspect of the electric arc synthesis of fullerenes. Characterization of the plasma would provide more insight into the undetermined mechanism of MNF fullerene formation. The research that has been done on fullerene formation in the electric arc plasma has focused on empty-cage fullerenes.[44,] [85-89] Therefore, there is much need for plasma analysis, particularly temperature studies, during the production of endohedral metallofullerenes (e.g., MNFs).

Plasma Physics

The term plasma refers to the fourth state of matter and is composed of one or more ionized gases.[90] The gases contain multiple charged particles with many cationic gas molecules and free electrons. This highly charged region of gas is very conductive and as a result, responds to an electromagnetic field. The net charge of a plasma is usually close to neutral since the positively charged particles are usually the parent atoms of the free electrons.

Plasmas are characterized by several important parameters[90] such as plasma temperature, degree of ionization, electron density, and the magnetic field of the plasma. For a plasma to exist, each particle must affect many other particles in a sphere of influence, also called a Debye Sphere. Another criterion of plasma formation is that the radius of the Debye Sphere, or Debye length, is fairly small relative to the size of the entire plasma. Finally, the plasma oscillations of the electrons, also called electron plasma frequency, must be high relative to the electron-neutral collision frequency (the frequency of electrons with neutral particles). This means that the electron collision frequency must be much higher with charged particles than with neutral particles.

Degree of ionization. The degree of ionization is a fundamental property of plasma.[90] This is the ratio of the number density of ionized particles to the total number of particles. This is given in the form: $\alpha = n_i/(n_i + n_a)$ where n_i is the number density of ions, and n_a is the number density of neutral atoms. Therefore, α is a dimensionless value and has a range of 0-1.0. However, plasma characteristics are usually not seen under 1% ionization (when $\alpha < 0.01$).

Plasma temperature. Plasma temperature is another fundamental parameter of a plasma.[90] Not only is temperature facile to measure with a tungsten-ceramic high temperature probe, but temperature also impacts degree of ionization, electromagnetism, and electron density.

Plasma temperature is measured in electron volts (eV) or Kelvin (K), but the two are interchangeable using dimensional analysis. The temperature refers to the kinetic energy per particle. However, when all the particles of a plasma are considered (e.g. electrons, ions, and neutral particles), the electrons reach thermal equilibrium much faster

than the ions due to their difference in mass. As a result, the electron temperature is usually hotter than the ion temperature. This is described using the Boltzmann Distribution, which relates the probability of a particle's velocity to temperature and mass. As the particle gets larger in mass, and the temperature increases, the distribution gets wider.[91] Therefore, the plasma temperature is an average of the temperature for all particles of the plasma. To accurately measure the plasma temperature, all the particles thermal energy would have to be considered. Using the standard "q = mcΔT equation, the "q" value for the electrons, neutral particles, and ions would have to be summed to calculate the thermal energy. Thus, the total thermal energey, or $q_{tot} = q_{elec} + q_{ion} + q_{neut}$, where q_{elec} is the thermal energy of the electrons, q_{ion} is the thermal energy of the ions, and q_{neut} is the thermal energy of the neutral particles of the plasma. In our system, we cannot determine these values due to mechanical limitations of temperature probes, and thus the thermodynamics must be based on averages and relative temperatures.

Based on these temperature averages, a plasma is classified as thermal or non-thermal. Thermal plasmas have their ions and electrons in thermal equilibrium with each other, whereas non-thermal plasmas have a large difference in their ion and electron temperatures. Temperature also directly affects the degree of ionization. Certain theoretical treatments show a direct relationship between ionization energy and electron temperature. Plasmas are therefore referred to as hot or cold. A hot plasma is nearly fully ionized (90-99%) and a cold plasma has only a small percentage of ionization, such as 1%. However, the threshold between a cold and hot plasma is not clearly defined. An example of a hot plasma would be the sun. Our electric arc plasma is considered a cold plasma.[90]

Plasma potential. The plasma potential[90] is the change in voltage between particles in the plasma. Since the particles are in close vicinity, this change is relatively smaller compared to the actual potential of the plasma. This is due to the Debye sheath, which is a result of having a larger positive charge density than negative charge density, despite the fact that the plasma experiences quasi-neutrality.

The Electric Arc Plasma

As previously described, the electric arc synthesis of fullerenes is the lowest yielding method, but has the highest productivity and one of the lowest costs.[44] This method, introduced by Krätschmer and Huffman (K-H) has been the most popular method of fullerene production. Figure 7 shows a diagram of a typical (K-H) arc reactor.
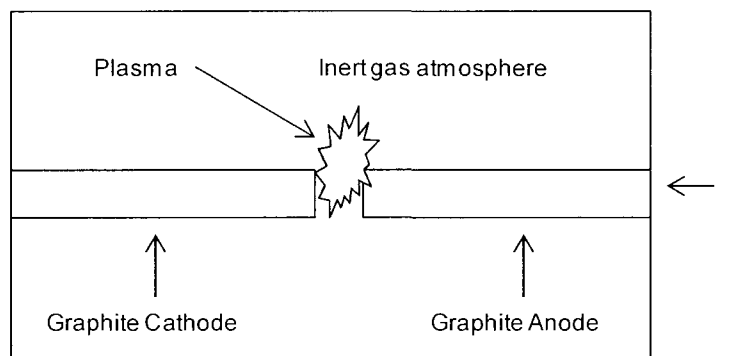
Figure 7. KH-Type reactor diagram

In the K-H reactor, the anode is consumed by vaporization of the graphite using a DC current. This vaporization depends on the amount of electrical discharge produced by the plasma. The resultant soot consists of a mixture of unreacted graphite, amorphous carbon, fullerenes, and sometimes nanotubes. Fullerene extraction from soot is typically done with CS_2, xylenes, or toluene. The experiments are usually done at low pressures

(200-400 torr), but high yields have been reported[83, 92] at pressures above atmospheric pressure (800-1000 torr).

Reactor parameters. Since the fullerene reactor is controlled with an arc welder, there are opportunities to investigate the effects of different welder settings. Particularly, the voltage, current, pressure, and gas flow rate can be adjusted. These parameters will have an effect on the state of the plasma and thus increase or decrease the yield and/or productivity. There are few reports of parameter optimization of this process.[93, 94]

The current produced by the arc welder is the electrical source of the plasma. Thus, the measured voltage of the system is dependent on the gap between the electrodes. A larger gap corresponds to a larger voltage. Therefore, a smaller gap would decrease the space between the plasma particles and increase the amount of ionization to some critical value. This potential is also dependent on the conductivity of the electrodes. Any additive to the typical carbon electrode (i.e. packed graphite rod) may increase or decrease the conductivity.

The pressure within the reactor chamber is another important parameter. The Debye sheath depends on the densities of ions and free electrons. Hence, the plasma volume is directly related to the state of the plasma and changes in pressure should have an effect on fullerene yield.

Plasma temperature of the arc plasma. The temperature of the plasma is a fundamental property. This parameter has been studied as a function of fullerene yield, and several temperature profiles for yield optimization have been obtained. However, there are few reports of temperature studies on synthesizing endohedral fullerenes[95-97]

and no published reports of MNF temperature profiles. Therefore, optimization for endohedral fullerenes (e.g., MNFs) requires the effects of temperature to be examined.

The three physical parameters described above (current, voltage, and pressure) have an effect on plasma temperature as described by Abanades et al.,[98] who demonstrated that plasma temperature was sensitive to current and voltage. These researchers also found that yield was affected by temperature. Variation in buffer gas pressure has been correlated with fullerene yield.[99-102] Reactor gases include He, He/N_2, and Ar. Gas dynamics (i.e. position of gas flow inside the chamber)[103] have also been examined in the formation of empty-cage fullerenes. The fullerene yield in this case was dependent on the gas flow rate and the existence of a turbulent jet between the discharge gap of the plasma.

Plasma temperature studies have been performed for C_{60} and C_{70}.[99, 104-107] These investigations suggest that not only does temperature have an effect on yield, but particular fullerenes as well as nanotubes require specific temperatures for optimization.[108] Changing the temperatures primarily comes from adjusting physical parameters.[106] The fullerene yield was correlated with the temperature gradient. The parameters varied included current, pressure, voltage, and carbon concentration.

Electron density and thermodynamics. Electron density, which is strongly related to temperature, is also believed to be a significant parameter in the formation of fullerenes. Churilov et al.[95, 97, 109] performed theoretical calculations to determine the optimal temperature and electron density to optimize the C_{60} formation rate.

Other studies use thermodynamic estimates[97, 109, 110] to conclude that charge highly affects the geometry of the carbon intermediates to form flat or spherical clusters.

Thus, formation of fullerenes would be primarily dependent on electron density. The

relationship between charge and geometry is fairly easy to conceptualize when

considering the changes in hybridization of an organic molecule when a charge is

induced (Figure 8).
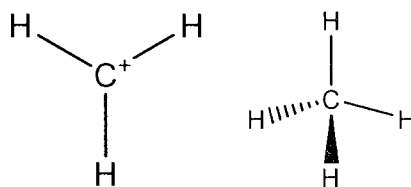
Figure 8. A planar sp^2 ion (left) and a tetrahedral sp^3 molecule

Bilodeau *et al.* used modeling to study the synthesis of C_{60} and C_{70}.[111] This

investigation assumed that the carbon vapor source is from the anode, which is supported

by experimental evidence. Thermodynamic properties were calculated as a function of

temperature and carbon mass. Experimental results supported the theoretical data. The

experiments were performed under argon and helium buffer gas. Electrode gaps ranged

from 1 mm to 4 mm.

Additives to the plasma. Takikawa *et al.* examined the effects of air leaks into the

plasma chamber.[112] This report concluded that air decreases the productivity of fullerenes

due to the formation of carbon derivatives with air components (i.e., CN and CO_2).

However, this investigation only considered empty-cage fullerenes. Our research group

has found that small amounts of introduced air may actually increase the percentage of

MNFs in the extract.[33]

The introduction of naphthalene to the plasma[113] was investigated by Geldard *et*

al. Their HPLC trace results demonstrate that naphthalene increases the relative ratio of

C_{70} to C_{60}. Under normal (i.e. without additives) conditions, C_{60} is the most abundant

fullerene in the HPLC trace (i.e. more than twice the amount of C_{70}, which is generally 30-32% of the fullerene extract). The data suggests that the naphthalene is better incorporated into the C_{70} molecule than C_{60}. The explanation of this change in distribution is that the C_{70} molecule can incorporate these fused 6-membered rings directly, while the C_{60} can only use this naphthalene after there is a rearrangement of the rings to give a 6-membered ring fused to a 5-membered ring.

The effects of alcohols, alkanes, and aromatics to the plasma have also been examined.[114] In this research, graphite electrodes were submerged in a liquid of choice. Fullerene yields were increased by factors of 8 to 100 times the typical yields. The carbon sources proved to originate from not only graphite, but also the organic compounds.

CCl_4 has also been introduced to the arc plasma as a vapor additive.[115, 116] At low flow rates (around 3% of the helium flow rate), the yield of fullerenes has a significant 3 fold increase in yield. However, at 10% - 13% of the helium flow rate, several chlorinated carbon clusters (CCCs) were produced. The data in this work suggested that the mechanistic pathway to these CCCs is similar to that of C_{60} fullerene. This finding may provide insight into the unknown mechanism of fullerene formation.

Ir and Pt metals have been suggested[117] to affect the yield of fullerenes, as well as the selectivity. Addition of Ir to the arc plasma shifted the fullerene production to selectively produce C_{60} at higher ratios than the control. Platinum metal increased the amount of C_{60} oxides and decreased the amount of higher fullerenes. These results indicate that solid additives can play a role in the mechanistic pathway of fullerene formation.

CHAPTER III

RESEARCH PLAN

Research Thrust I – Effect of Chemical Additives to the Plasma

The effect of chemical additives was investigated to determine the most efficient method for synthesizing our targeted fullerenes (MNFs, Oxo-Metallic Fullerenes (OMFs), and Metallic Nitride Azafullerenes (MNAFs)). This research includes modifying the chemical nature of the solid packing material and introducing volatile, reactive vapors into the plasma generator.

Since $Sc_3N@C_{80}$ is the highest yielding MNF, this species was evaluated as a starting point for optimizing other MNFs. For these experiments, an array of different solid packing materials in the cored graphite rods (i.e. changing the ratios of Sc_2O_3, Cu, $Cu(NO_3)_2$, and graphite) was examined followed by the incorporation of other metals and nonmetals to the packing material. We also delivered measured quantities of vapors (e.g. air) into the low pressure plasma chamber and expected to find a correlation with yield.

Optimization of MNF yields has shown to be possible through the use of additives to the packing material and plasma. To test this hypothesis, we designed an array of experiments and characterized our results using HPLC to determine peak areas and percentage of MNF produced in the extract. The amounts of MNFs produced were correlated to the additives being investigated.

Metals and nonmetals can work as conductors, semiconductors, or insulators in an electrical system. Therefore, we hypothesized that by adding different types of materials (e.g., metals, salts, nonmetals) to the packed carbon electrode, the electrical flow would

also change as a result of higher or lower resistance/conductivity if the current and voltage remain constant. This change depends on the type and quantity of additive and, in turn, modifies the state of the plasma. To evaluate the hypothesis, a set of experiments was designed in which reactor parameters were held constant and the packing ratios of chemicals were changed from one extreme to another (i.e. 0% to 100% additive). The weight percentages of additives were plotted as a function of yield. Once a satisfactory recipe was established, other materials were gradually added to the mixture until an optimum yield was achieved. This research area also involved the use of volatile solids (e.g. nitrate salts) to alter the type of atmosphere in the reactor chamber. This area is discussed further in Chapter V.

<div align="center">Research Thrust II – New Endohedral Fullerenes</div>

This research focuses on the selective synthesis, isolation, and identification of two new classes of endohedral fullerenes. This includes the encapsulation of new clusters inside the cage (e.g. OMFs) as well as the inclusion of heteroatom in the cage structure (e.g. MNAFs).

OMFs include any endohedral fullerenes with the generic formula $M_xO_y@C_{2n}$, where "M" is the metal targeted for the cluster that is impregnated inside the graphite rod, "x" and "y" refer to the number of metal atoms and oxygen atoms encapsulated as the endohedral cluster. "n" refers to the number of carbon atoms in which 2n is most likely no less than 80, due to spacial constraints. This research has led to the successful identification of the crystal structures for $Sc_4O_3@ I_h\text{-}C_{80}$ and $Sc_4O_2@ I_h\text{-}C_{80}$.

MNAFs are any endohedral fullerene with the generic formula $M_3N@C_xN_y$, where "M" is any MNF metal, "x" is the number of carbon atoms and "y" is the number of nitrogen as long as x + y equals an equal number ≥ 60 (e.g. 80, 82, 88).

These molecules could provide new applications for fullerenes based on the judicious selection of the cluster atoms. Heteroatoms as cage substituents should provide different reactivities of the cage for subsequent adduct formation. For instance, if there exists a lone pair of electrons on the nitrogen of an azafullerene (some researchers believe it is delocalized on the cage, but the preferred pyramidal structure of a nitrogen with three bonds would provide more stability to the spherical cage structure, as opposed to the preferred planar structure of an sp^2 carbon), an sp^3 nitrogen in an MNAF may provide a Lewis Base reaction to a targeted Lewis acid, which would result in an adduct formation at a specific cage location. Evidence suggests that the nitrogen of the cage provides stability for the cluster as well. This is discussed further in Chapter VI.

We hypothesized that each class of fullerenes requires specific energy profiles for optimal synthesis. It has been shown that temperature profiles have been established for empty cage fullerenes and nanotubes. Different types of fullerenes require different temperatures for optimized formation. Therefore, MNFs should require different energy profiles for their optimal synthesis. Data suggests that synthesis of our new endohedral fullerenes has been achieved as we introduce highly reactive atmospheres into the reactor to shift the plasma environment to energy more favorable to MNFs. Our results were characterized by HPLC for product distribution of MNFs and MALDI-TOF for new endohedral fullerenes. This topic is discussed further in Chapter VI.

Research Thrust III – Design, Fabrication, and Evaluation of a

New Electric Arc Reactor

The focus of this research is based on scale-up of equipment to use larger

quantities of starting material in order to produce increased fullerene extract yields. There

were two main focal points to achieve this scale-up. (1) The scale-up of graphite rod

diameter to increase the amount of starting materials and (2) the design and evaluation of

a newly designed reactor to overcome limitations of scaling-up on a traditional reactor.

This new design is necessary to scale-up to larger rod diameter sizes due to the

mechanical limitations following the scale-up of power required to vaporize the larger

diameter rods. Our results were evaluated by HPLC to monitor the new reactor's ability

to produce a variety of MNFs, OMFs, and MNAFS. This research has demonstrated our

success in the design, fabrication, and evaluation of a new 2nd generation reactor.

Research Thrust IV – Green Chemistry and Recycling of

Waste Nano Soot

This research focus stems from our ability to scale-up larger quantities of starting

materials. This scale-up resulted in much larger increases in yields, but larger quantities

also resulted in increased cost of starting materials and larger amounts of waste. X-ray

Photoelectron Spectroscopy (XPS), discussed in Chapter VIII (Figure 62), shows that

waste soot from a 100% scandium oxide experiment contains only scandium, oxygen,

and carbon. Therefore, the removal of carbon should be sufficient to retrieve the metal

content for use in subsequent reactions.

We hypothesized that removal of carbon from waste soot could be achieved using

thermal oxidation. In this process, we used an oxidative atmosphere at elevated

temperatures to remove carbon by chemical conversion to carbon dioxide. This is liberated from the mixture and vented through a fume hood. The remaining material is predominantly Sc_2O_3.

Thermogravimetric Analysis (TGA) was used to determine the time and temperatures required to completely remove the carbon in an oxidative atmosphere for small (micro-scale) samples (e.g. < 50 mg). A muffle furnace was used to carry out bulk (macro-scale) sample (e.g. > 20 g) experiments followed by XPS to compare our oxidized product to the original waste soot and the commercial "virgin" metal oxide. Finally, graphite rods were packed with both virgin and recycled metal oxides and used to obtain fullerene extracts. Extracts were characterized using HPLC to compare fullerene extracts from 1st generation metal oxide versus our 2nd generation recycled metal oxide material.

CHAPTER IV

EXPERIMENTAL

Equipment List

High Performance Liquid Chromatography (HPLC) Information

Our lab utilized HPLC for analysis of fullerene extracts to determine

quantitatively and qualitatively the type and amount of each fullerene present in the

extract. Our HPLC system uses an M-45 Waters reciprocating pump, a Model 500

variable wavelength detector (Lab Alliance), a pyrenyl-ethyl (PYE, 10mm wide and

250mm, Phenomenex). Integrations were performed with Logger Pro software from

Vernier. The wavelength for detection of fullerenes was set at 360 nm.

Matrix Assisted Laser Desorption Ionization – Time of Flight (MALDI-TOF) Information

Matrix assisted laser desorption ionization – time of flight mass spectrometry

technology is useful for determining the m/z value for each type of fullerene in our

samples. The MALDI-TOF detector is more sensitive than that of the HPLC so some of

the fullerene peaks at the UV detection limits can be found in the mass spectrum. Routine

mass spectral analysis was performed using a Bruker Daltonics Microflex instrument.

The sample plates are made of ground steel (Bruker). Carbon disulfide (see Table 5 for

solvent details) was typically used to transfer fullerene samples to the stainless steel

plates. The matrix, when used, was anthracene-1,8,9-triol (dithranol).

Thermogravimetric Analysis (TGA)

Thermogravimetric analysis (TGA), using a TA Q500 instrument was used to

investigate any changes in the mass of soot as a function of temperature and time under a

controlled atmosphere. Platinum pans were used for sample placement under air at temperature ranges from 22-1000°C. A heat-and-hold method was employed for our purposes.

X-Ray Photoelectron Spectroscopy (XPS)

X-ray Photoelectron Spectroscopy (XPS) is a useful tool for analyzing elemental composition, empirical formula, electronic state, and chemical state within a material. For our purposes, we used this technique (in collaboration with the Navy Research Labs (NRL)) to determine elemental composition of soot samples as well as thermally oxidized samples of soot during the development of our metal oxide recovery method (CHAPTER VIII). Acquisition of data was obtained using a Perkin-Elmer 5400 X-Ray photoelectron spectrometer.

Chemicals

The synthesis of endohedral fullerenes requires various chemicals. The following tables (Table 1 - Table 5) include the chemical name, formula, vendor, part number, purity and/or size of the chemicals used in our lab. This includes: metal oxides, metals, nonmetals and salts, reactor gases, and solvents, respectively.

Table 1. Metal Oxides

Chemical Name	Formula	Vendor	Part #	Purity/Size
Cerium Oxide	CeO_2	HEFA	CEO -4N	99.99% 325 mesh
Dysprosium Oxide	Dy_2O_3	HEFA	DYO -4N	99.99% 325 mesh
Erbium Oxide	Er_2O_3	HEFA	ERO -4N	99.99% 325 mesh
Gadolinium Oxide	Gd_2O_3	HEFA	GDO -4N	99.99% 325 mesh
Holmium Oxide	Ho_2O_3	HEFA	HOO -4N	99.99% 325 mesh

Table 1. (continued)

Lanthanum Oxide	La_2O_3	Sigma Aldrich	L4000	99.99% 325 mesh
Lutetium Oxide	Lu_2O_3	HEFA	LUO-4N	99.99% 325 mesh
Neodymium Oxide	Ny_2O_3	HEFA	NYO-4N	99.99% 325 mesh
Praseodymium Oxide	Pr_6O_{11}	HEFA	PRO-4N	99.99% 325 mesh
Scandium Oxide	Sc_2O_3	HEFA	SCO-4N	99.99% 325 mesh
Terbium Oxide	Tb_4O_7	HEFA	TBO-4N	99.99% 325 mesh
Yttrium Oxide	Y_2O_3	HEFA	YO-4N	99.99% 325 mesh

Table 2. Metals

Chemical Name	Formula	Vendor	Part #	Purity/Size
Cerium	Ce	HEFA	CEMP-3N	99.9% 325 mesh
Copper	Cu	Cerac	C1133	99.5% 325 mesh
Dysprosium	Dy	HEFA	DYMP-3N	99.9% 325 mesh
Erbium	Er	HEFA	ERMP-3N	99.9% 325 mesh
Gadolinium	Gd	HEFA	GDMP-3N	99.9% 325 mesh
Holmium	Ho	HEFA	HOMP-3N	99.9% 325 mesh
Scandium	Sc	HEFA	SCMP-3N	99.9% 325 mesh
Yttrium	Y	HEFA	YMP-3N	99.9% 325 mesh

Table 3. Nonmetals and salts

Chemical Name	Formula	Vendor	Part #	Purity/Size
Graphite Powder	$C_{(s)}$	Carbone of America	014145-004	99.99% 325 mesh
Graphite Rods	$C_{(s)}$	Carbone of America	AGKSP & UF4S	99.9% (6" x 0.5")
			UF4S	99.9% (6" x 1")
Copper (II) Nitrate	$Cu(NO_3)_2$	Fluka	61197	98-103%
Ammonium Nitrate	NH_4NO_3	Sigma-Aldrich	A9642	99.0%

Table 4. Reactor Gases

Chemical Name	Formula	Vendor	Part #	Purity/Size
Helium	He	Nordan Smith	UN1046	Ultra High Purity
Nitrogen	N_2	Nordan Smith	UN1066	Ultra High Purity
Air	N_2, O_2, CO_2	Nordan Smith	UN1032	Ultra High Purity

Table 5. Solvents

Chemical Name	Formula	Vendor	Part #	Purity
o- Xylene	$C_6H_4(CH_3)_2$	Sigma-Aldrich	X1040	97%
Toluene	$C_6H_5CH_3$	Sigma-Aldrich	34866	99.9%
Carbon Disulfide	CS_2	Sigma-Aldrich	676918	99.9%
Acetone	$(CH_3)_2CO$	Sigma-Aldrich	179124	99.5%
Diethyl Ether	$(CH_3CH_2)_2O$	BDH	BDH1121	99.0%
Chloroform	$CHCl_3$	BDH	BDH1109	99.8%

Procedures

Electric-Arc Synthesis of Endohedral Fullerenes

The electric-arc synthesis of fullerenes employs a custom designed Krätschmer Huffman (KH – type) arc reactor (Figure 9). First, a solid graphite cathode of varying length is inserted into the electrode sleeve of the reactor (i.e. cathode). A second graphite rod, six inches in length, is core drilled to approximately four inches using a lathe so that only a carbon shell remains. The inside of the shell is packed with the metal or metal oxide of choice, depending on which endohedral metal is targeted. Alternatively, this packed rod may also include additives that affect the yield and distribution and is placed in another electrode sleeve and serves as the anode. The reactor chamber is closed and sealed by vacuum, and the air is purged from the chamber. The chamber is filled with helium to create an inert atmosphere. This purge and fill technique is repeated two additional times for further removal of residual air. Water coolant is supplied to water jackets surrounding the chamber and electrodes. If air is used as an additive, the flow meter is set to obtain the desired pressure change as a function of time. An arc welder (Idealarc 600A) is used to apply a current to form a plasma between the two graphite electrodes (Figure 10). The portion of the graphite rod (e.g. the cathode) containing the packing material and surrounding graphite shell has been vaporized and condensed as soot in the chamber. Once the current is discontinued (switching the arc welder off), the chamber is purged and filled with helium and given approximately twenty minutes to cool. The chamber is opened and the soot content is harvested for the extraction process.
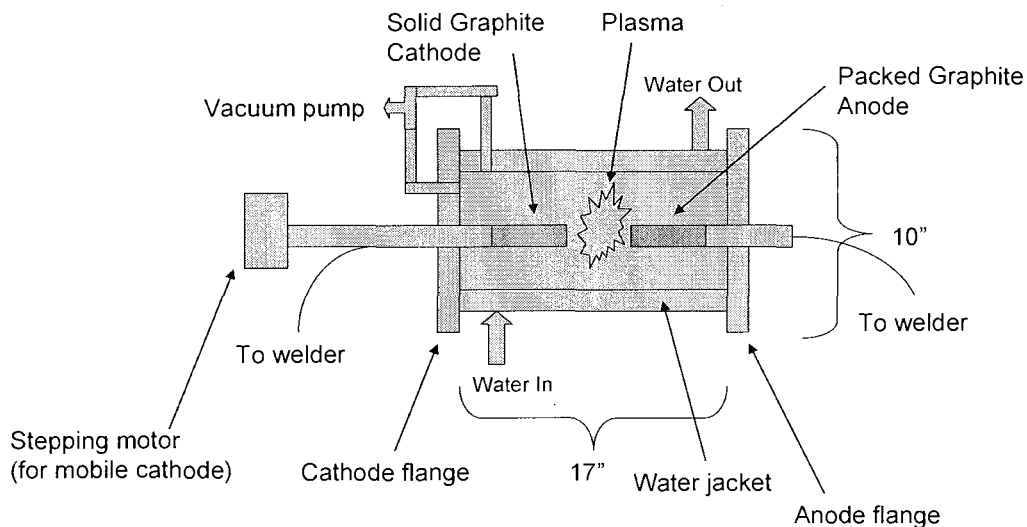
Figure 9. KH-type arc reactor used at USM
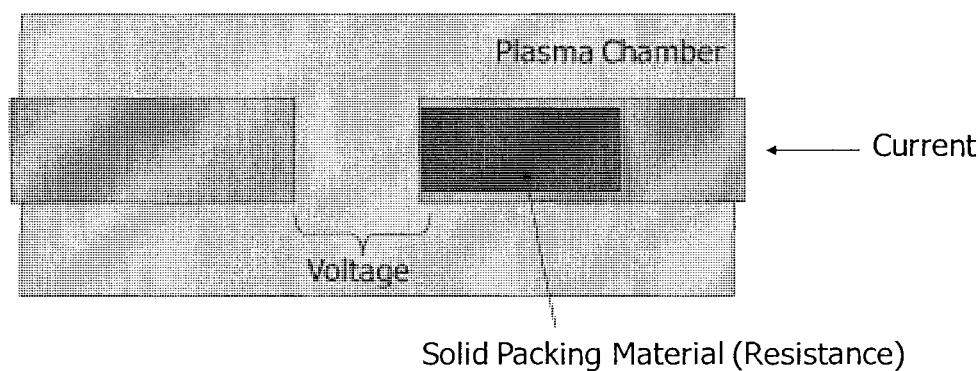
Figure 10. Diagram of the electric arc chamber during plasma formation

Extraction of Fullerenes from Reactor Soot

The soot collected from the reactor chamber (described in the previous section) contains a variety of components. This includes fullerenes, unreacted metals and metal oxides, and usually two or three other allotropes of carbon (e.g. amorphous, graphite, and nanotubes). Extraction of the fullerenes is performed by placing the soot in a glass beaker with approximately 100 to 300 mL of solvent (e.g. CS_2 or xylene) to form a slurry, which is poured into a Buchner funnel attached to a vacuum flask (Figure 11) using #3

Whatman filter paper to remove the majority of the soot under vacuum (step 1). The

filtrate is then poured through a PTFE membrane filter (< 1 µm pore size, Millipore) for

removal of fine soot particles (step 2), as shown in Figure 12. Solvent from the filtrate is

removed using a rotovap to produce solid samples of fullerene extract, which is washed

with diethyl ether.
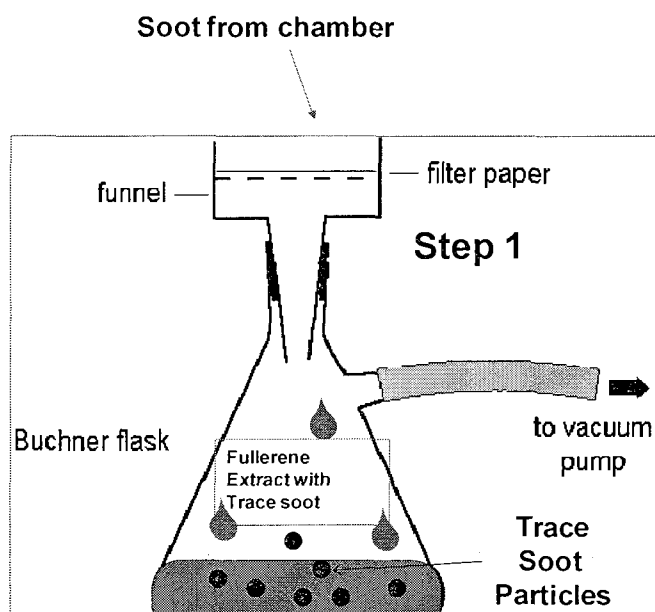
Figure 11. Vacuum filtration of reactor soot to remove fullerene extract
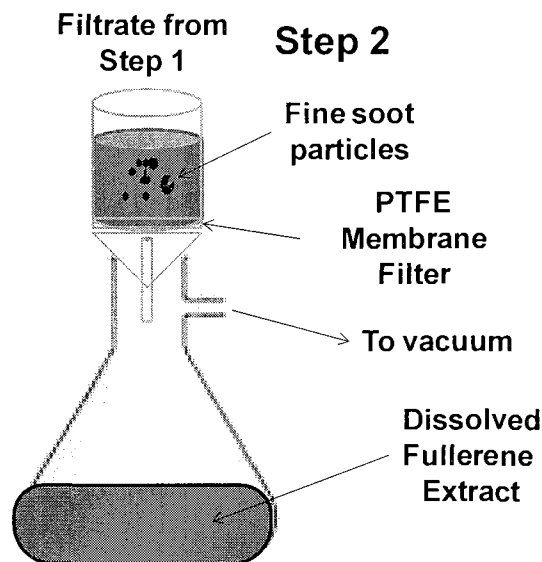
Figure 12. Membrane filtration to remove trace soot particles

HPLC Analysis of Fullerene Samples

Each experiment is initially analyzed by high performance liquid chromatography

(HPLC). This is a separation technique that uses a packed column (stationary phase) to

separate, identify (from retention times), and quantify various compounds relative to each

component in a mixture by integration of the chromatogram peaks. The stationary phase

contains a chromatographic material that retains different compounds at different rates as

they move through the packed column. The mobile phase moves the compounds through

the column to the detector, often UV-Vis, in which the output results in peaks of different

retention times and peak area, depending on the concentration and settings of the HPLC.

The peak area of an HPLC is proportional to its relative abundance in the mixture. This

technique is crucial in our research to determine product distribution. Figure 13 shows an

example of a fullerene extract that contains several types of fullerenes with different

retention times as well as peak areas. As shown, the dominant species are C_{60} and C_{70}.

These are considered contaminant fullerenes for our purposes. The large abundance of

C_{60} and C_{70} makes selective synthesis of MNFs a worthwhile goal.
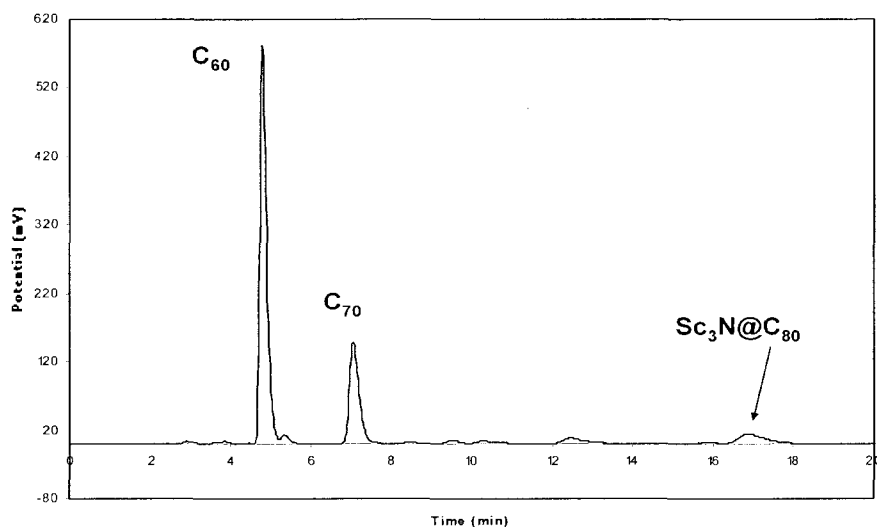
Figure 13. Chromatogram of scandium fullerene extract

MALDI-TOF Analysis of Fullerene Samples

MALDI-TOF MS or matrix assisted laser desorption-time of flight mass

spectrometry is another instrument used in the analysis of fullerenes. This technique

utilizes a soft laser (usually a nitrogen laser) to vaporize and ionize typically large

molecules (peptides, polymers, fullerenes, and other macromolecules). The detector of

the mass spectrometer is sensitive to ions and monitors ions of the particular analyte that

are ablated by the laser. The matrix is used to protect the analyte(s) from being destroyed

during ablation.

Most of our studies often do not require a matrix to assist the vaporization of

fullerenes. However, dithranol is used when matrix is required. This instrument is useful

to detect fullerenes which cannot be readily distinguished by HPLC, due to overlapping

peaks, similar retention times, or the insufficient quantities for HPLC detection. Detected

metallofullerenes include MNFs, metallic nitride azafullerenes (MNAFs), and oxo-metallic fullerenes (OMFs) (discussed in CHAPTER VI). MALDI-TOF MS is primarily used for qualitative rather than quantitative data, although the relative abundances of fullerenes are reflected using this method. HPLC is more reliable for quantitative data but MALDI-TOF MS overcomes the detection limits of HPLC. Figure 14 shows the separation of OMFs with HPLC (a), followed by several fraction collections of the $Sc_4O_2@C_{80}$ OMF (b) and $Sc_4O_3@C_{80}$ (c)). Figure 15 displays the MALDI-TOF mass spectra of OMFs at various air flow introductions into the reactor. The air flow introductions shown in the figure do not reflect MALDI – TOF conditions, which is under vacuum. They refer only to the reactor conditions that result in the fullerene extract analyzed by MALDI – TOF.
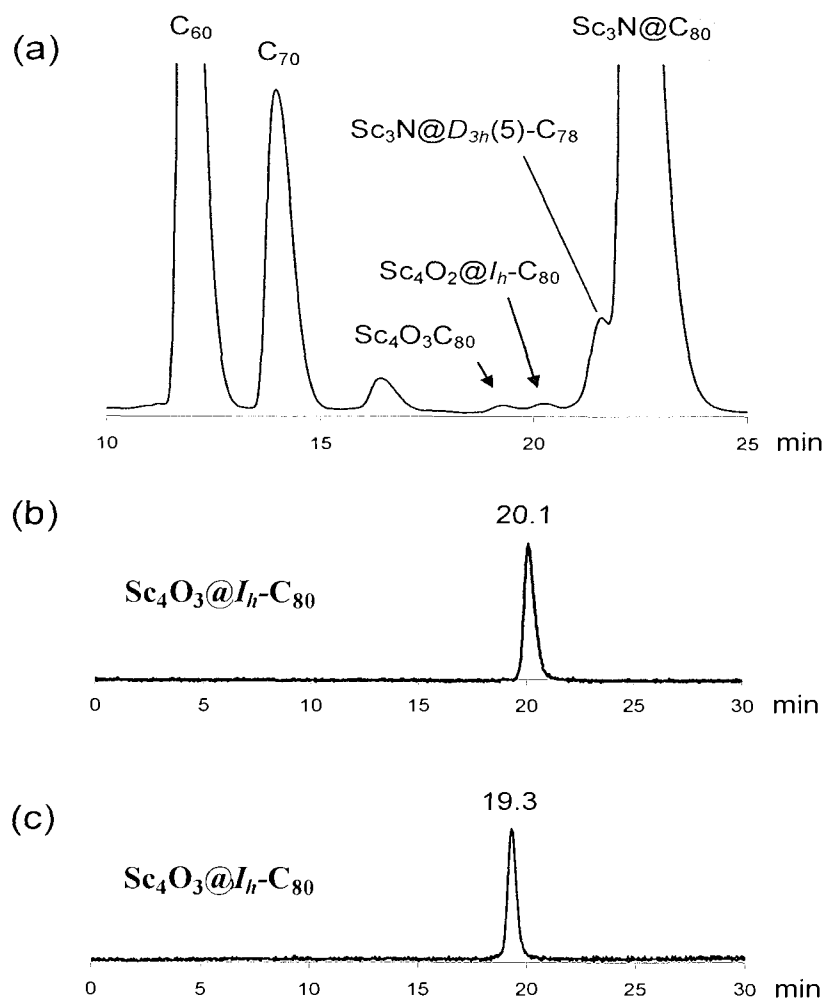
Figure 14. (a) HPLC of OMFs, MNFs, and empty caged fullerenes; (b) HPLC after several fraction collections of $Sc_4O_2@C_{80}$; and (c) HPLC of $Sc_4O_3@C_{80}$ after several fraction collections
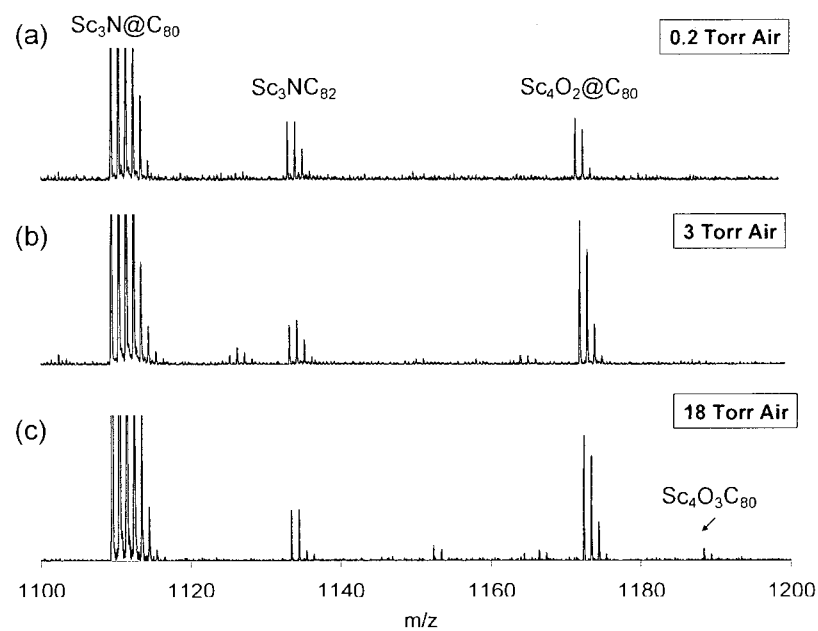
Figure 15. MALDI-TOF of fullerene extract with various reactor conditions including (a) $Sc_4O_2@C_{80}$

at 0.2 torr air, (b) $Sc_4O_2@C_{80}$ at 3 torr air, and (c) $Sc_4O_2@C_{80}$ and $Sc_4O_3@C_{80}$ at 18 torr air

CHAPTER V

EFFECT OF CHEMICAL ADDITIVES ON FULLERENES

Effect of Copper (Cu) on Scandium Experiments

Introduction

Since the discovery of MNFs, much effort has been placed into increasing their

yield and purity[12, 14, 15, 33, 97, 118] Recent advances include the introduction of NH_3[48] gas to

the arc reactor chamber to suppress the empty cage yield and thereby increase MNF

purity. However, efforts to achieve higher MNF purity resulted in a significant decrease

of their milligram yield.

In this study, a goal is to increase the overall mg yield of fullerene extract and

MNFs. Although this will increase the amount of empty cage contaminant fullerenes,

recent advances in our lab include a novel non-chromatographic separation[12] of MNFs

from the extract. This SAFA technique allows for empty cage contamination to be of

little consequence.

Our hypothesis is that solid additives to the packing material should affect the

yield and product distribution of fullerene and MNF yield. Little success has been

achieved in previous studies, such as the addition of CoO.[4] A cost effective material, such

as copper metal, is very attractive to this research since it decreases the amount of Sc_2O_3

used, which is very expensive. An overview of this process is shown in Figure 16.

$$C, Sc, N \xrightarrow{\text{Cu}} \text{Arc-Plasma} \rightarrow Sc_3N@C_{80}$$
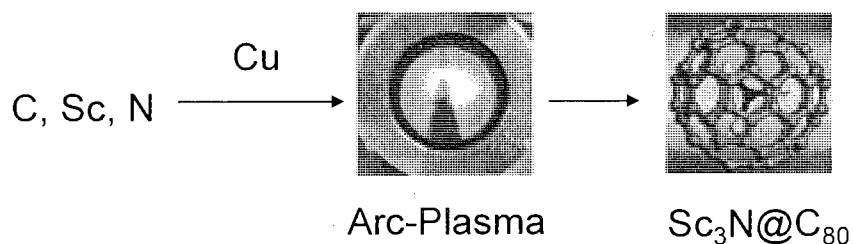
Figure 16. Schematic overview of synthesizing $Sc_3N@C_{80}$ metallic nitride fullerenes produced in an electric-arc reactor[15]

Experimental

In each experiment, the graphite rods (from Carbone of America, Table 3) were 1 inch in diameter and 6 inches long. Each rod was core drilled 4 inches deep using a 0.75 inch diameter drill bit. The cored rods were packed with copper and Sc_2O_3 (~28 g) only. The control used a rod packed with 100% Sc_2O_3. The reactor parameters include 220 amps, 40 volts, 300 torr inside the chamber, dynamic ambient air flow that resulted in a pressure change of 6 torr/min and 12 torr/min for a nitrogen source and oxygen, and 630mL/min of helium gas (ultra high purity tank from Nordan Smith's Welding Supplies) used as a buffer gas. Each experiment was repeated and plotted in triplicate in lieu of using error bars. After the electric arc process, each soot sample was extracted with xylenes and analyzed via HPLC for product distribution. The extract was dried and washed with diethyl ether prior to obtaining mg masses.

Results and Discussion

Copper is widely used as an electrical conductor. By adding copper into the packing material, we increased the conductivity of the anode, and this was demonstrated to have a beneficial effect on the fullerene extract yield.

6 torr/min air. The graphs below show the effects of copper on fullerene type, including C_{60} and C_{70}, (Figure 17) as well as the $Sc_3N@C_{80}$ MNF at an ambient air flow responsible for a pressure change of 6 torr/min (Figure 18).
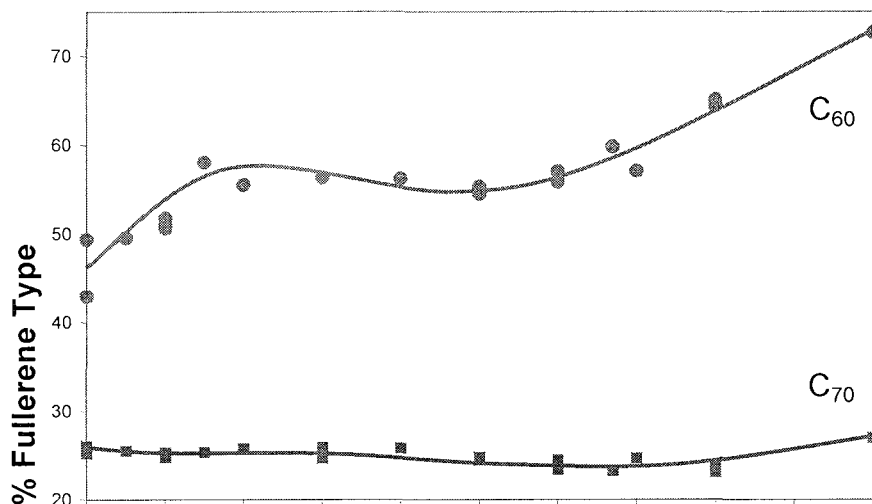
Figure 17. Effect of Cu additive on fullerene type (% of C_{60} and C_{70})[15]
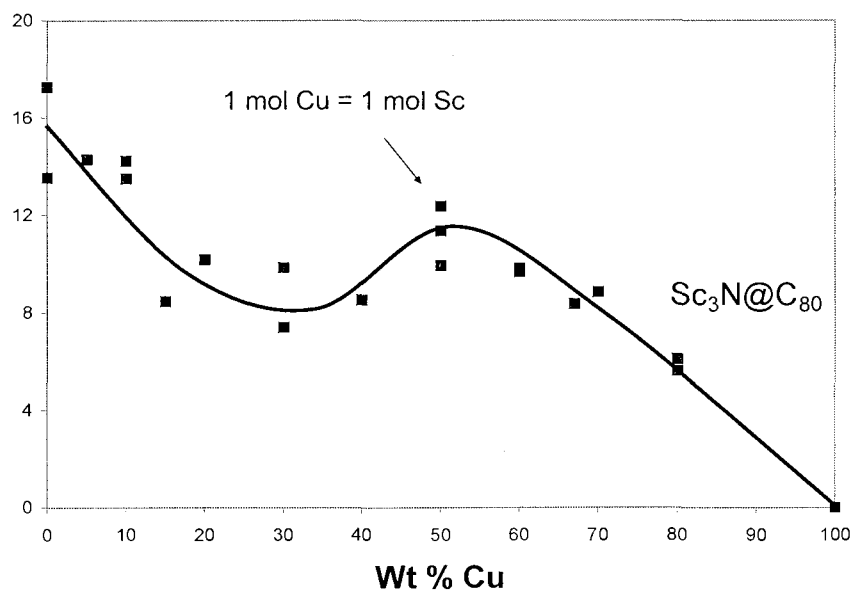
Figure 18. Effect of Cu additive on fullerene type (% $Sc_3N@C_{80}$)[15]

These graphs include two observations. (1) The C_{70} remains virtually constant throughout the addition of copper. (2) The C_{60} and $Sc_3N@C_{80}$ show an inverse relationship. This inverse proportionality indicated that the C_{60} and Sc-MNF are related in some way that is not relevant to the formation of C_{70}. Therefore, the optimization of the MNFs in this study corresponds to minimizing the C_{60} portion of the extract. This is a novel discovery since C_{60} generally dominates the fullerene extract. We have obtained a rich MNF extract with simultaneous suppression of C_{60}. This opens many questions into the unknown mechanism of fullerene formation. Perhaps the two types of molecules are related in their synthesis, but conditions in the plasma atmosphere favor one species over the other. However, without proper probing of the plasma, these questions remain unanswered for now and are not a focus of our reactor research and development. The mass of extract was also investigated for this study, and these results are shown in Figure 19.
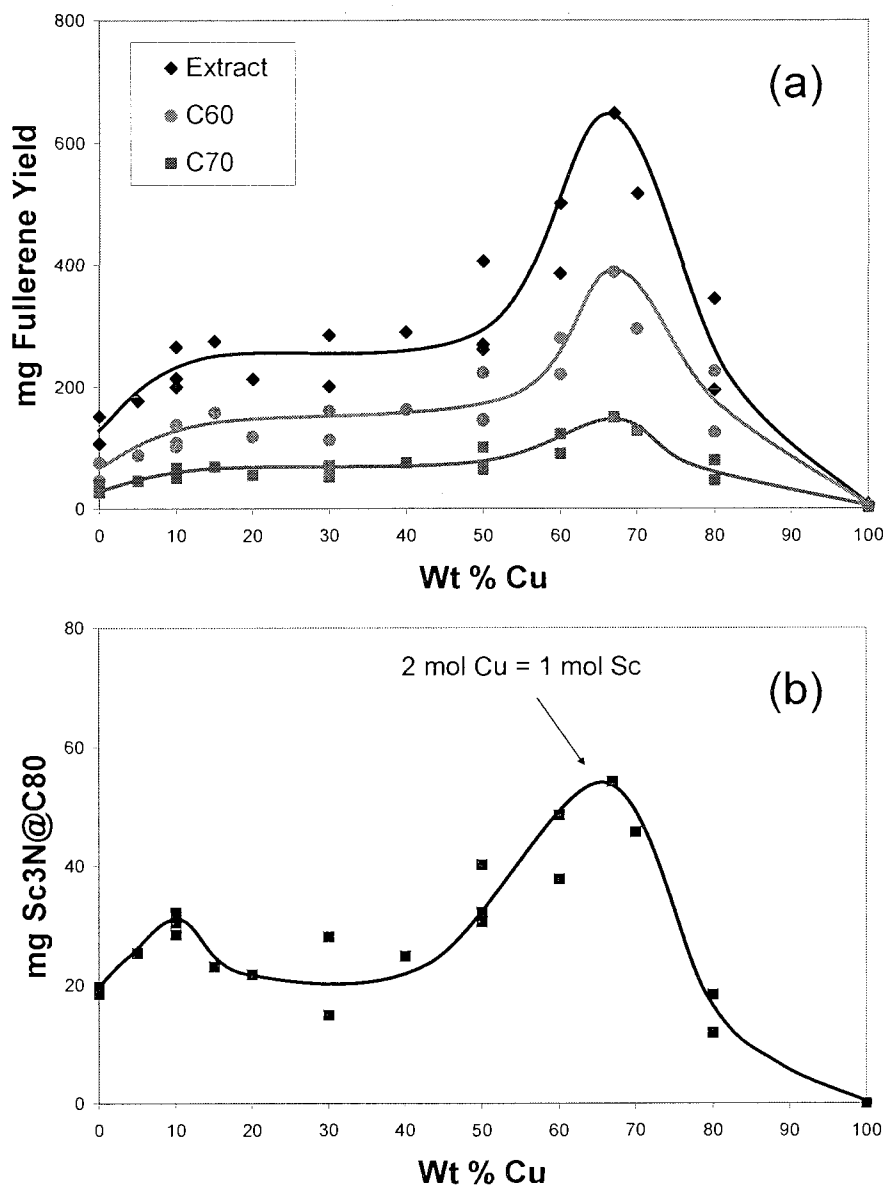
Figure 19. Effect of Cu additive on the milligrams produced of (a) extract, empty-cage fullerenes, and (b) $Sc_3N@C_{80}$[15]

The data in the above graph (Figure 19(a)) shows one maxima at 67% Cu loading (~650 mg of extract). However, Figure 19(b) shows a local maximum of MNFs at 10% cupper loading (~35 mg), but the other components remain dominant in this region (e.g. $C_{60} \sim 100$ mg and C_{70} ~50 mg). The second maximum of MNFs occurs at 67% (~55 mg),

which is still the lowest yielding fullerene of the extract. We can conclude that the Cu

increases the overall fullerene yield by 3-4 times the value of the control rod (i.e. 100%

Sc_2O_3). The MNF maximum at 10% suggests we can increase the ratio of MNFs, but the

empty cage components remain the dominant species. The MNF yield can be increased

by factors of 2-3 with addition of 67% copper and 33% Sc_2O_3 at 6 torr/min air.

12 torr/min air. The same copper profiles for the 6 torr/min air addition were

repeated for the addition of 12 torr/min of air to determine what effects resulted from the

increased oxidizing atmosphere. All reactor parameters were comparable to the 6 torr/min

air data. The results are shown below. The graphs below in Figure 20 and Figure 21

display the effects of copper on the % MNFs ($Sc_3N@C_{78}$ and $Sc_3N@C_{80}$, respectively) at

12 torr/min air as an additive. A maximum occurs again at approximately 10% for both

graphs.
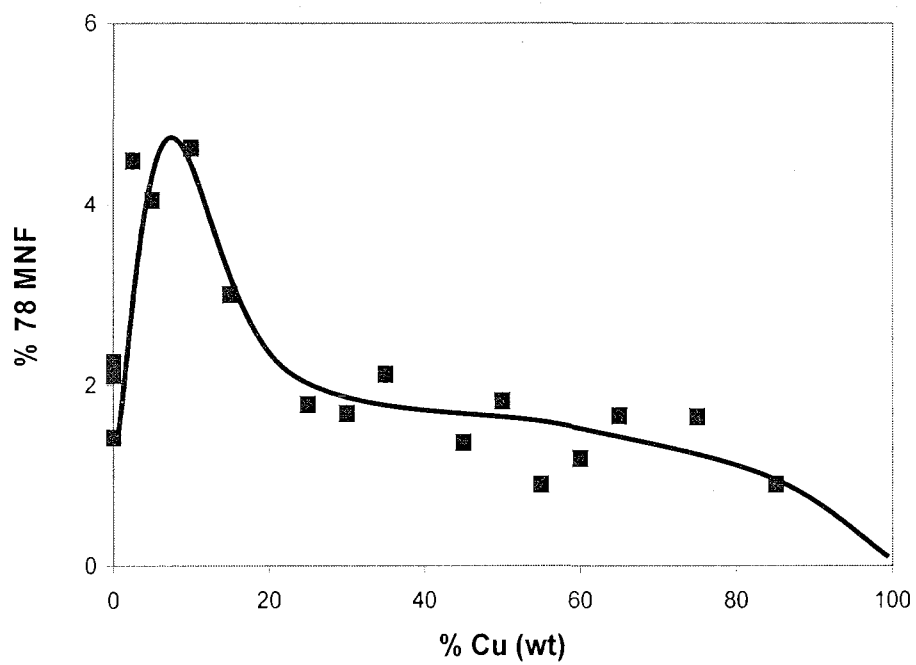
Figure 20. Effect of copper on $Sc_3N@C_{78}$ (12 torr/min air)[119]
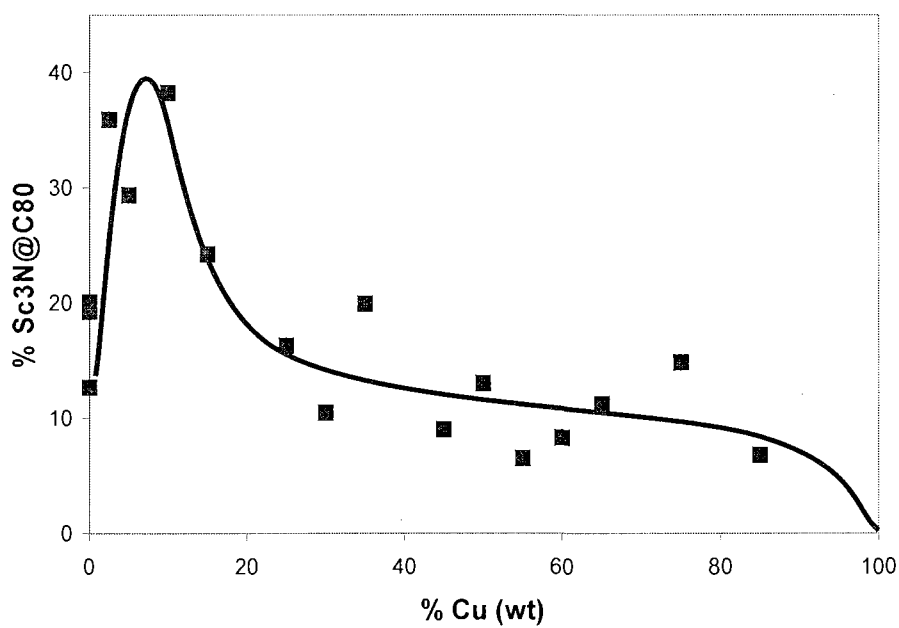
Figure 21. Effect of copper on $Sc_3N@C_{80}$ (12 torr/min air)[119]

However, the extract yield shows a new maximum of 50% for the 12 torr data (Figure 22)

rather than the 67% maximum for the 6 torr data.
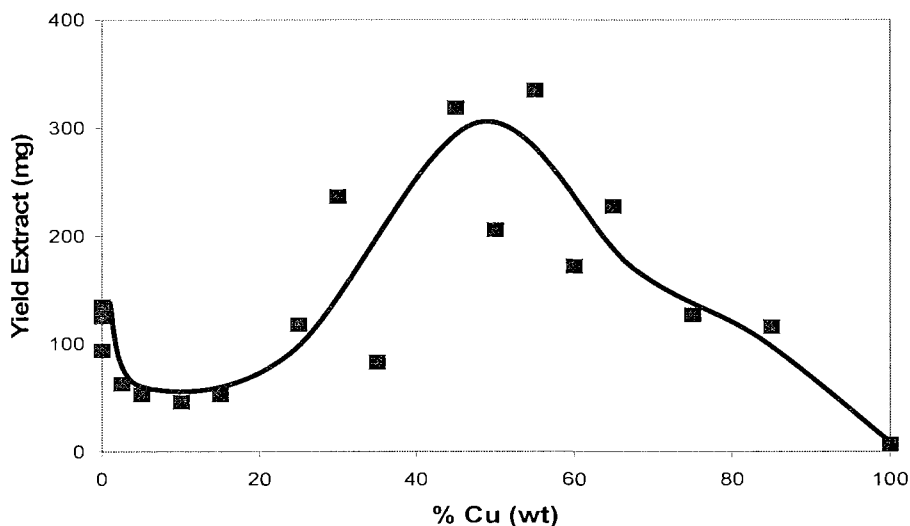
Figure 22. Effect of copper on extract yield (12 torr/min air)[119]

This shift in maximum indicated that the difference in air affects the interaction of

Cu and Sc. We believe that increasing oxidizing conditions not only lowers the threshold

for the maximum yield produced (i.e. from ~600 mg to ~350 mg extract), but also shifts

this maximum to a lower percentage from the increase in demands for the copper to

perhaps protect the fullerenes from oxidative damage. The purity of the MNFs remains

selective at 10% despite the shift of the extract maximum. However, when the masses of

MNFs were examined, the 10% maximum proved to be the lowest yielding (Figure 23

and Figure 24). Thus, quality is traded for quantity under these conditions.
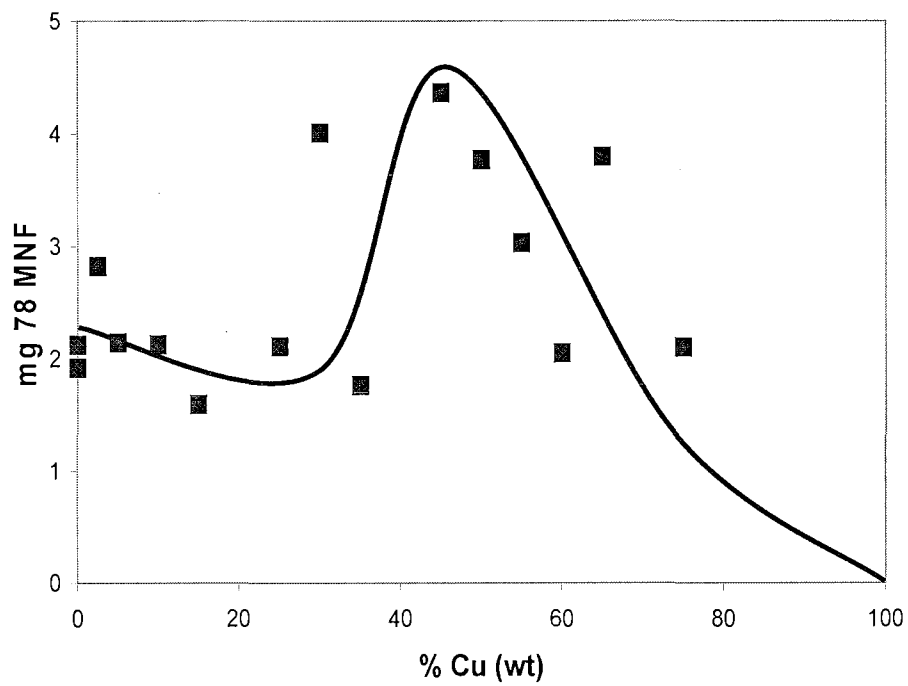
Figure 23. Effect of copper on $Sc_3N@C_{78}$ $(mg)^{119}$
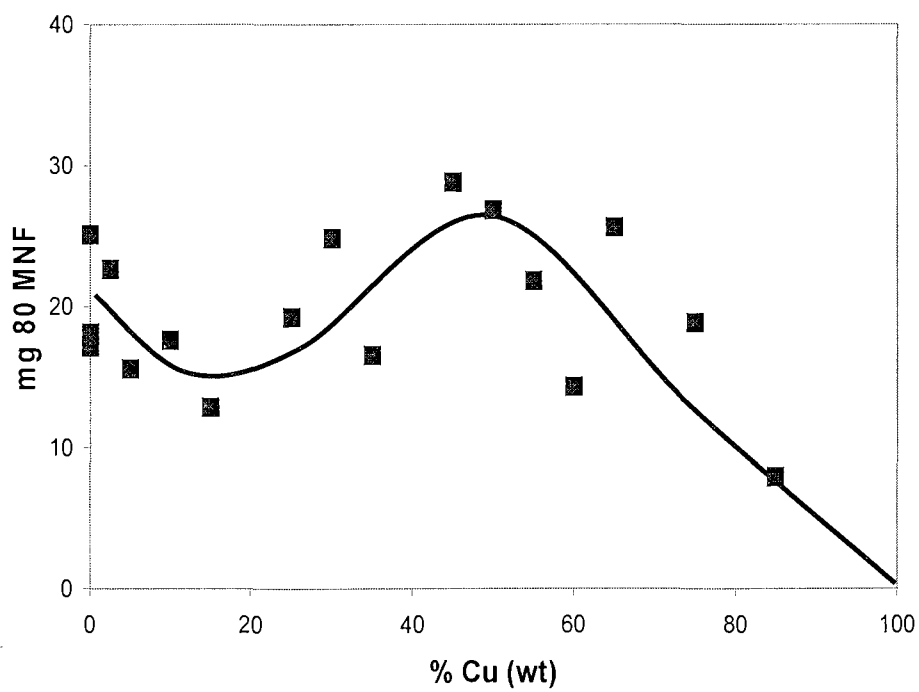
Figure 24. Effect of copper on $Sc_3N@C_{80}$ $(mg)^{119}$

Overall, copper metal is a cost effective metal that greatly improves the yield of fullerenes. We also believe there to be a "protective feature" of the copper to fullerene formation that results in a maximum shift to a lower percentage as we increase the amount of air into the plasma. At higher concentrations of oxygen, the copper interacts with the oxygen to form CuO, with the remaining copper to interact with the scandium oxide. Therefore, the shift of the maximum extract yield from 67% to 50% as a result of increasing air may be due to the reduced amount of copper available to aid in fullerene yield increases. Thus, after 50% Cu at 12 torr air, the copper is no longer able to increase the fullerene yield.

The Effect of Copper Addition on Productivity

Productivity, as defined by the quantity of fullerenes produced over a time period, has a significant role in the experiments in the previous section. Productivity is proportional to efficiency. If productivity is low for an optimal set of experimental parameters, the production may not be more efficient than a set of parameters that has low productivity. Therefore, we examined the burn times as a function of increasing copper to determine whether this optimization was efficient. The results are shown in Figure 25.

Cu (12 torr air/min)

Cu (6 torr air/min)

Wt. % Cu

100

80

60

40

20

0

20   40   60   80   100   120
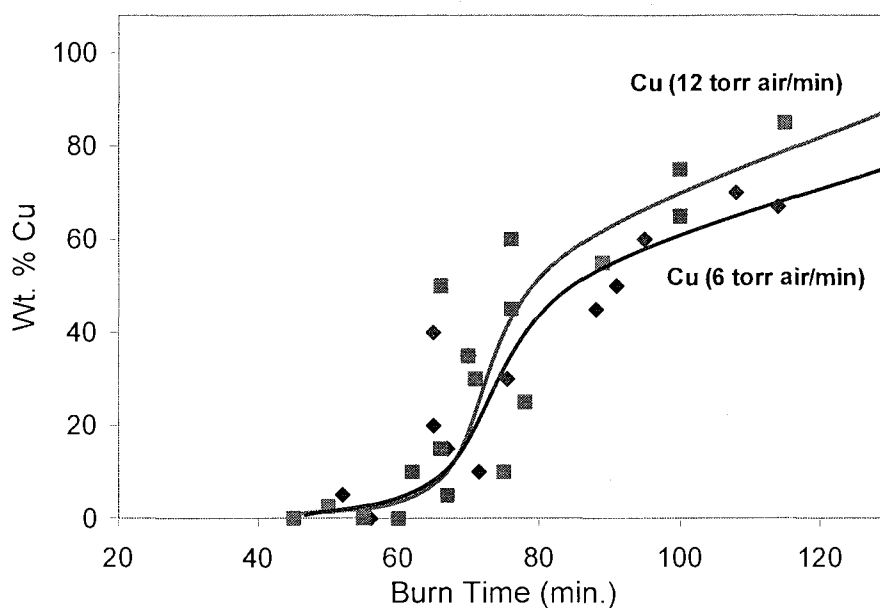
Burn Time (min.)

Figure 25. Effect of burn time on weight % copper loading[119]

The graph shows that increasing copper causes an increase in burn time.

However, when considering the 6 torr data, the 67% region of copper is ~100 minutes,

whereas the 0% copper is ~50 minutes. This is double the time, but the extract increase is

4 times higher than the control experiment. The 12 torr data, with a 50% maximum,

results in ~75 minutes of burn time and the same ~50 minutes of burn time for the

control. The mg increase is 3 times higher than the control yield. Therefore, we can

conclude that this process is productive and efficient.

Our final observation of the copper studies involved determining how burn time

affected each type of fullerene (mass and percentage of extract). The results are shown in

Figure 26 on the next page.
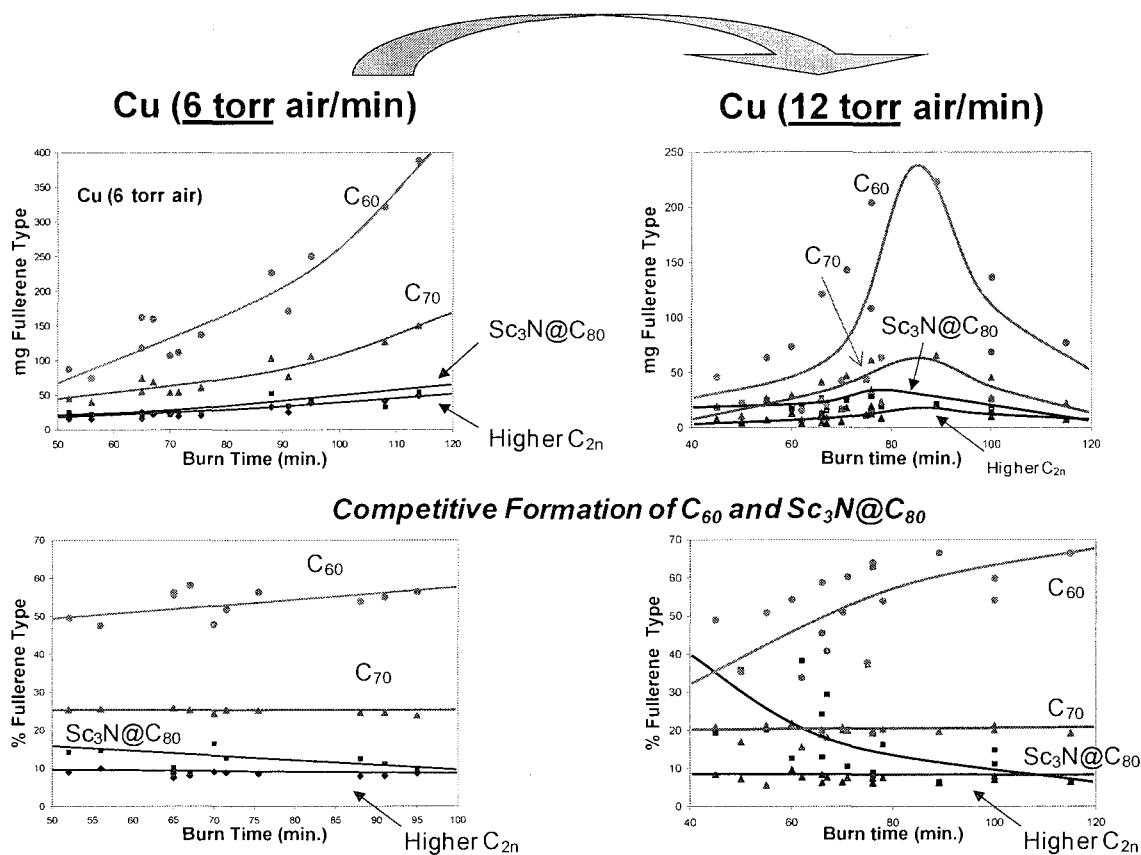
Figure 26. Mass of fullerenes as a function of burn time for the 6 torr data (top left) and the 12 torr data (top right) and % fullerene type as a function of burn time for 6 torr (bottom left) and 12 torr (bottom right)[119]

The graphs show that increasing the burn time under fairly low oxidative conditions (6 torr) is of no consequence to the mass produced (top left). There is, however, an inflection in the C_{60} and C_{70} curves, whereas the $Sc_3N@C_{80}$ is approximately linear. This indicates that the longer burn times result in preference toward empty cage formation. The percentages (bottom left) of fullerenes indicate that the C_{70} and C_{2n} remain constant while the C_{60} and $Sc_3N@C_{80}$ show an inverse relationship. This relationship is greatly exemplified under higher oxidative conditions (12 torr). Yet the other percentages of fullerenes remain constant even under high oxidation. The mass of

fullerenes at 12 torr/min air shows a yield maximum at ~ 90 minutes (as is the case for C_{60}) before the fullerenes start to decay in the highly oxidative atmosphere. This maximum likely exists at the lower air introduction rate but the time required for decay may be much higher for this to occur. These results indicate two conclusions. (1) The C_{60} and $Sc_3N@C_{80}$ display competitive formation that is not exhibited by other types of fullerenes. The % C_{60} is inversely proportional to the % MNFs as burn time proceeds. (2) The oxidative atmosphere is favorable to yield until a certain burn time, in which the decay of all fullerenes overcomes their formation. The graphs involving percentages were generated using integration values from HPLC. The peaks that were integrated were consistent with known retention times for certain fullerenes. No elemental analysis was performed on these extracts since no unknown peaks were found in the HPLC.

The Effect of Graphite Addition in Cu/Sc Mixtures

We also evaluated a third ingredient into the copper/scandium rods, to determine whether graphite addition to cored rods proved valuable in this research. This involved a short study with varying ratios of the three ingredients. Our hypothesis was that the addition of graphite would also increase the fullerene extract yield with minimal effect to the product distribution.

Table 6 shows the effect of varying the ratios of Sc_2O_3, C, and Cu. Graphite has traditionally been packed with metal oxide powder to ensure the availability of carbon for fullerene cage formation. However, addition of extra carbon to the rod increases the resistance relative to a copper/metal oxide mixture.

Table 6 also suggests that an increase in resistance from excessively added graphite (50% graphite) has a deleterious effect on the MNF yield (1%), despite the

increase in fullerene yield (367 mg). Only 4 mg of MNF is produced at this excessive

50% carbon loading. In contrast, 31 and 40 mg of MNFs are produced with the lower

25% and 33% graphite loadings. The percentage of MNFs in the extract are also much

improved for the lower loadings of graphite. Relative to the highest carbon loading (1%

MNF produced), the lower 25% and 33% graphite loadings permit a large jump to 15 and

18% MNFs produced, respectively.

Table 6. Effect of graphite on fullerene yields using Cu/Sc mixtures[98]

% Sc_2O_3 (By Mass)	% Carbon (By Mass)	% Cu (By Mass)	% MNF (of Fullerene Extract)	Total Mass of Extract (mg)	Total Mass of MNF (mg)
25%	25%	50%	6	537	31
50%	25%	25%	15	203	31
33.3%	33.3%	33.3%	18	220	40
25%	50%	25%	1	367	4

Curing experiments were performed in a furnace containing 1" diameter packed

rods that were cured for 18 hours under helium gas at 1100 °C. Each experiment was

performed at 220 A, 40 V, 350 torr, and an ambient air flow resulting in a pressure

change of 12 torr/min.

Packed rods are typically placed in a furnace under an inert gas blanket to cure the

packing materials. However, there are no publications to our knowledge on the effect of

cure time versus MNF yield and extract. Our data suggests that uncured rods yield the

lowest percent MNF yield in the extract. However, the mass of extract is significantly

higher and thus the overall mass of MNFs produced is the highest in the uncured rods

(Table 7). There is no known target weight or ceiling of a maximum amount of fullerenes

which should be produced. A possible disadvantage to this uncured rod approach is the

boost of empty-cage fullerenes also made. In the isolation strategy for purifying MNFs,

these contaminant fullerenes (e.g. C_{60}, C_{70}) must be removed. There is a trade-off

between synthesizing more MNFs versus more empty-cage fullerenes. The data for 18

hour and 72 hour furnace cure times in Table 7 indicate a slightly improved percent MNF

yield, but with a slightly lower total mass of MNF produced.

Table 7. Effect of furnace cure time on MNF yield[98]

Furnace Cure Time (hr)	% Sc_2O_3 (By Mass)	% Carbon (By Mass)	% Cu (By Mass)	% MNF (of Fullerene Extract)	Total Mass of Extract (mg)	Total Mass of MNF (mg)
Uncured	33.3%	33.3%	33.3%	15	325	50
18 hr	33.3%	33.3%	33.3%	18	220	40
72hr	33.3%	33.3%	33.3%	17	242	47

These results support our hypothesis that additives do have an effect of the plasma

(depending on quality and quantity of the additive), which in turn have an effect on the

type and quantity of fullerene produced. These results also suggest that there are TWO

sets of electric-arc reactor parameters – one set for maximizing empty-cage fullerenes

(e.g. C_{60}) and a second set of conditions for optimizing MNF yields. We have also

concluded that curing the rods decrease the yield of MNFs, but slightly increases relative

percentages for MNFs. However, this increase is negligible and results in low

productivity (mg MNF per unit of time).

The CAPTEAR Method – Effect of Copper Nitrate [$Cu(NO_3)_2$]

on Scandium Experiments

Introduction

In our efforts to increase the yield of fullerenes, we found that copper was an

excellent additive to improve overall fullerene yield[15] but at the expense of MNF

selectivity. However, when experiments were performed under different oxidizing

conditions (6 and 12 torr/min air), there were notable differences in selectivity depending on burn time. The shorter burn times favored MNF formation and longer burns favored C_{60} formation. Another import aspect of the copper profile results was that air was used as the oxidative atmosphere. We hypothesized that MNF selectivity would still be possible under harsher oxidizing conditions and therefore, chose copper (II) nitrate as our additive. This compound has several advantages over other oxidizing agents. (1) We knew that copper would assist in increasing the yield. (2) Copper (II) nitrate is a solid at room temperature and could therefore decompose to introduce NO_x gas vapor through the packing material rather than from a gas cylinder, which is more expensive and harder to control and quantify. (3) The NO_x gas produced by combustion (refer to Figure 27 below) would not only provide the oxidizing atmosphere, but also a possible source of nitrogen for our MNFs. (4) Thermal decomposition occurs in two high temperature stages (identified at 350°C an 850°C). (5) Water and NO_x are lost simultaneously and over all decomposition ranges. (6) The amount of copper (II) oxide produced is higher than anticipated and it is suggested that the copper oxide surface produced during the decomposition of copper nitrate reduces the NO_2 to NO. (7) There was no known use of this compound (or other oxidizing agents) as an additive in previous literature.

$$Cu(NO_3)_2 \cdot 3H_2O \rightarrow CuOH \cdot NO_3 + HNO_3 + 2H_2O$$
$$2HNO_3 \rightarrow H_2O + 2NO_2$$
$$NO_2 + (CuO) \rightarrow NO + \tfrac{1}{2}O_2$$

Oxidizing Environment
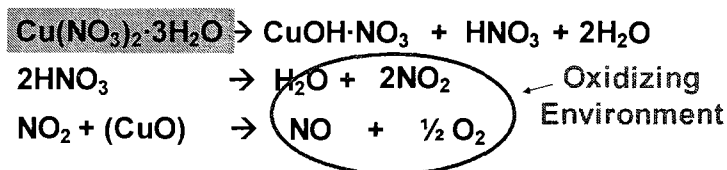
Figure 27. Combustion scheme for the thermal decomposition of copper (II) nitrate trihydrate[33]

Experimental

In each experiment, the graphite rods (from Carbone of America) were 1 inch in diameter and 6 inches long. Each rod was drilled 4 inches deep using a 0.75 inch diameter drill bit. The cored rods were packed with various ratios $Cu(NO_3) \cdot 3H_2O$ and Sc_2O_3. The control experiments used 100% Sc_2O_3. Reactor parameters include 220 amps, 40 volts, 300 torr inside the chamber, 6 torr/min air for a nitrogen source and oxygen, and 630 ml/min (~21 torr/min) of helium gas (ultra high purity tank from Nordan Smith) used as a buffer gas. After the electric arc process, each soot sample was extracted with xylenes and analyzed via HPLC for product distribution. The extract was dried to a solid and washed with diethyl ether to obtain mg masses. MALDI-TOF was employed for verification of fullerenes produced.

Results and Discussion

Copper (II) nitrate proved not only to provide the desired oxidative atmosphere, but also created a highly energetic and reactive atmosphere that favored our targeted MNFs. Our lab coined this method as the CAPTEAR shift or **C**hemically **A**djusting **P**lasma **T**emperature, **E**nergy, **A**nd **R**eactivity.[33] A scheme of how this process works is shown in Figure 28. Based on this diagram, the increased energy, temperature, and reactive environments should result in a high purity sample of MNFs with contaminant suppression of empty cage fullerenes that would otherwise dominate the extract.
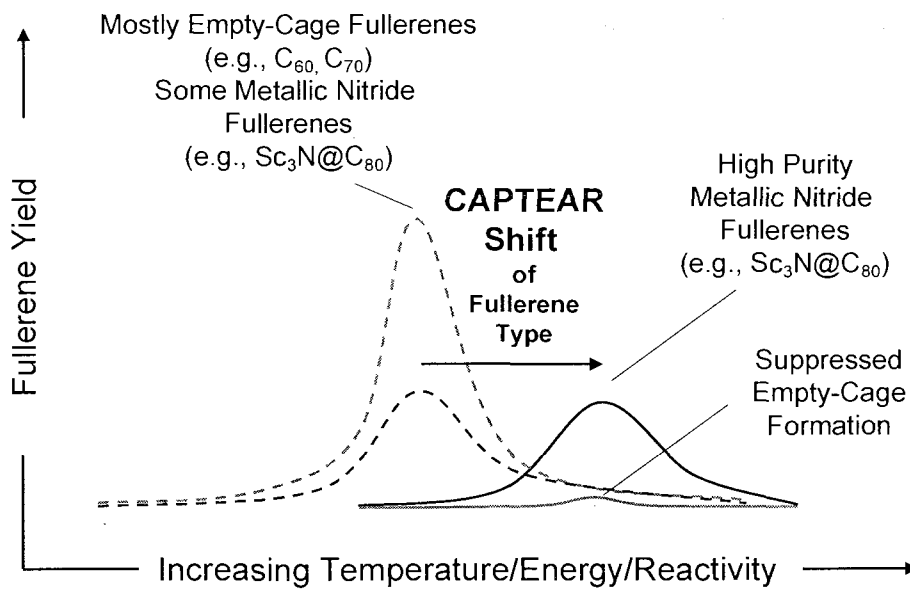
Figure 28. Concept of using the CAPTEAR method to adjust and optimize the temperature, energy, and reactivity of the plasma environment to "tune" the type of fullerene produced[33]

The $Cu(NO_3)_2 \cdot 3H_2O$ study was performed in the same manner as the copper studies. The control rod was packed with 100% Sc_2O_3 powder (325 mesh). All reactor parameters and gas additions were held constant while 5-10% increments of the $Cu(NO_3)_2 \cdot 3H_2O$ were added. Soot from each rod was extracted, followed by HPLC analysis to determine product distribution. The following graph (Figure 29) provides results from these studies.
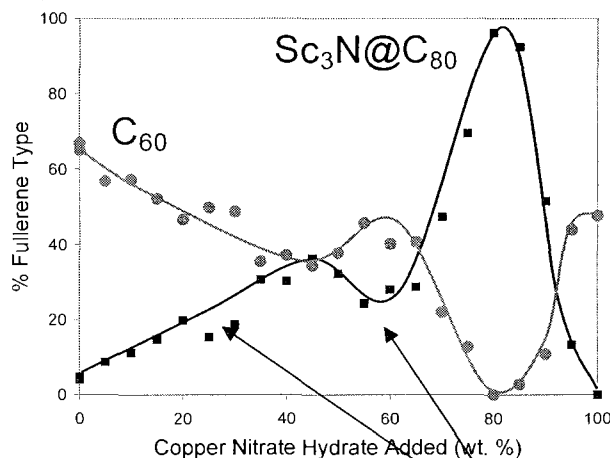
Figure 29. Effect of $Cu(NO_3)_2 \bullet 3H2O$ on C_{60} and $Sc_3N@C_{80}$

Just as the copper studies demonstrated, the copper (II) nitrate hydrate addition resulted in an inverse relationship between the C_{60} and $Sc_3N@C_{80}$. This indicates a competitive formation of the two molecules. Clearly, there must be complex kinetics that play a role in this "double maxima" graph.

Results from copper studies revealed that C_{70} and other C_{2n} species had little effect from the addition of copper. This also remains true for the copper (II) nitrate data except for one differentiation. The downward inflection experienced by C_{60} at 80% copper (II) nitrate loading is shared with the other fullerenes as well (Figure 30). Hence, we have finally created an atmosphere that was totally selective for MNFs and suppressive for all other fullerenes as shown in Figure 31.
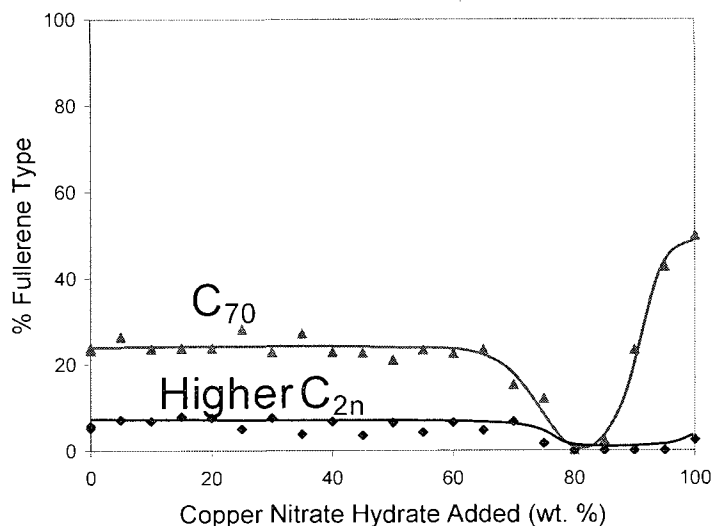
Figure 30. Effect of $Cu(NO_3)_2 \bullet 3H_2O$ on C_{70} and the higher C_{2n} [33]
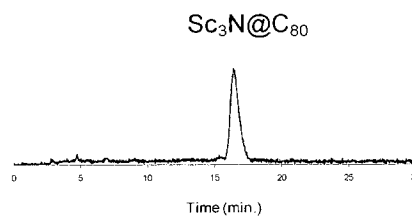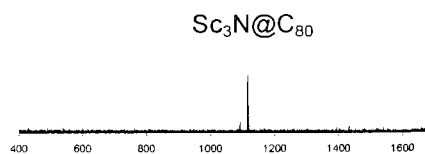
Figure 31. HPLC of soot extract at 80 % weight $Cu(NO_3)_2$ containing pure $Sc_3N@C_{80}$ (top) and the resulting mass spectrum (bottom) [33]

Not only is there a region of MNF purity in the copper nitrate profiles, this region

has one of the most favorable burn times as well. Recall that increasing copper resulted in

increased burn times (Figure 26). Due to the increase in temperature, energy, and

reactivity of the CAPTEAR method, the burn times actually shortened as the amount of

$Cu(NO_3)_2$ increased. The comparison of burn times (or productivity) for the CAPTEAR method when compared to the copper addition burn times is shown in Figure 32.
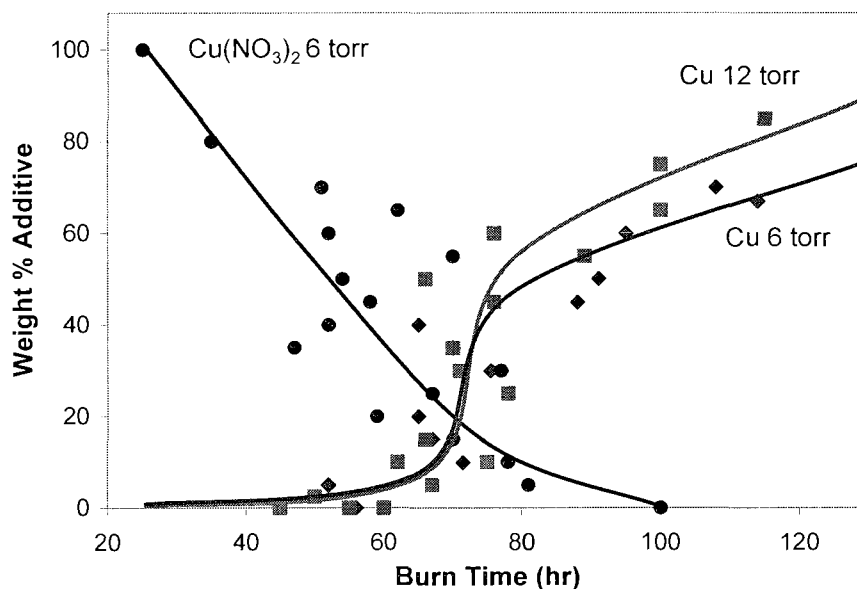
Figure 32. Weight % additive as a function of burn time for the CAPTEAR method (circles), the 6 torr-air copper data (diamonds) and the 12 torr copper data (squares)

As shown in the graph, the CAPTEAR method favors shorter burn times, which also favor high MNF purity. This clearly indicates that the CAPTEAR method is a novel method that favors both productivity and MNF purity by shifting the energetic environment to favor MNF production. Our CAPTEAR method not only produces a high % MNF (>99 %), but without a significant loss of mg yield and a short burn time, as shown in Figure 33.
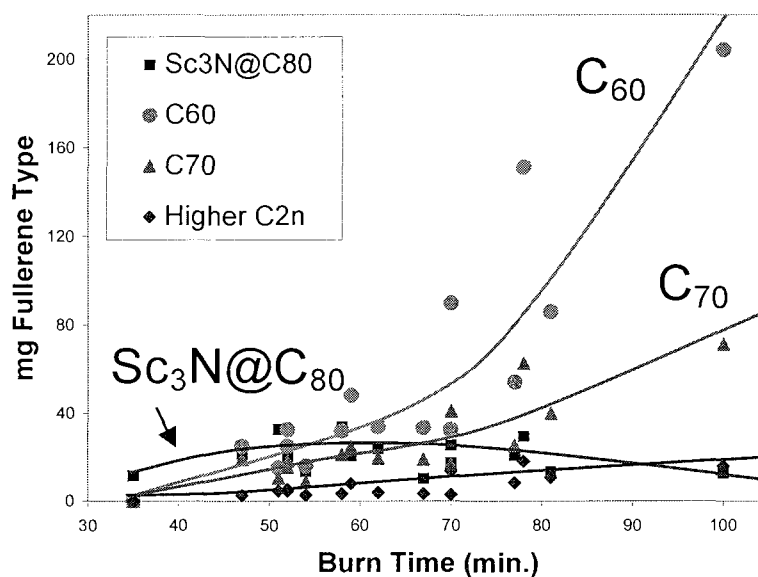
Figure 33. mg of fullerene type versus burn time[33]

This graph demonstrates that there is little cost of yield for purity. In the 35-40

minute region, our MNF yield ~ 16 mg is comparable with its yield at 100 minutes.

Therefore our CAPTEAR approach has the best of purity, productivity, and yield. This is

also the first known method to produce these targeted molecules under an oxidizing

atmosphere. Most scientists in this field (including Dorn, Dunsch, Yang, Echegoyen, Cai,

Duchamp, and Olmstead) until now, believed oxidation was deleterious to fullerene

production and thus have never attempted such a feat from the norm. We also

demonstrate that the % fullerenes at these low burn times greatly favor MNF purity,

when compared to the other extract components (Figure 34).
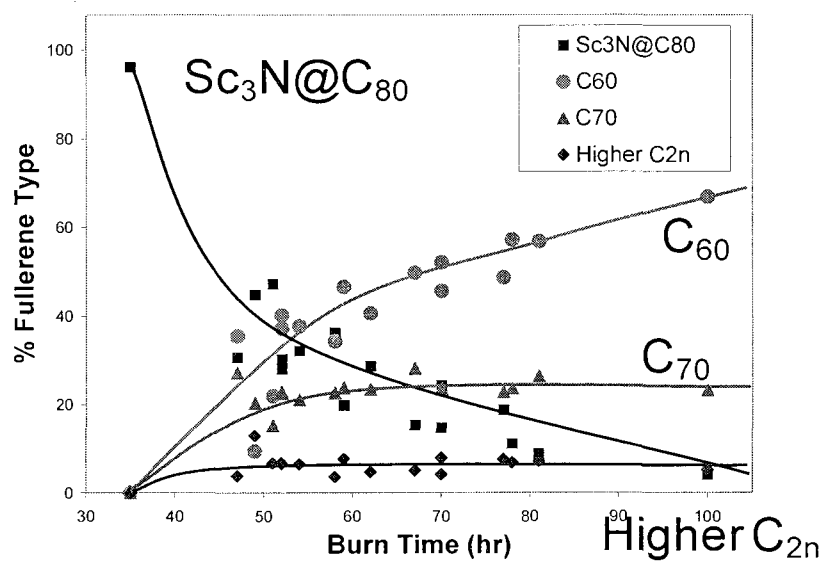
Figure 34. % fullerene type versus burn time[33]

In conclusion, the CAPTEAR method has proven to be a novel method to selectively synthesize MNFs in high purity without much penalty to the yield. It is also, by far, the most productive method to synthesize these molecules and is the first method to synthesize fullerenes in an oxidizing atmosphere.[33]

CHAPTER VI

NEW ENDOHEDRAL FULLERENES

This chapter focuses on two new classes of fullerenes. These molecules were discovered while attempting to scale-up the yield of MNFs. CHAPTER V introduced a new concept of producing fullerenes with targeted selectivity under an oxidizing environment (CAPTEAR). The CAPTEAR method was not only capable of selectively producing MNFs, but also was necessary to create these two new classes (metallic nitride azafullerenes (MNAFs)[18] and oxo-metallic fullerenes (OMFs).[47, 120]

Metallic Nitride Azafullerenes (MNAFs)

Azafullerenes have been isolated and characterized[121-125] since 1995. Empty cage fullerenes (i.e. $(C_{59}N)_2$) have been used in thin film transistors.[126] Recently, a new class of azafullerenes were discovered (MNAFs).[127] MNAFs are endohedral fullerenes that have one or more nitrogens incorporated within the carbon cage. MNAFs have the generic formula $M_3N@C_xN_y$, where "M" is any metal of the MNF family, "x" and "y" represent the number of carbons and nitrogens that make up the cage composition, respectively. Thus far, x + y has only been shown to be ≥ 80, as in the case of $Sc_3N@C_{79}N$. In addition to the favorable 80 atom cage size, data suggests that the structure also favors having only one nitrogen in cage composition.[128, 129] Though azafullerene chemistry is still a relatively new field, there remains great potential for structural diversity as well as applications. Changing a carbon to a heteroatom on a fullerene cage has the potential to (1) change the reactivity of the molecule and (2) serve as a particular linking site for functionalization.[130] Figure 35 is an example of an MNAF, with the typical nitrogen substitution of one carbon atom.
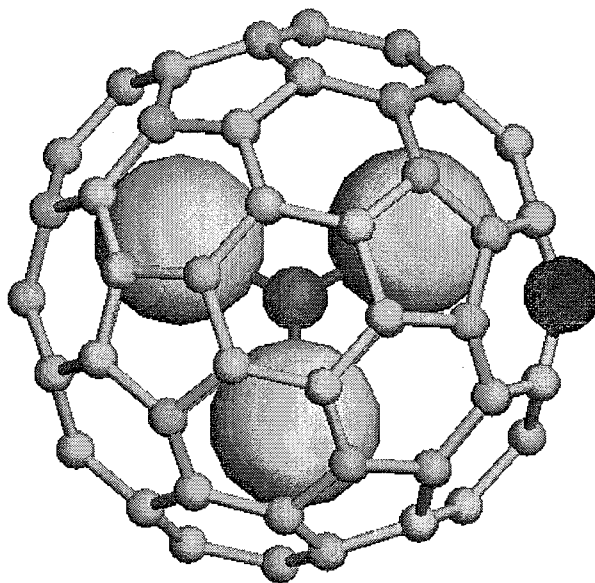
Figure 35. Example of a metallic nitride azafullerene

Selective Synthesis of MNAFs Using CAPTEAR

Our lab first found this new class while characterizing a mixed metal MNF extract

of lanthanum and scandium. Our research was focused on these mixed metal MNFs to

study separation methods for these mixed metal compounds. This extract should have

included three C_{80} cage MNF species: $LaSc_2N@C_{80}$, $La_2ScN@C_{80}$, and $Sc_3N@C_{80}$. The

$La_3N@C_{80}$ would usually be a fourth MNF species, but this MNF has not been detected

before on an 80 atom cage. Our first suspicion of the existence of the MNAF was evident,

and serendipitous, while analyzing the $Sc_3N@C_{80}$ using MALDI-TOF. The mass

differences of the MNF versus the MNAF is only 2 amu or in the case of the mass

spectrum, 2 m/z units. The Sc-MNF has a m/z value of 1109 and the Sc-MNAF has a m/z

value of 1111. Therefore, the MNAF was difficult to differentiate from the isotopic

pattern of the MNF. Therefore, HPLC was used to remove the MNF to determine if the

isotopic ratios of 1109 to 1111 changed in the mass spectrum. Figure 36 shows the mass

spectra of the extract containing the Sc-MNF and MNAF before and after HPLC fraction collection of the MNF.
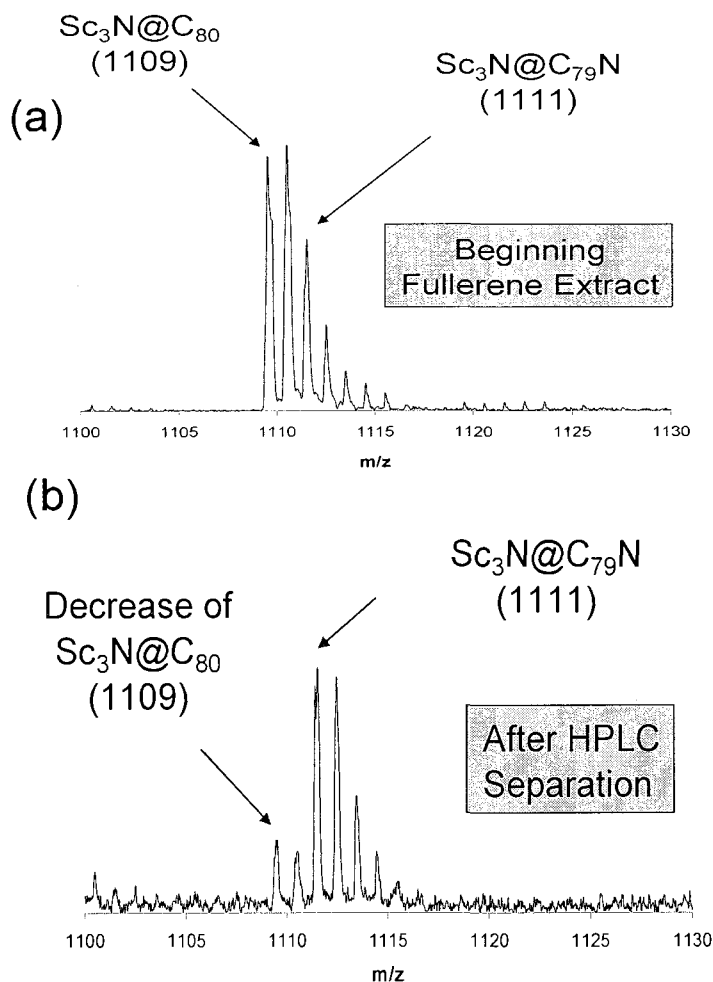
Figure 36. Mass spectrum of (a) Sc-MNF and Sc-MNAF before HPLC fraction collection and (b) after HPLC fraction collection[18]

If the 1111 m/z peak was just an isotope of 1109, then all the peaks in Figure 36(b) would decrease simultaneously. However, since the 1109 m/x peak decreased and the 1111 m/z peak did not decrease as well, this data suggested that the 1111 m/z peak was $Sc_3N@C_{79}N$.

The preferential method for production of MNAFs involves the use of reactive gases (i.e. CAPTEAR method). We used copper (II) nitrate since this chemical is inexpensive and its use has been well established in our studies. This process is currently patent pending.[130] Our investigations have shown that increasing the amount of reactive gases into the plasma chamber changes the product distribution to favor MNAFs over MNFs. Figure 37 shows the mass spectral data for the MNFs and MNAFs of a lanthanum/scandium based fullerene extract.
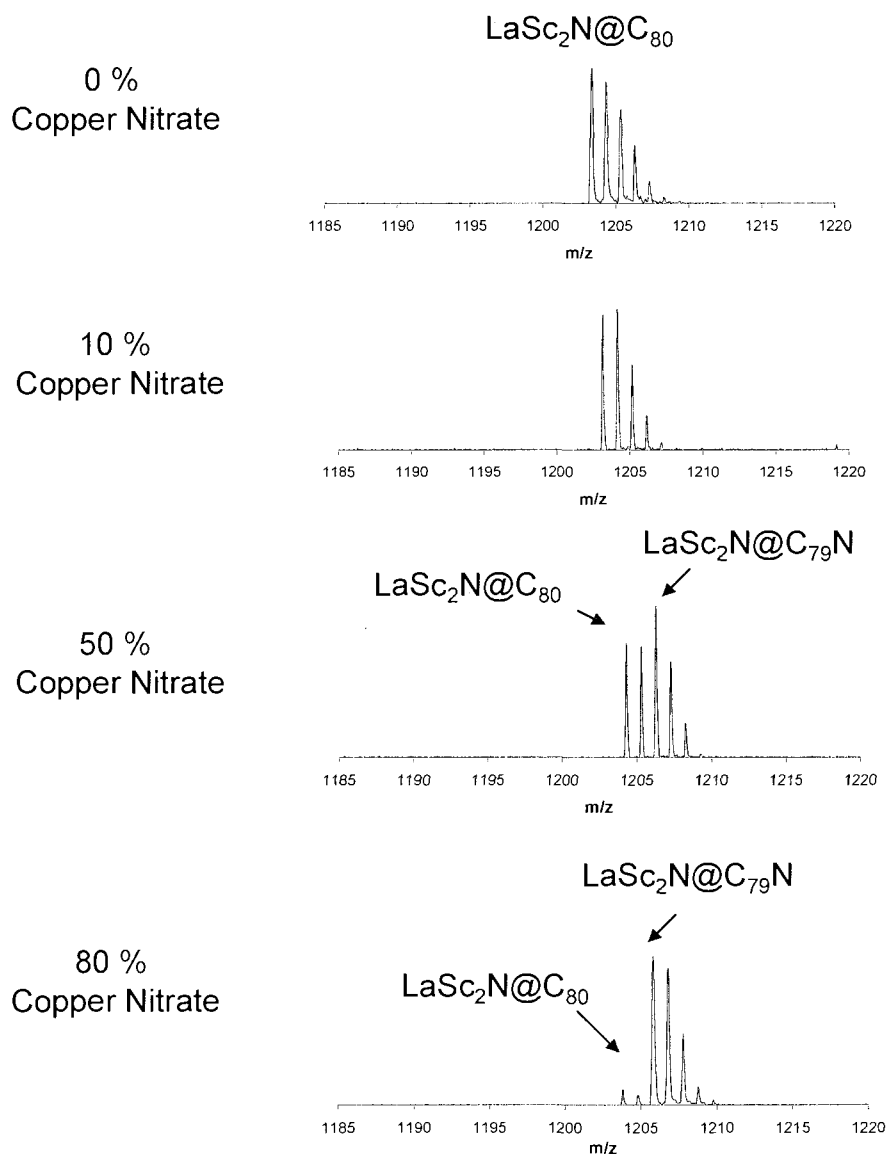
Figure 37. Mass spectra showing the effect of increasing Cu(NO3)2 on La/Sc based MNFs and MNAFs[18]

As shown in Figure 37, increasing copper (II) nitrate packing material for the arc synthesis of $La_2Sc@C_{80}$ and $La_2Sc@C_{79}N$ favors the MNAF at these highly oxidative conditions. Conversely, when only the traditional N_2 gas introduction method was used, the MNAF did not appear in any of the extracts Figure 38.

(a) $Sc_3N@C_{80}$

1090	1100	1110	1120	1130

m/z

(b) $LaSc_2N@C_{80}$

1180	1190	1200	1210	1220

m/z

(c) $La_2ScN@C_{80}$ $La_2ScN@C_{79}N$
(At Detection Limit)   (not detected)

1280	1300	1320

m/z

(d) $La_3N@C_{80}$ $La_3N@C_{79}N$
(not detected)   (not detected)

1380	1400	1420

m/z
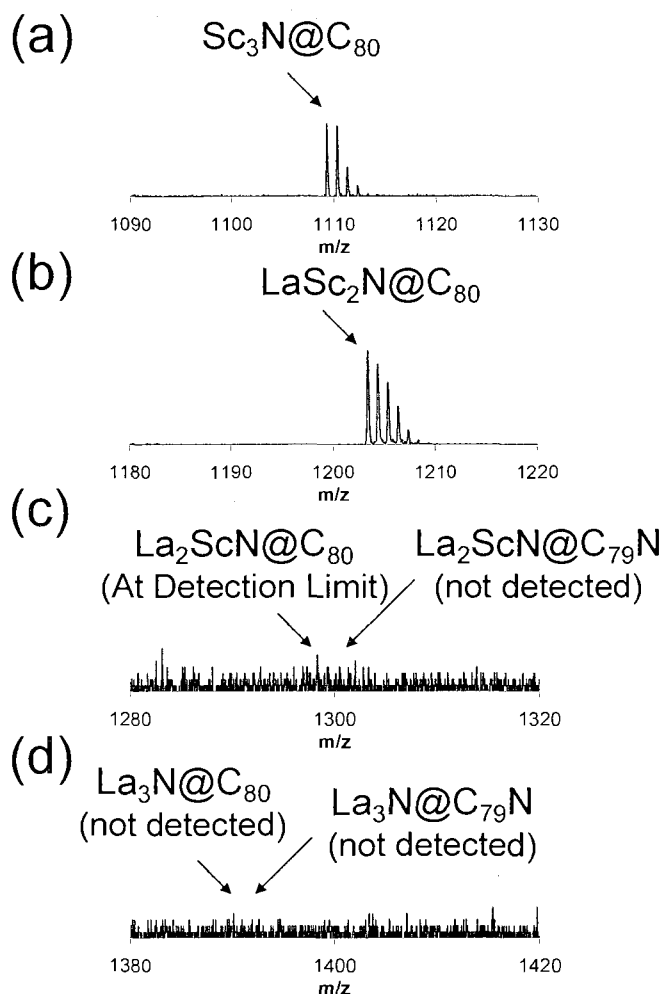
Figure 38. Mass spectral data (using N_2 as an additive) showing no evidence of MNAFs[18]

Preferential Encapsulation and Stability of MNAFs

Trimetallic nitride clusters (from group IIIB (Sc,Y,La) and 4f-block metals (Lu,Er,Gd)) show preference for MNF cage sizes (C_{80}, C_{88}, C_{96}) depending on their ionic radius.[1, 131-133] After discovering the MNAFs, several MNF metals were tested for their ability to synthesize the MNAFs. Mixed metal (heterometallic) MNFs and homometallic MNF clusters (e.g. La_3N) that would ordinarily prefer large cage sizes (e.g. C_{88} and C_{96}) were analyzed via MALDI-TOF to determine if the nitrogen provided stabilization for the cluster in an atypical cage size. The mass spectral data is shown in Figure 39.

(a) $Sc_3N@C_{80}$

$Sc_3N@C_{79}N$

1090   1110   1130

m/z

(b) $LaSc_2N@C_{80}$

$LaSc_2N@C_{79}N$

1180   1200   1220

m/z

(c) $La_2ScN@C_{80}$ $La_2ScN@C_{79}N$

1280   1300   1320

m/z

(d) $La_3N@C_{79}N$

$La_3N@C_{80}$
(not detected)

1380   1400   1420

m/z

(e) $LaSc_2N@C_{82}$ $LaSc_2N@C_{81}N$

1210   1230   1250

m/z

(f) $La_3N@C_{87}N$

$La_3N@C_{88}$
(not detected)

1470   1490   1510

m/z
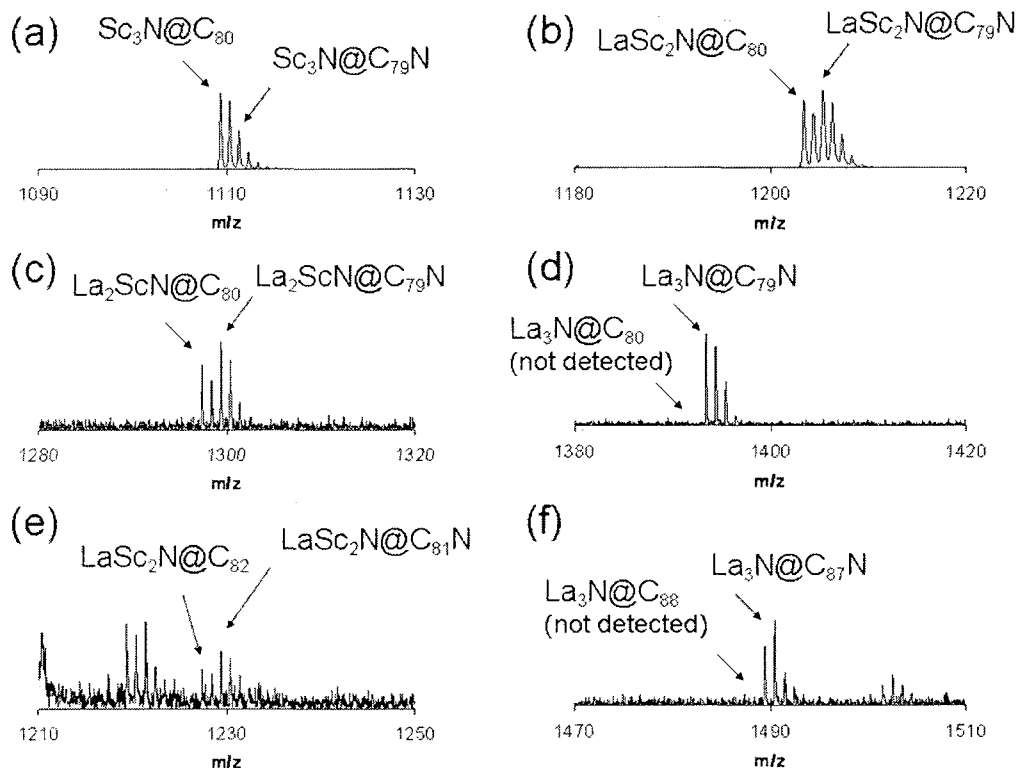
Figure 39. Mass spectra of mixed metal MNFs and MNAFs that show preference to MNAFs (b,c, and e) and MNAFs of smaller cage sizes that would otherwise prefer larger cages for their MNF analogs (d and f)[134]

The mass spectra show a tendency for the large clusters in the MNFs to have smaller m/z values than the MNAF analogs. Although mass spectroscopy doesn't rely on peak area to be a true comparison of relative ratios, the peak heights are indicators of which species is dominant. The propensity for the MNF cluster to prefer larger cage sizes, based on their ionic radii, is shown in Figure 40.
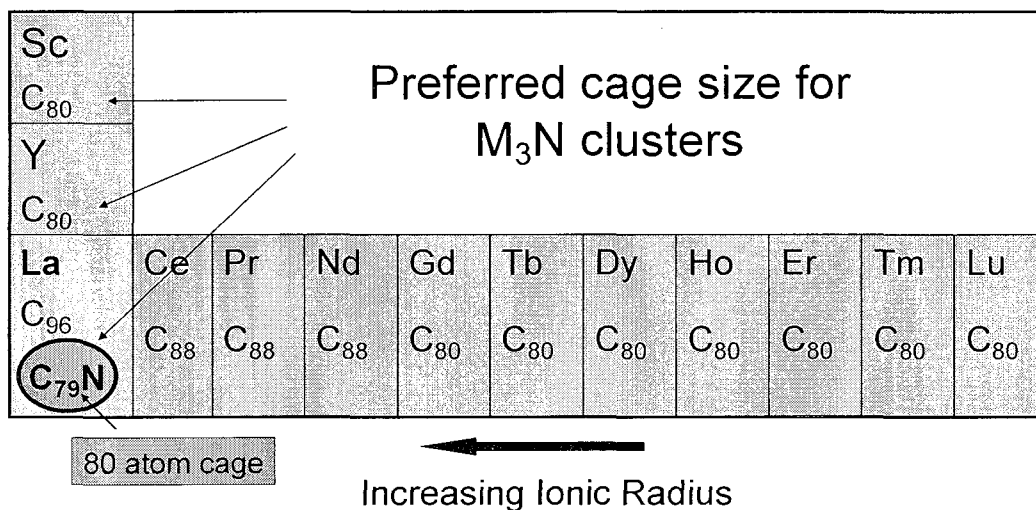
Figure 40. Overview of preferred cages for M_3N clusters with C_{80} (blue), C_{88} (green), and C_{96} (yellow). The preferred 80 atom cage for $La_3N@C_{79}N$ is circled[18]

As shown, the C_{80} cage is preferred for metals ranging from lutetium to gadolinium, followed by the C_{88} cage for neodymium to cerium, and the lanthanum MNF prefers the C_{96} cage. However, the $C_{79}N$ cage provides stability that supercedes the $La_3N@C_{96}$. This is further demonstrated in Figure 41, in which the MNAF of La_3N is detected without any trace of the corresponding MNF. In addition, the $La_3N@C_{79}N$ has a larger peak height than $La_3N@C_{96}$ and $La_3N@C_{104}$. The base peak in these mass spectra is C_{60} and the relative intensities are not shown since the MNFs and MNAFs needed resolution enhancement. The isotopic patterns typically show a "staircase" pattern in which the $[M]^+$ peak is the most intense peak and every following peak is smaller. Therefore, the magnitude of the MNAFs can be seen in the mass spectra by comparison of the $[M]^{2+}$ peak.

A

C$_{60}$

C$_{70}$

Sc$_3$N@C$_{80}$

LaSc$_2$N@C$_{80}$

La$_3$N@C$_{80}$
(1391)
not detected

La$_3$N@C$_{79}$N
(1393)
detected

1380   1400   1420
m/z

700 800 900 1000 1100 1200 1300 1400 1500
m/z

B

La$_3$N@C$_{79}$N

La$_3$N@C$_{96}$

La$_3$N@C$_{104}$

1300   1350   1400   1450   1500   1550   1600   1650   1700
m/z
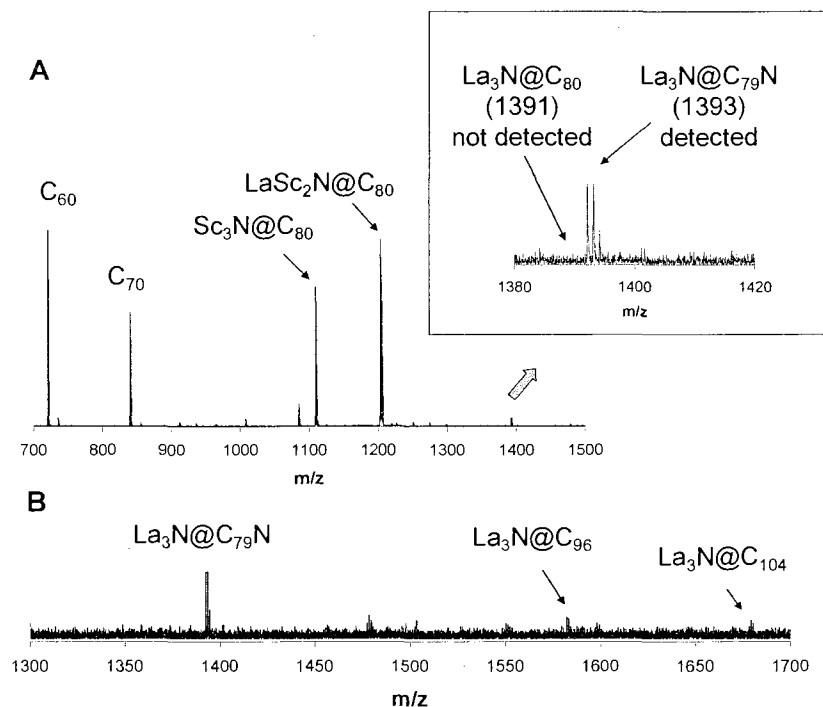
Figure 41. MALDI mass spectral data of soot extract obtained under CAPTEAR conditions[18]

Our data concerning MNAFs suggests that these molecules are selectively

synthesized under oxidizing conditions (i.e. CAPTEAR method). The nitrogen

heteroatom provides reactivity in fullerene functionalization that was not possible with

the MNFs. The MNAFs also provide stabilization of the cluster and has enabled many

large clusters to favor smaller cage sizes than their MNF analogs. Currently, the yields of

these new molecules have not been obtained due to a lack of separation method.

However, collaboration efforts are showing promise to further characterize these

compounds through molecular modeling. This class of fullerenes should provide the

scientific community with fullerene characterization and functionalization that has not yet

been possible.

Oxo-Metallic Fullerenes (OMFs)

Oxo-metallic fullerenes (OMFs) are another new class of fullerenes discovered by our lab. These molecules have the generic formula $M_xO_y@C_n$, where "M" represents a class of metals in the IIIB or 4-f block, "x" and "y" refer to the number of metal and oxygen atoms encapsulated in the fullerene cage, and "n" refers to the number of carbon atoms in the fullerene cage. Thus far, only two known OMFs have been isolated, $Sc_4O_2@C_{80}$[120] and $Sc_4O_3@C_{80}$.[34] These molecules are the first to encpsulate more than 5 atoms in a C_{80} cage and are one of the two known classes (OMFs and MNAFs) to be synthesized preferebly in an oxidizing atmosphere. In this section, the isolation, identification, and characterization of this new class of endohedral fullerenes is discussed.

Synthesis, Isolation, and Characterization of $Sc_4O_2@C_{80}$ and $Sc_4O_3@C_{80}$

The CAPTEAR method has revealed that targeted fullerenes can be selectively synthesized, and has also resulted in the discovery of this class of fullerenes. The OMFs first appeared as a mere "blip" on the HPLC chromatograms, while using CAPTEAR to isolate MNFs. Since these peaks were currently unidentified, our lab utilized the SAFA technique[135] to simplify the mixture of fullerenes by removing a large portion of empty cage fullerenes. Diamino silica gel was used for the SAFA process for approximtely two hours followed by several HPLC fraction collections (as shown in Figure 42).
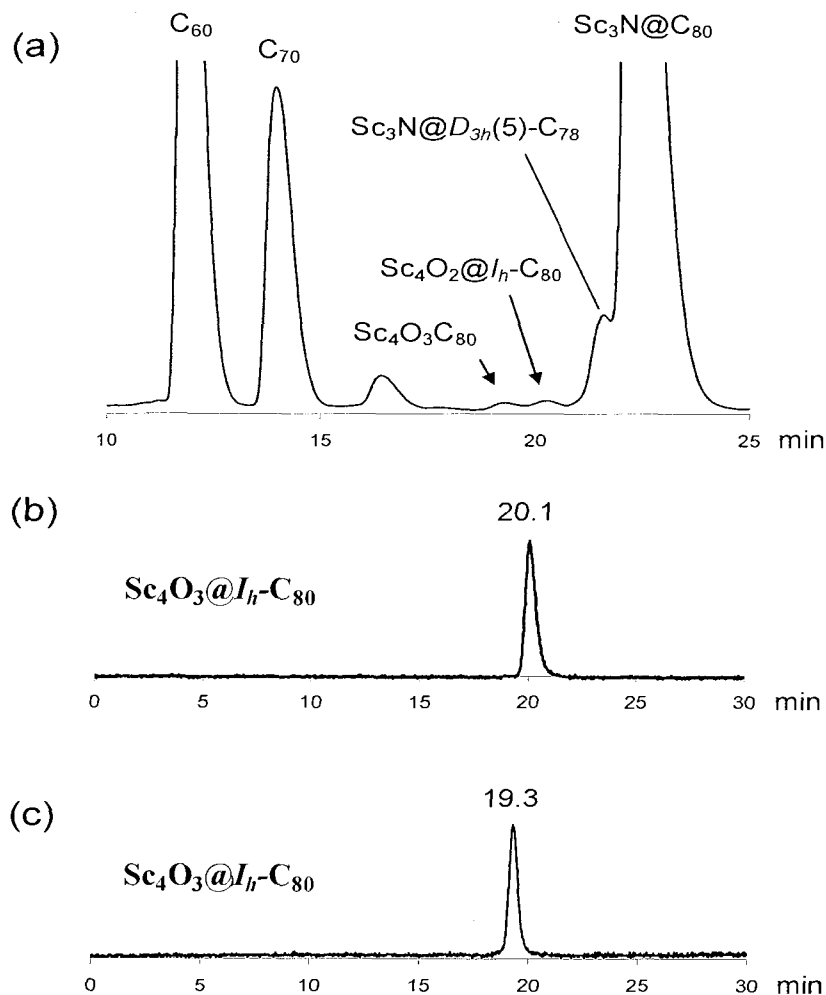
Figure 42. HPLC of (a) the extract containing OMFs, (b) fraction collection of $Sc_4O_2@C_{80}$ and (c) fraction collection of $Sc_4O_3@C_{80}$[34, 120]

After sufficient quantities (e.g. 50 – 100 μg) were obtained from fraction collection, samples were sent for crystallization to the University of California – Davis to obtain crystal structures. MALDI-TOF analysis was used to determine the m/z values and isotope patterns. The resultant m/z values were 1172 and 1188. After deliberation on the possibilities, candidate formulas were $Sc_4O_2C_{80}$ and $Sc_4O_3C_{80}$. The "@" symbol was left out of the previous statement since (at that time) we did not know whether the cluster was endohedral or exohedral. Therefore, isotope patterns (Figure 43) were compared to the

theoretical patterns and were found to be consistent with the proposed formulas. The peak after 1100 is 1109, which is contamination from the $Sc_3N@C_{80}$.
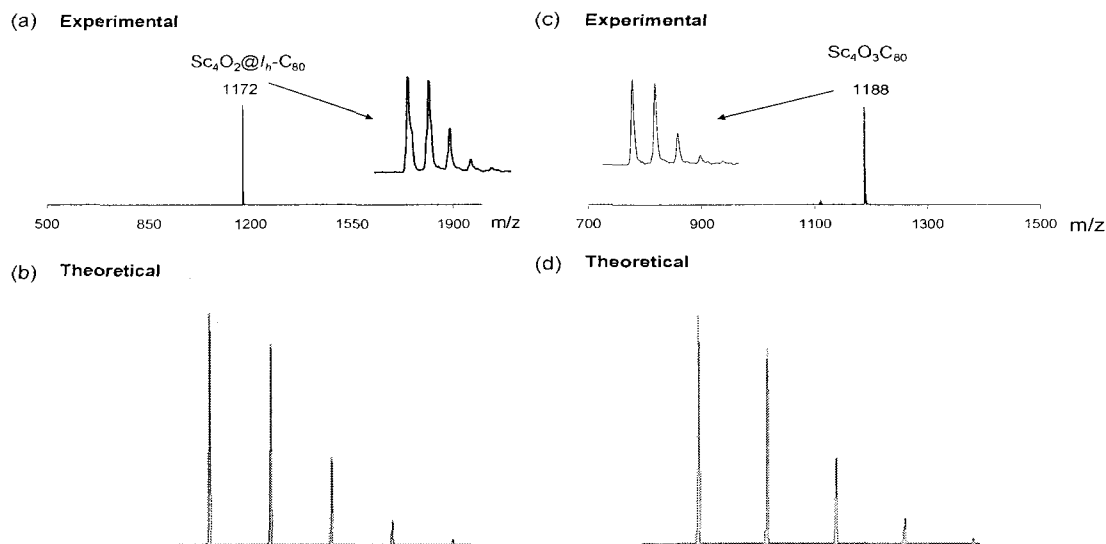
Figure 43. MALDI of (a) $Sc_4O_2C_{80}$ with isotope pattern and (b) comparison theoretical isotope pattern; and (c) MALDI of $Sc_4O_3C_{80}$ with isotope pattern and (d) comparison isotope pattern[34, 120]

High resolution mass spectral experiments were also performed on several fullerenes to compare m/z values with theoretical values. The values are shown in Table 8. The experimental versus theoretical values suggest reasonable error.

Table 8. High resolution mass spectral data for C_{60}, C_{70}, $Sc_3N@C_{80}$, and both OMFs[34, 120]

Fullerene	Experimental	Theoretical	Error
C_{60}	719.99940 721.00276 722.00605	719.99945 721.00281 722.00616	78 ppb
C_{70}	839.99943 841.00262 842.00619	839.99945 841.00281 842.00616	28 ppb
Sc_3NC_{80}	1108.87029 1109.87357 1110.87766	1108.87026 1109.87360 1110.87696	29 ppb
$Sc_4O_2C_{80}$	1171.81296 1172.81650 1173.81966	1171.81292 1172.81628 1173.81963	36 ppb
$Sc_4O_3C_{80}$	1187.80762 1188.81099 1189.81438	1187.80784 1188.81119 1189.81454	100 ppb

To isolate the variables that contribute to the formation of these molecules, an array of experiments were done using reactor R&D techniques. Table 9 shows the effect of several additives on the mg yields and percentages of C_{60}, C_{70}, and $Sc_4O_2@C_{80}$. The data suggests that CAPTEAR is necessary to synthesize the OMFs.

Table 9. Identification of key variables and comparison of soot extracts[34, 120]

Wt % Additive to Sc_2O_3	Air (torr/min)	mg C_{60}	mg C_{70}	mg $Sc_4O_2@C_{80}$	% C_{60}	% C_{70}	% $Sc_3N@C_{80}$	% $Sc_4O_2@C_{80}$
Control Rod (Sc_2O_3 + Air)								
No Additive	0.6	588	225	**0**	65	25	1.8	**0**
Effect of Increasing Cu								
33% Cu	2	523	201	**0**	65	25	2.0	**0**
50% Cu	2	254	85	**0**	70	23	0.98	**0**
67% Cu	2	214	73	**0**	69	23	1.8	**0**
Effect of Increasing Air								
67% Cu	**2**	214	73	**0**	69	23	1.8	**0**
67% Cu	**6**	137	47	**0.016**	68	23	2.0	**0.0081**
67% Cu	**12**	57	27	**0.11**	59	28	5.2	**0.11**
Effect of Increasing CAPTEAR								
No Additive	0.6	588	225	**0**	65	25	1.8	**0**
33% Cu	0.6	421	146	**0**	69	24	1.0	**0**
33% $Cu(NO_3)_2$	0.6	222	91	**0.9**	63	26	3.6	**0.25**
50% $Cu(NO_3)_2$	0.6	194	83	**2.4**	59	25	5.7	**0.75**
80% $Cu(NO_3)_2$	0.6	1.5	5.3	**9.1**	1.3	4.4	76	**7.6**
Optimization of CAPTEAR + Air								
80% $Cu(NO_3)_2$	**0.1**	20	55	**15**	11	31	54	**8.8**
80% $Cu(NO_3)_2$	**0.2**	15	31	**19**	9.5	19	67	**12**
80% $Cu(NO_3)_2$	**0.6**	1.5	5.3	**9.1**	1.3	4.4	76	7.6
80% $Cu(NO_3)_2$	**6**	1.0	1.7	**0.56**	4.2	7.5	82	**2.5**

The table above does not include the $Sc_4O_3@C_{80}$ due to its requirements for synthesis. The data table utilizes air up to 6 torr/min, but according to Figure 44, $Sc_4O_3@C_{80}$ requires at least 18 torr/min of air just to obtain a peak in the mass spectrum.
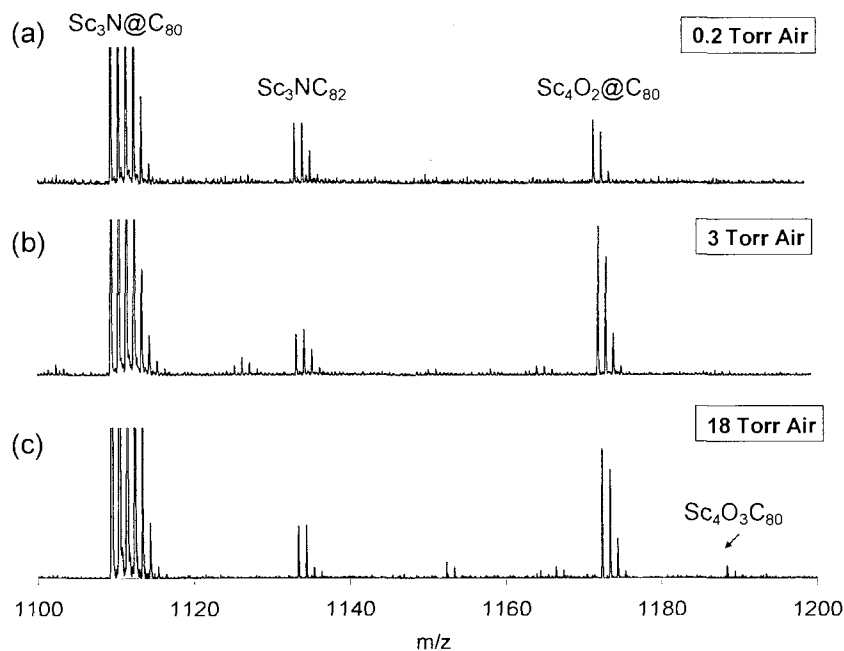
Figure 44. Effect of air using CAPTEAR method on the formation of OMFs[34, 120]

The researchers at Cal-Davis successfully obtained X-ray crystallographic data using Ni-porphyrin co-crystallizers to determine the structure of our OMFs, confirming that the clusters were, in fact, endohedral to the fullerene cage. Figure 45 and Figure 46 show the crystal structures of $Sc_4O_2@C_{80}$ and the endohedral cluster of the $Sc_4O_2@C_{80}$ molecule, respectively. LDI has not been performed on the crystals, only the HPLC fraction collected samples.
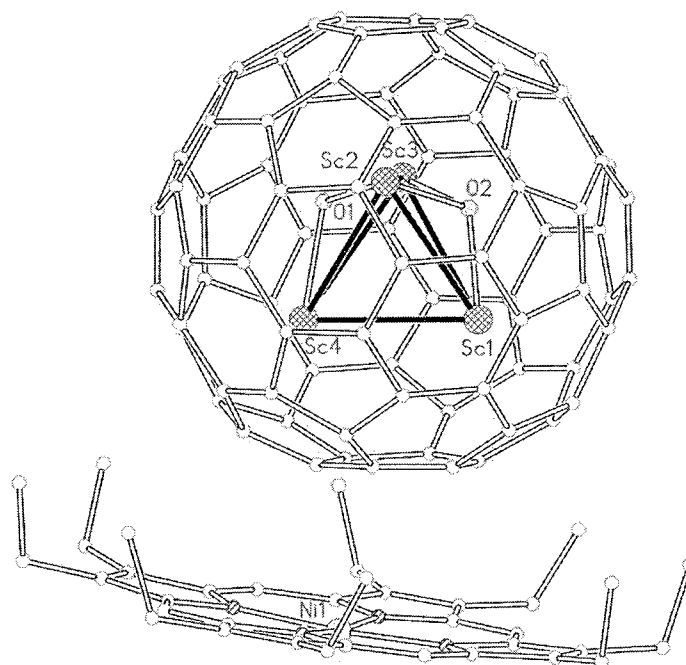
Figure 45. Crystal structure of $Sc_4O_2@C_{80}$[120]
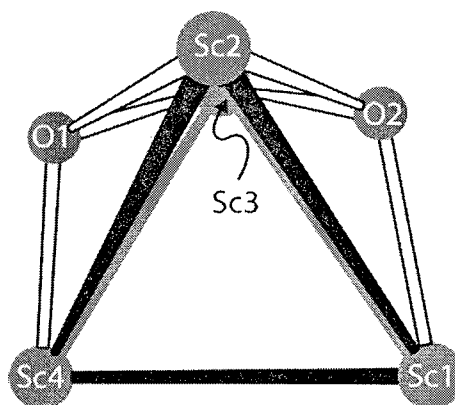
Figure 46. Endohedral cluster of the $Sc_4O_2@C_{80}$ molecule[120]

The next two figures (Figure 47 and Figure 48) show the $Sc_4O_3@C_{80}$ and its corresponding endohedral cluster, respectively.
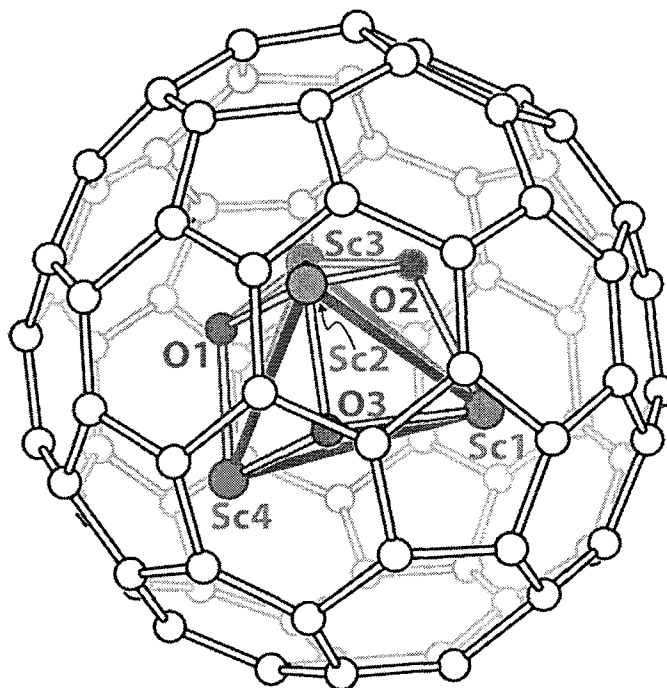
Figure 47. Crystal Structure of $Sc_4O_3@C_{80}$[34]
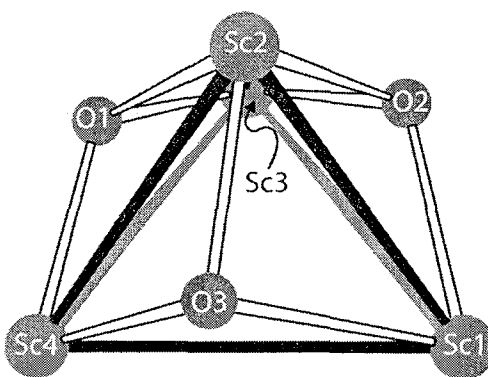
Figure 48. Endohedral cluster of the $Sc_4O_3@C_{80}$ molecule[34]

The synthesis of OMFs has only been possible by the use of the CAPTEAR method. Since most researchers have believed that reducing atmospheres were required for fullerene synthesis, these molecules have only just began to take notice in the scientific community. Therefore, researchers will soon be able to determine their structural and physical properties, which will be valuable to science and technology.

CHAPTER VII

DESIGN, FABRICATION, AND EVALUATION OF A NEW ELECTRIC-ARC

REACTOR

Limitations of Traditional Electric-Arc Reactors

The electric arc method, as previously stated, is one of the most popular and

efficient methods for generating fullerenes. Our lab utilizes this method for all fullerene

studies.[44] The schematic for our reactor is shown below in Figure 49.
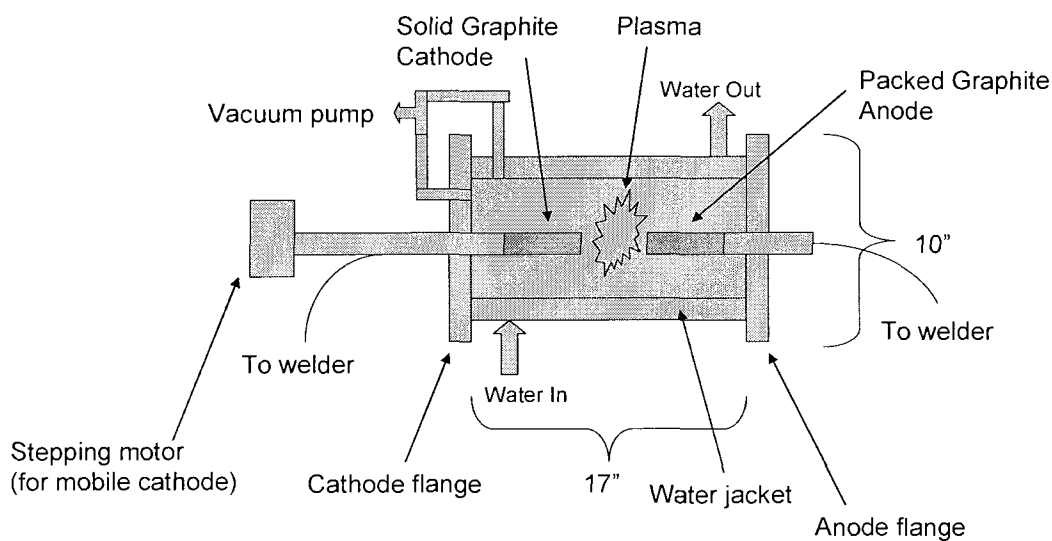
Figure 49. KH-Type reactor used at USM[15]

This reactor was assembled and available for use in June 2006. Since then, this

reactor has undergone several modifications to accommodate sample demands. This

includes two new stepping motors (more power and efficiency), water jackets added to

the cathode and anode flange (to reduce overheating of the flanges), larger diameter

electrode cables to reduce overheating and increase the maximum electrical current

capabilities, as well as designing new maintenance protocols to maintain the optimum

working condition of the reactor. However, several drawbacks remained, and these flaws

required designing a new reactor.

Thus far, the modifications described in the above paragraph have allowed the

scale up from 0.5 inch (~1.3 cm) to 1.0 inch diameter (~2.5 cm) graphite rods. However,

on average, the scale up from 0.5 inch to 1 inch diameter requires a minimum of double

the current (i.e. 120 amps for 0.5 inch and 240 amps for 1 inch diameter). The current is

adjusted to maintain reasonable experimental times (i.e. 1-2hr) and to ensure vaporization

of the graphite and packing materials. This large increase in power results in a generation

of extra heat from the plasma and electrodes. Since the surface area is unchanged the

water coolant is at a constant flow rate, the extra power increases the internal plasma

temperature as well as the reactor components. Table 10 shows the external flange

temperatures for given currents at 45 minutes after beginning an experiment. Each

temperature was taken manually using a common mercury thermometer attached to the

flange.

Table 10. External flange temperatures of the traditional reactor for different electrical currents[119]

Current	120 A	160A	220 A	260A
External Flange Temperature at 45 min	115°C	130°C	189°C	205°C

The data in Table 10 (previous to the addition of water jackets to the flanges)

shows a continual increase in the external flange temperature as the current increases.

Thus, scaling up to 220 or more amps for long periods of time (i.e. >1 month) causes

warping of the flanges from heat damage and the electrode components. Realizing the

upper limitations of the reactor involved damaging and replacing expensive mechanical parts. Hence, the previously mentioned modifications were implemented to maintain this scalability. Despite best efforts to increase the functionality of the reactor, the modifications only increased the time intervals between replacing heat damaged components. The water jacketed flanges have allowed for the temperatures from Table 10 to maintain close to that of room temperature, but the electrode upgrades have only made it possible to allow for a continuous burn time at approximately 280 amps as the upper limit. However, when highly dense packing materials (copper, 8.96 g/cm^3; cobalt, 8.90 g/cm^3; and other free metals) and thicker graphite shells (i.e. > 0.3 cm) are used to obtain high extract yields and reasonable experimental times, these experiments required much more electrical current than 280 amps. Figure 50 shows some examples of current requirements for different packing material recipes and as well as different graphite thickness to maintain desired experimental times. An estimation based on the data below shows that the current required to maintain experimental times depends on quality and quantity of packing materials and the thickness of the shell. To maintain the desired experimental times, the equation that fits most circumstances is shown in equation 7.1, where I is current, E_{spm} is the vaporization energy required to vaporize the shell and packing material and "x" is an undetermined proportionality constant in units of(amps/kJ). More data is needed to determine the value of "x."

$$(I = x(E_{spm})) \text{ equation } 7.1$$

0.3 cm graphite thickness

220 A	240 A	250 A
100 % Sc$_2$O$_3$	50 % Cu 50 %Sc$_2$O$_3$	67 % Cu 33 %Sc$_2$O$_3$
100 % Sc$_2$O$_3$	50 % Cu 50 %Sc$_2$O$_3$	67 % Cu 33 %Sc$_2$O$_3$
240 A	280 A	>280 A

0.8 cm graphite thickness
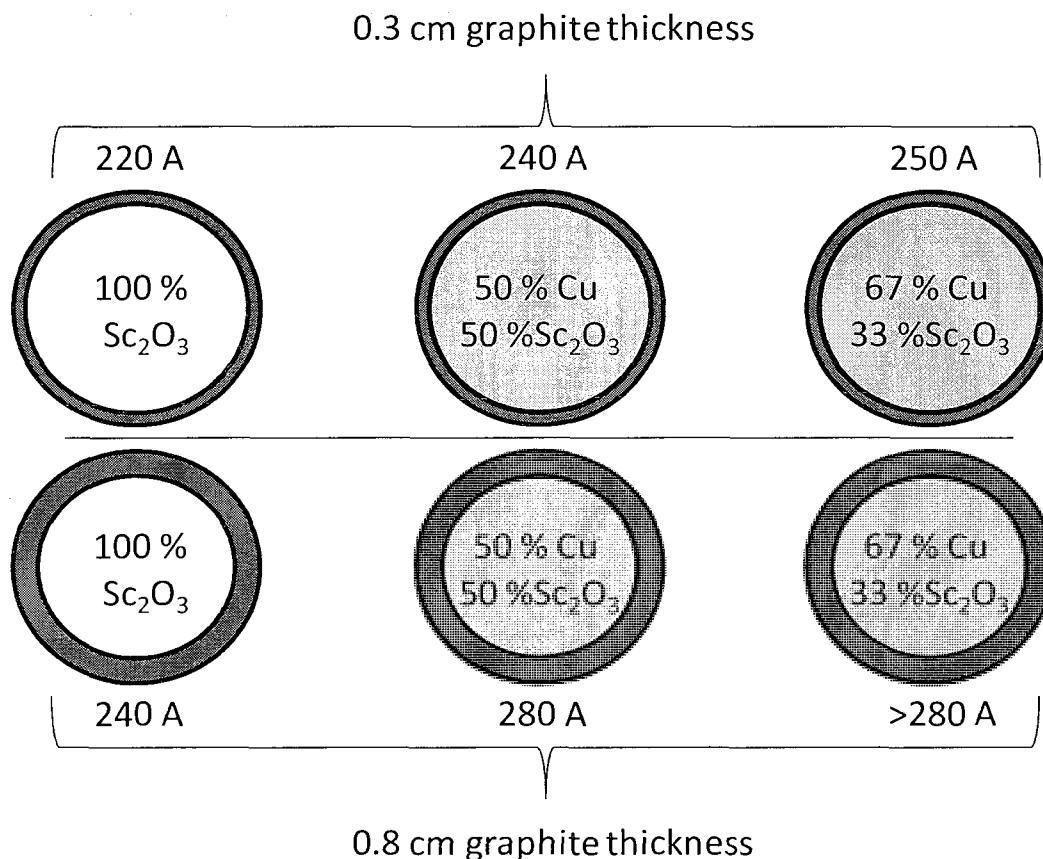
Figure 50. Approximate currents used to obtain experimental times between 50-60 minutes[119]

The purpose of changing the graphite thickness is to find the optimum thickness

for product distribution and extract yield prior to attempting an additive study. In general,

the thickness of the graphite shell is directly proportional to the fullerene extract yield,[119]

but this depends on the packing material quality. Some volatile packing materials yield

better results with smaller shell sizes, although full studies with adequate statistical data

have not been evaluated in our lab at this time due to limited reactor capabilities to obtain

more than three shell thickness sizes. This evidence suggests a need for a newly designed

reactor that is capable of using higher currents and better coolant capabilities.

Another less important flaw (for scientific purposes) in the traditional design is

the ergonomic features. However, user friendly features on many technological

improvements have allowed for better productivity and less experimental error. Thus, ergonomic improvements described in the following section allow for the user to maintain the reactor parameters more precisely and with a less probability of error during the experiment as well as the sample collection process.

The traditional reactor design includes two unfavorable features that are generally noticeable only to the reactor technician after several experiments. The first design flaw is the stepping motor that is used to move the solid graphite rod through the reactor chamber as the packed graphite rod is consumed to maintain the gap voltage. The plasma of the reactor is considered to be somewhat chaotic in the sense that reactor parameters are difficult to control. The voltage readings vary by approximately 5-7 volts due to the movement of the plasma (rotationally between rods) and the non-uniform vaporization rate of the graphite rods. The average voltage is close to the desired voltage but this involves constant in-and-out movement of the motorized arm. Figure 51 shows an example of this overall movement throughout the experiment.
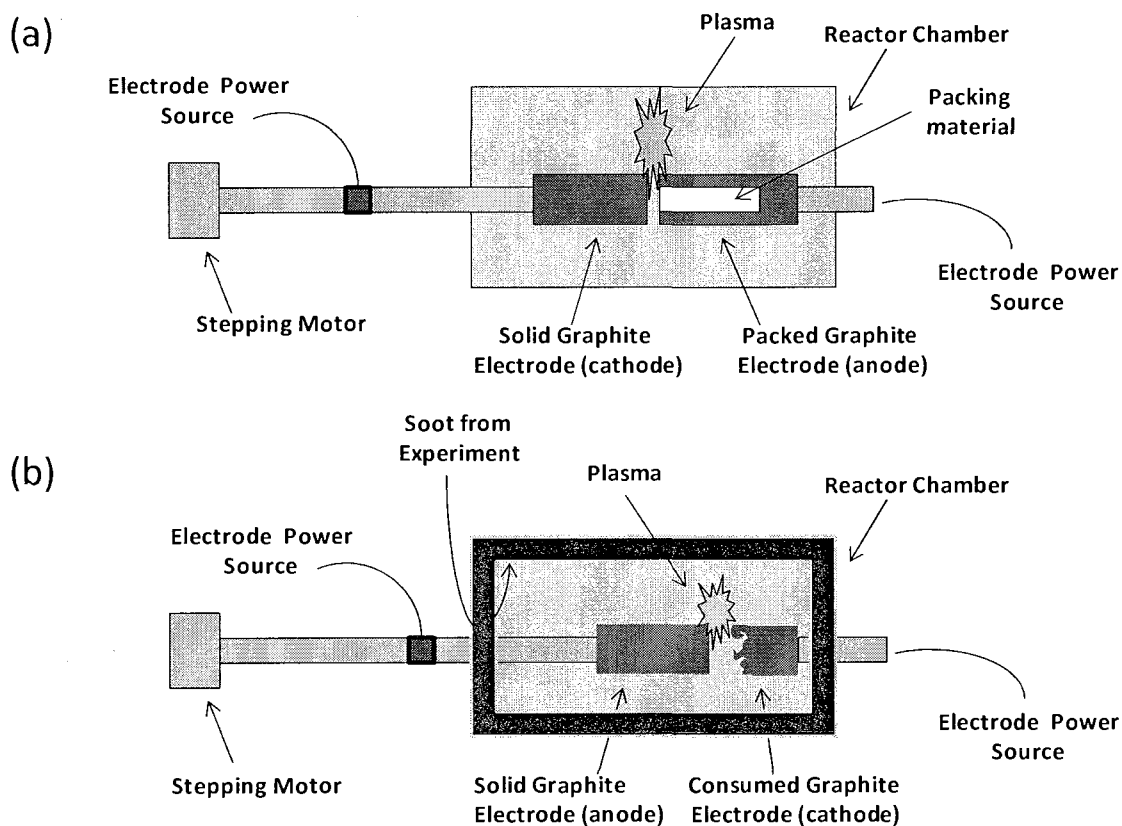
Figure 51. Reactor schemes (a) at the beginning of an experiment and (b) after several minutes of experimental burn time[119]

In Figure 51, the packed portion of the rod has been consumed into soot on the walls of the chamber, and has somewhat of a jagged shape. Although the task at hand ultimately gets accomplished, the motorized arm component could be responsible for some error when considering the mechanical limitations of the variation in gap voltage during the experiments. Another flawed component relates to both the stepping motor and the overheating issues discussed earlier. The electrode arm connected to the stepping motor was previously cooled with small water jackets inside the steel arm. Despite the coolant, the arm produced large amounts of heat (>200°C) at the higher currents.[119] This heat caused the metal of the mechanical arm to expand when in use and contract after

being cooled. Not only did this cause warping over 2 to 3 months of use, but also put more strain on the motor as the heat expanded the tubular steel. The strain caused the motor to wear out faster and slowing of the solid rod linear movement and its ability to maintain a constant gap voltage (i.e. the linear movement of the solid cathode would be halted for 30 seconds to 1 minute time periods while the plasma consumed the anode, which caused a larger gap between the rods and thus a larger voltage). These time lapses caused undesired voltage variations ($\pm$ 5 to 7 volts) and uneven surface vaporization and resulted in the jagged edges of the cathode (Figure 51 (b)). Thus, electrode coolant and mechanical motor improvements was one other focus in our new reactor design.

As mentioned above, there are two ergonomic flaws in the traditional reactor design. The stepping motor has speed issues as well as the electrode heating problem. The second ergonomic feature is the sample collection. After the experiment is complete and sufficient time has elapsed to cool the steel components, the soot must be collected by removing the right side flange (refer again to Figure 49) and sweeping the soot from the inside of the reactor into a sample collection vessel with a large funnel. A diagram of this collection method is shown in Figure 52.
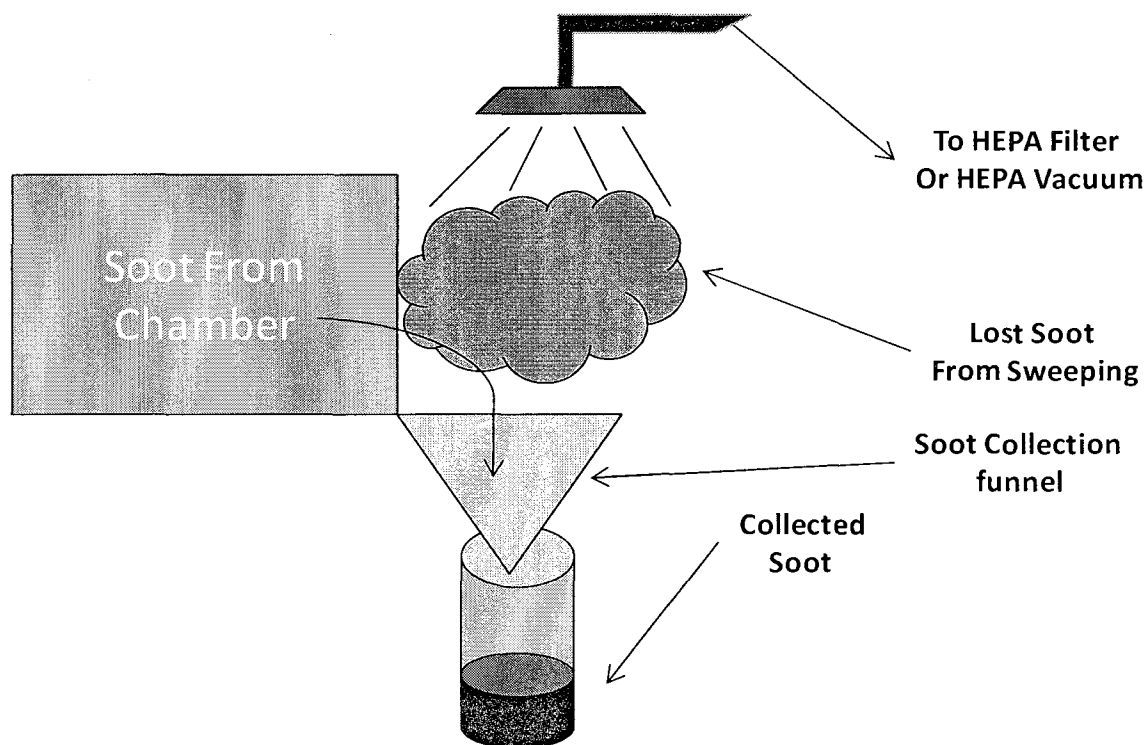
Figure 52. Diagram of soot collection method[119]

The "lost soot" refers to the soot sample amount that is lost from the inefficiency of this method. This collected amount is only estimated since it is not reasonably possible to obtain the actual mass that dissipates. However, the soot particles generally have a very low density and easily float through the air and attach to the HEPA filters in the lab. This amount is perhaps negligible but may represent several grams after sweeping the chamber 5-10 times. This is evident by the amount of waste disposal when replacing the lab filters. The last drawback with this chamber design is the light source from the lab's ceiling does not provide adequate visualization of the chamber to identify when all particulates have been removed. Therefore, an external light source has to be used every time the chamber is removed of soot.

With all factors considered, there were some flaws that allowed for a scale up of the rod diameter size from 0.5 inch to 1 inch, but with limitations in the electrical

components from overheating as well as the ergonomic limitations that could contribute to systematic error. Therefore, these limitations inspired a newly designed reactor that would overcome these issues and produce larger quantities a better statistical sample representation.

<div align="center">Advantages of a Newly Designed Electric-Arc Reactor</div>

The implementation of a new design has been a necessary tool to enable our lab to obtain better representative analytical samples as well as allowing the scale up process to be of little consequence to the reactor machinery. For example, larger samples sizes allow for better statistically favorable samples, durability allows for less down time for maintenance, and the ergonomic improvements allow for less error due to sample loss and better accuracy (such as the mechanical arm speed that maintains more precise gap voltage averages).

The first improvement with this new design involved a scale – up of the mobile, motor driven arm. The traditional electrode arm was 1.3cm (0.5 inches) in diameter, which limited coolant flow through the electrode. The electrodes, being directly exposed to the electrical current flow external to the reactor chamber and internally exposed to the plasma arc, have shown the most propensities to absorb heat. Thus, in order to scale up the electrical current, the first idea for the electrodes was to increase the diameter of the steel tubes to allow for larger amounts of coolant flow. In collaboration with a machinist (Jim Bridges, USM), the decision was made to increase its diameter from 1.25 cm (0.5 in)to 5.0 cm (2 inches). With this diameter, the coolant flow covers a much larger surface area and the increase in coolant volume enables the heat to be dissipated more efficiently. Another addition to the electrode was a coolant upgrade. The coolant used previously was

water. However, this new reactor design utilizes ethylene glycol as a coolant that is recycled through an industrial chiller. This enables our experiments to use chilled fluid (<0°C), rather than room temperature tap water (~22°C) as a coolant through the electrodes. An example of this set up is shown in Figure 53.
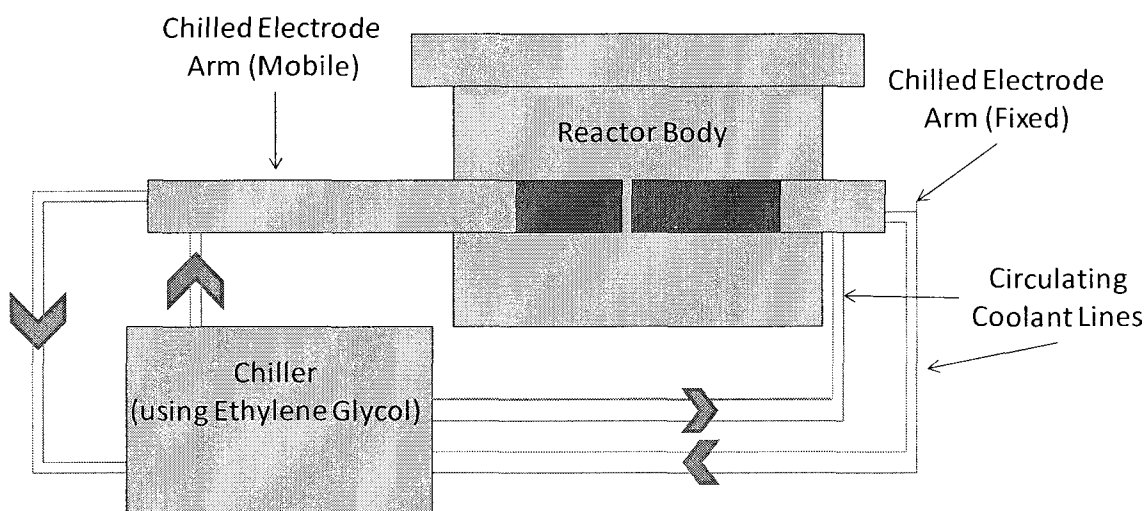
Figure 53. Scheme of electrode chiller addition to the new reactor[119]

The chiller in the above figure not only increases the capacity for heat (i.e. the ability to utilize more electrical current and the heat generated as an electrical byproduct), but also allows our lab to recycle the fluid, which reduces water waste and ultimately the production costs. The traditional design used water that was sent to drain rather than being reused. Therefore, this new design enables better cooling capabilities while offering more production efficiency.

The next component that required modification is the reactor chamber and flanges. The traditional design lacked the coolant capacity needed for scale up past 280 amps. This was due to the chamber volume (21.9 L) being unable to dissipate heat over a

large surface area as well as the lack of water jackets on the side flanges that were easily

warped by excess heat. The new reactor design is shown in Figure 54 and Figure 55.
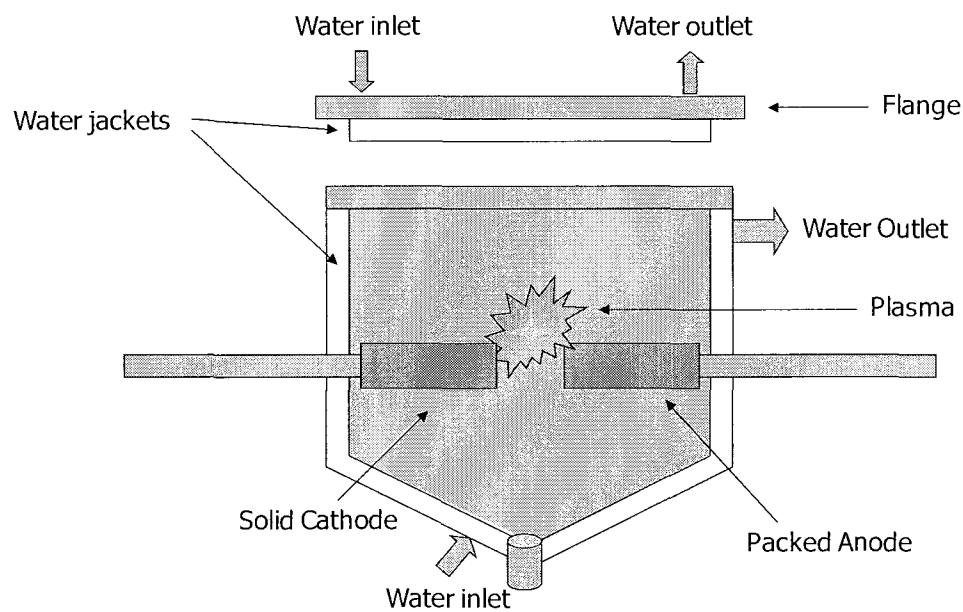
Figure 54. Slice diagram of the new reactor chamber with electrodes[136]
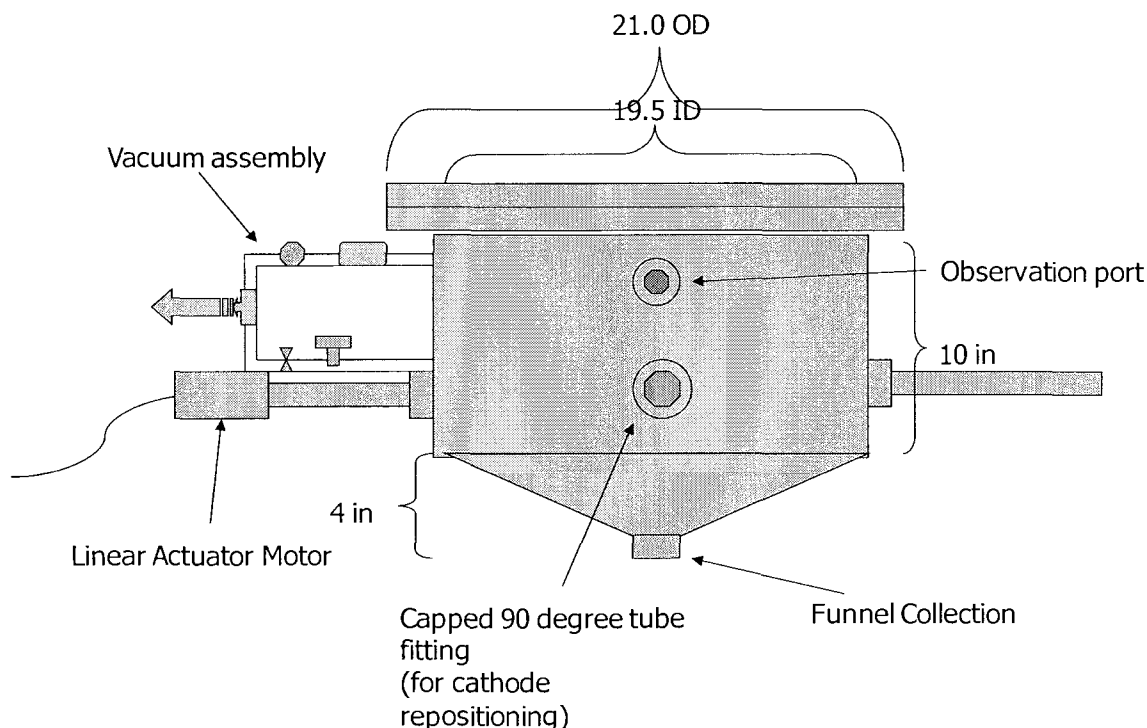
Figure 55. Scheme of new reactor design with dimension measurements (frontal view)[136]

The new reactor has several advantages over the traditional design. First, the chamber volume is much bigger (53 L) as compared to the traditional reactor (22L). Since the volume of the new design is ~2 times the volume of the old design, we also doubled the water jacket thickness (from 1.25 cm to 3 cm). However, the electrodes of the old design were responsible for the most heating problems so we increased the diameter by a factor of 6 (from 1.25 cm to 7.5 cm). Thus, the equations for these scale-up features are shown below in equations 7.2, 7.3, and 7.4. V_{tc} is the volume of the traditional reactor chamber, V_{nc} is the volume of the new chamber; T_{twj} is the thickness of the traditional water jackets, T_{nwj} is the new water jacket thickness, d_{te} is the diameter of the traditional electrode tubes, and d_{ne} is the diameter of the new electrode tubes.

$$(2V_{tc} = V_{nc})\ \text{equation 7.2}$$

$$(2T_{twj} = T_{nwj}) \text{ equation 7.3}$$

$$(4d_{te} = d_{ne}) \text{ equation 7.4}$$

This allows for a better heat distribution and also give the plasma between 6" and 8" (15 -20 cm) of clearance around the electrodes. Another advantage is having the entire chamber surrounded by water jackets. There is only one flange, which lessens the possibility of unwanted air leaks. This flange also will have a water jacket and is therefore less likely to warp. Also important is that the electrodes are now attached through the chamber and thus through a water jacket, which will be able to handle the heat produced by high current.

The ergonomic features discussed in the previous section have also been addressed in this new chamber design. The funnel shaped sample recover port allows the user to sweep in a downward motion rather than sideways. The sample recovery port has an air sealed cap to maintain atmospheric gas control during the burn, but is easily removed and replaced by the sample collection vessel during the recovery process. Therefore, less sample is lost because the downward sweeping motion is assisted by gravity and the funnel shaped chamber directly collects sample rather than the indirect method of the traditional reactor (which uses an external funnel). The other ergonomic improvement is the linear actuator motor. This new motor is more powerful and adjusted with a faster linear in-and-out rate (i.e. the mobile arm's linear movement is faster and able to maintain the desired gap between the graphite electrodes). Therefore, the gap voltage maintains the desired settings with little or no variance. The old motor varied between 5-7 volts of the desired potential but the new motor only varies approximately 1-2 volts.

The gas delivery system for the new reactor is more efficient as well. The traditional reactor has a gas port around the anode that ensures that the gas enters the chamber and not directly into the plasma. This new system involves a tube with a pinhole that can direct gas or vapor additives directly into the plasma. Since the tube is connected though the inside of the mobile cathode tube, its relative position to the plasma remains constant. This tube is also threaded, and thus interchangeable. This allows different gas fittings for positioning, splitting, and maintenance.

The last new feature includes three access ports through the top of the flange (Figure 56) for probe analysis and additive introduction. These ports are able to accommodate a temperature probe for plasma temperature and electron density measurements, a fiber optic probe for emission spectroscopy, and addition of plasma additives. Thus far, the temperature probe has been the only component used. This is a standard thermocouple temperature probe that is connected to a digital temperature gauge purchased from Fisher.
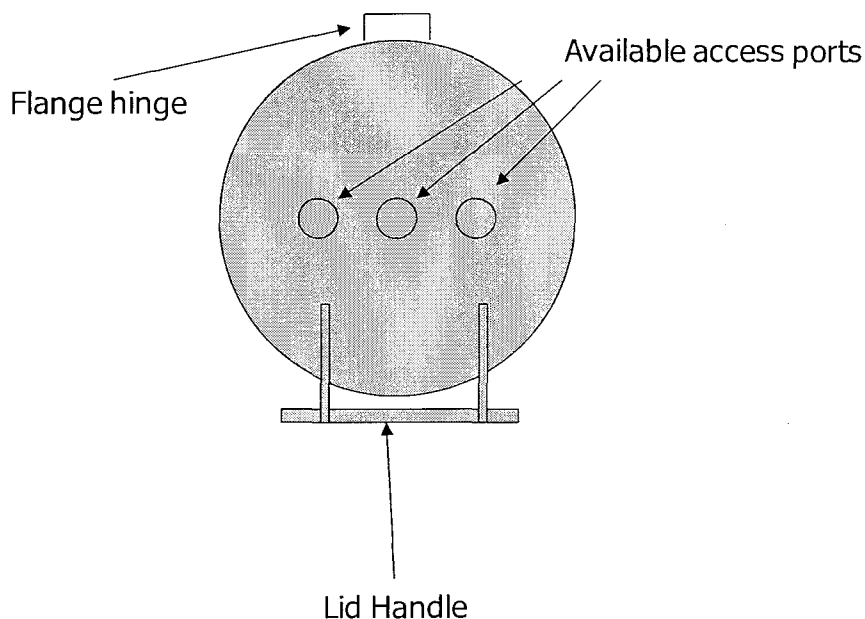
Figure 56. Top view of the new reactor lid with plasma accessory points[136]

The dimensions of this new reactor design are more compact than the traditional

reactor and could, therefore, fit within a traditional fume hood. Soot loss is diminished by

the funnel collection feature that allows the soot to be swept to the bottom of the chamber

and out of a tube with a threaded, vacuum-sealed cap. Commercialization of our new

reactor is not a focus.

Evaluation and of a New Electric-Arc Reactor

This reactor fabrication was complete in the summer of 2007. Since then, several

types of MNFs have been synthesized, as well as OMFs and MNAFs. Parameters have

been established (e.g. current, voltage, pressure) and additives have been tested for

product distribution and yield (i.e. Copper and copper (II) nitrate). Our reactors are now

noted as the α-reactor (for the traditional reactor) and β-reactor (for the newly designed

reactor). Figure 57 is an HPLC of a 100% Sc_2O_3 experiment on the β-reactor. This

chromatogram is similar to what is expected from the α-reactor under the same

conditions. Thus, the β-reactor is capable of producing similar arrays of fullerene products.
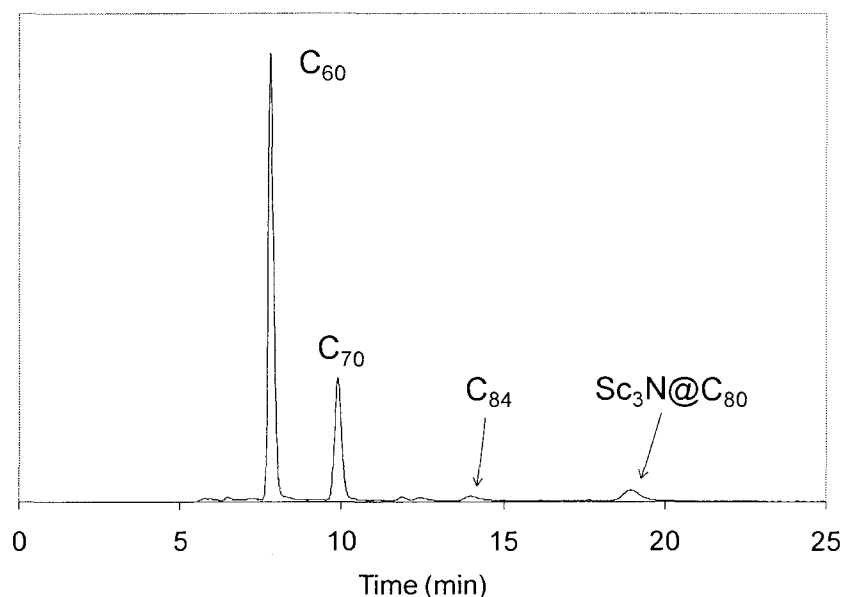
Figure 57. HPLC of a scandium based fullerene extract: 100% Sc_2O_3, no additives, 1 torr/min air; HPLC: 50μl, 0.5 mL/min, PYE, 360 nm[79]

Using $Cu(NO_3)_2$ as an additive, the β-reactor suggests that the CAPTEAR method is independent of different reactors. The following chromatogram in Figure 58 shows $Er_3N@C_{80}$ in high purity using the CAPTEAR method. This experiment required 260 amps of current, which is unfavorable to the electrical capacity of the α-reactor. However, this experiment indicated no external heating problems that would otherwise be a common feature of the α-reactor.
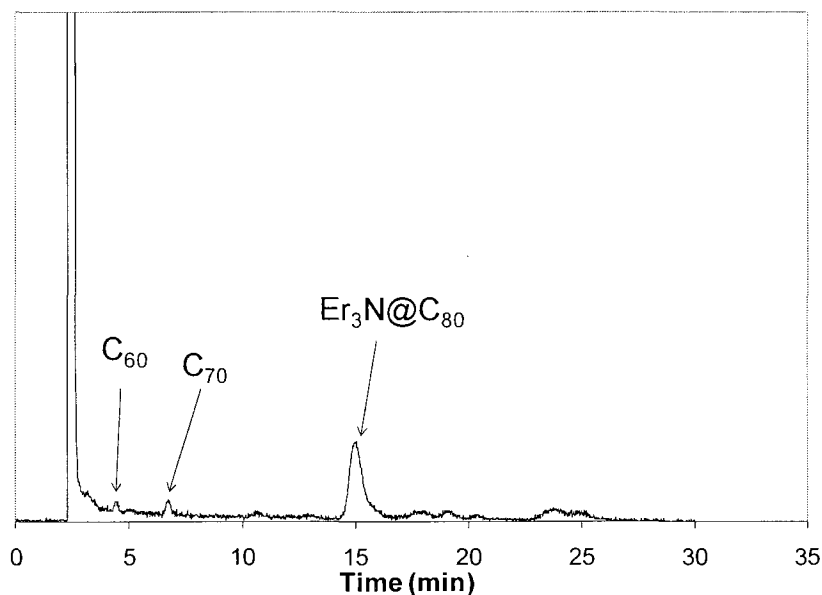
Figure 58. HPLC of an erbium based fullerene extract: 90% Er_2O_3, 10% $Cu(NO_3)_2$, 6 torr/min air; HPLC: 50μl, 1.0 mL/min, PYE, 360 nm[79]

The chromatogram above suggests than the β-reactor is cable of synthesizing rare earth MNFs using the CAPRTEAR method to obtain high purity extracts without the heating problems associated with the α-reactor. The large peak at ~3 minutes is toluene, the mobile phase.

Mixed metal MNFs were synthesized on the β-reactor as well. In general, the LaSc extract generally favors the Sc-MNF over the LaSc-MNF. The chromatogram in Figure 59 suggests that $La_2Sc@C_{80}$ is the dominant MNF.
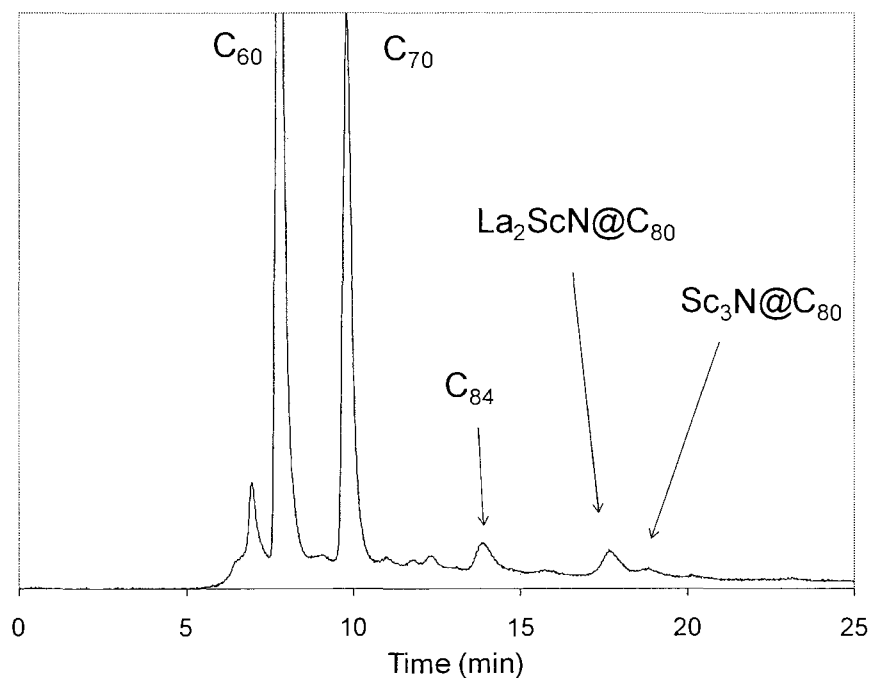
Figure 59. HPLC of a lanthanum/scandium based fullerene extract: 65% La_2O_3, 25% Sc_2O_3, 10% $Cu(NO_3)_2$ 1 torr/min air; HPLC: 50μl, 0.5 mL/min, PYE, 360 nm[79]

This experiment utilized the CAPTEAR method, which is likely to be responsible for the shift to the mixed metal MNF. However, this chromatogram is yet another example of the versatility of the β-reactor.

We conclude that the new reactor design is capable of synthesizing a wide range of fullerene products with and without the CAPTEAR method. Thus, the new features did not result in a loss of efficient or effective production.

The heating problems that occurred with the α-reactor have not occurred with the β-reactor. Therefore, our design has been successful in eliminating scale up limitations. Thus far, the β-reactor has used currents as high as 420 amps without mechanical malfunction! Flange temperature measurements are shown below in Table 11.

Table 11. External flange temperatures of the Beta-reactor for different electrical currents[119]

Current	120 A	160A	220 A	300A	360A	400A
External Flange Temperature at 45 min	28°C	29°C	32°C	58°C	70°C	112°C

As shown in the table, external heat is no longer a factor over a large array of currents. This suggests that the β-reactor is much more durable than the α-reactor and should therefore require less maintenance and/or modification. Many experiments have been performed using thicker carbon shells (i.e. up to 0.95 cm) with high percentages of copper metal (>67%), while still maintaining the optimal experimental times (50-60 min). Recall that Figure 50 suggests that these parameters are unattainable using the α-reactor. This requires current ranges above 300 amps, but the data in Table 11 shows that the β-reactor is capable of using this electrical current range without consequence to the mechanical integrity.

Scaling-up of yield was also a primary goal of the β-reactor design. As demonstrated, the new features allow for a higher electrical current capacity. The typical carbon shell thickness used is 0.95 cm. This allows extract yields to be much higher than what the α-reactor would allow. To date, yields as high as ~700 mg of extract for one experiment have been achieved using the 0.95 cm carbon shell with 100% Sc_2O_3 (380 amps).[137] The α-reactor, which was only capable of using up to 0.8 cm shell thickness, could only produce ~250 mg using the same recipe (240 amps). The 0.3 cm shell thickness was capable of ~180 mg at a safer and lower current of 220 amps.

In conclusion, our new reactor (β-reactor) is sufficient for use with much higher currents and a larger array of parameters (i.e. shell thickness and/or additives that require

high currents). It has been used to produce several types of MNFs. The OMFs and

MNAFs from Chapter VI utilized the new reactor to produce most of the extracts

containing these molecules. The ergonomic design reduces the oppotunities for user error

and experimental variables (i.e. deviations in potentials and less chance of unwanted air

leaks). This reactor is more cost effective due to its ability to maintain mechanical

function with fewer maintenance requirements. Therefore, this reactor was needed to

accomplish the original scale-up goals our lab has sought.

CHAPTER VIII

GREEN CHEMISTRY AND RECYCLING OF WASTE NANO SOOT

Introduction

In recent years, green chemistry has become an important topic within the scientific community. As natural resources are being consumed at accelerated rates (i.e. petroleum, other fossil fuels, etc.),[138] the need for green processes has increased tremendously. It is becoming more evident that these resources will eventually be depleted and therefore, much scientific research has shifted to both research and development of new green methods for reducing waste, or changing methods to generate less waste.[139] Our efforts to contribute to green chemistry have yielded very promising results and continue to aid our research as well as others.

Our research requires large quantities (e.g. 20 -100 g) of metal oxide powder for each experiment. Most of these metal oxides are very expensive (e.g. scandium oxide ~$3000/kg)[46]. Even when relatively large quantities of MNFs are produced, the fullerene product only accounts for 5-10% of the stoichiometrically predicted product based on starting reagents. The waste soot produced accounts for a majority of waste and metal products not related to fullerenes. Thus, there has been a great need for the recovery of metal oxides.

In the development of our recycling method, some assumptions have been made. The first assumption is that the soot waste produced is composed of the same elements as the starting material and no contamination has occurred. For instance, if Sc_2O_3 is packed in a graphite rod, then the soot should only be comprised of scandium, oxygen, and carbon. The second assumption is that there is a cheap and efficient way to selectively

separate the metal oxides from the carbonaceous portion of the soot. Results indicate that both assumptions are valid.

In this study, we report a new approach to recycling soot waste.[31, 32] Thermal oxidation was used to remove carbon, in the form of carbon dioxide, leaving only Sc_2O_3. X-ray photoelectron spectroscopy (XPS) is a technique used to determine the elemental content of a substance in addition to the relative ratios of the elements. Thus, XPS was employed by Wynne et al[140] to analyze soot as well as the thermally oxidized products. Our results indicate that thermal oxidation is sufficient for recycling waste nano soot into a second generation metal oxide.

<div align="center">Experimental</div>

Sc-based Soot

Each rod (1 in diameter, 6 in length) was core drilled (4 in depth and ¾ in diameter) and packed with either virgin Sc_2O_3 powder (Stanford Materials, CA) or 2nd generation Sc-based materials from our recycling of waste soot. The packed rods were cured for 8 hr under He flow at 1050°C in a tube furnace. The reactor parameters were as follows: 300 torr reactor chamber pressure, dynamic flow, 630 mL/min He (buffer gas), 220A, 38V, and 6 torr/min air (e.g. nitrogen source). Reactor soot was extracted with ~1L *o*-xylene (which was recycled and reused via reduced pressure, using a rotovap) to obtain dry fullerene extract, which was washed with diethyl ether and/or acetone. Fullerene extract was analyzed via HPLC (Specifications in CHAPTER IV) to determine product distribution, and peaks were integrated for quantitative data.

The effect of thermal oxidation was monitored by thermogravimetric analysis (TGA), using a TA Q500 instrument to investigate any changes in mass as a function of

temperature and time under a controlled atmosphere. Waste soot was homogenized using a mortar and pestle, and 5-10 mg samples were placed on platinum pans under air at temperature ranges from 22-1000°C. A heat-and-hold method was employed, with a temperature rate increase of 28°C/min to temperatures of 600, 750, and 1000°C, and held for 60 minutes. Waste soot, thermally oxidized samples, and virgin Sc_2O_3 samples were characterized with XPS for elemental content and relative ratios. Recovery of bulk quantities of recycled Sc-material was performed using a standard laboratory muffle furnace. The effluent was vented to the hood with no evidence of significant particulates in the effluent trap or on the interior of the furnace.

Er-based Soot

All conditions for the scandium experiments were repeated for erbium experiments with the following reactor parameter exceptions: 5/8 inch rod core diameter, 330A, 40V, and an ambient air flow resulting in a pressure change of 0.5 torr/min (nitrogen source).

Results and Discussion

Thermal Oxidation Process for Recycling Sc2O3

Figure 60 shows an overview of the recycling process for scandium based soot. This process has proven to be very efficient in recycling nano waste soot as well as mitigating the cost of production.
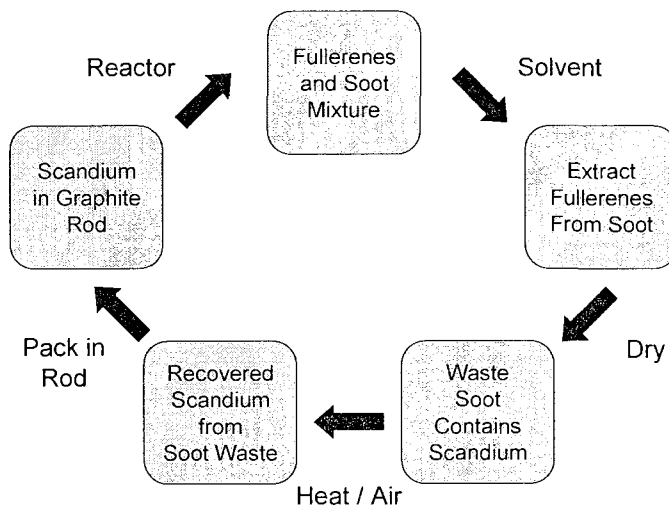
Figure 60. Overview of Waste Soot Recycling Process[31, 32]

Thus far, our method has been useful in bulk samples with up to 100 g of waste soot placed in the furnace. Most scandium experiments only produce 30-40 g of soot and only produce ~70-150 mg of scandium fullerene extract. Therefore, this process should be able to undergo an unlimited number of cycles (i.e. 3rd, 4th, 5th generation).

Our recycling method was first monitored by TGA (Figure 61 on the next page) to determine the proper temperature and time profiles.
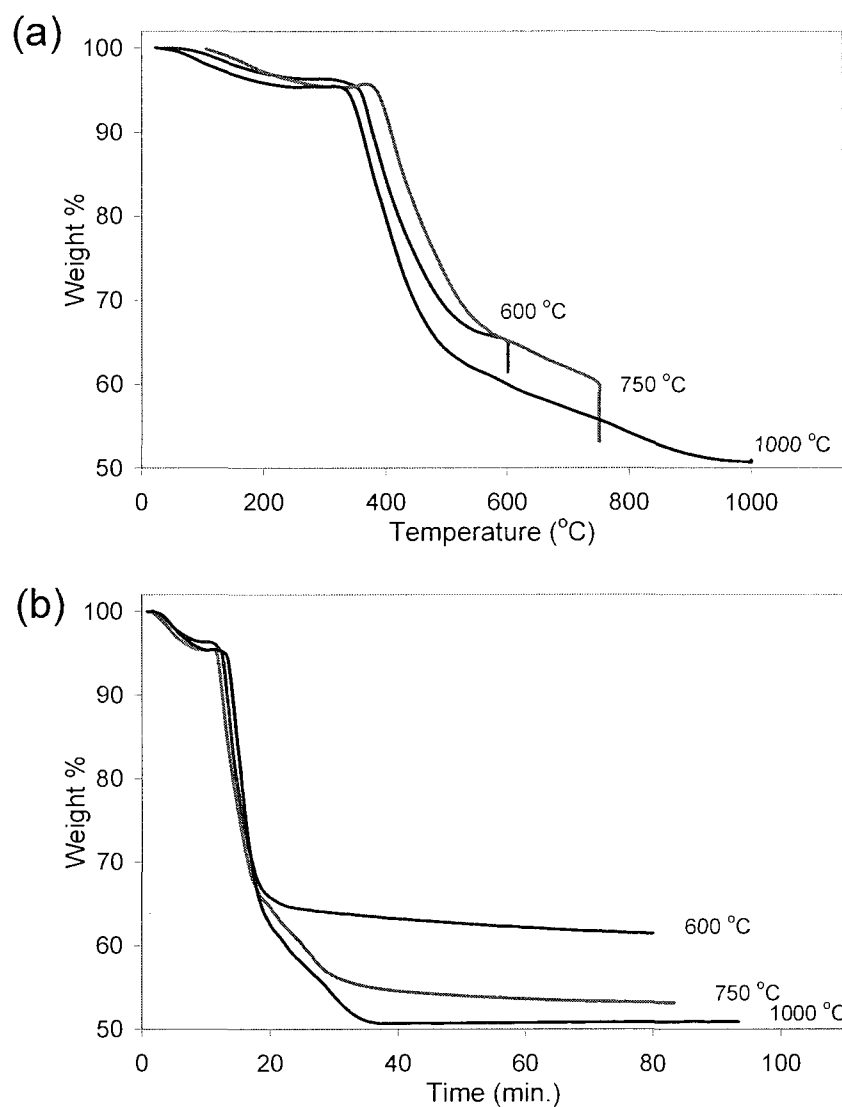
Figure 61. TGA of soot samples (a) as a function of temperature and (b) as a function of time[31, 32]

Figure 61(a) shows the weight change as a function of temperature. The graph

shows that there is still significant weight loss when the temperatures were held at 600

and 750°C. However, at 1000 °C, there is no significant weight loss. This indicates that

neither 600 nor 750 °C is sufficient for complete removal of contaminant materials. Since

there is no weight loss at 1000°C, this indicates that this is an appropriate temperature for

the recycling process to undergo completion. Figure 61(b) shows the times at which each

temperature has vaporized the maximum amount of material. This point on the graph is

signified by an inflection followed by a relatively flat line (no weight change). The

maximum weight loss occurs at 1000 °C (~48% weight loss) and is reached between 30

and 40 minutes. As stated earlier, the sample size for TGA was typically 5 to 10 mg.

Therefore, the bulk experiments (using a muffle furnace), in which sample size was 50

grams, utilized oxidization and heat for much longer periods of time (13 h) to ensure

complete removal of contaminant materials. This resulted in 37% mass loss (31.5 g) at

600°C and leveled off at a 44% mass loss (28 g) at 750 and 1000°C. Figure 62 shows the

elemental composition (via XPS) of soot before and after thermal oxidation as well as the

percent composition of standard Sc_2O_3 stock from a commercial source.
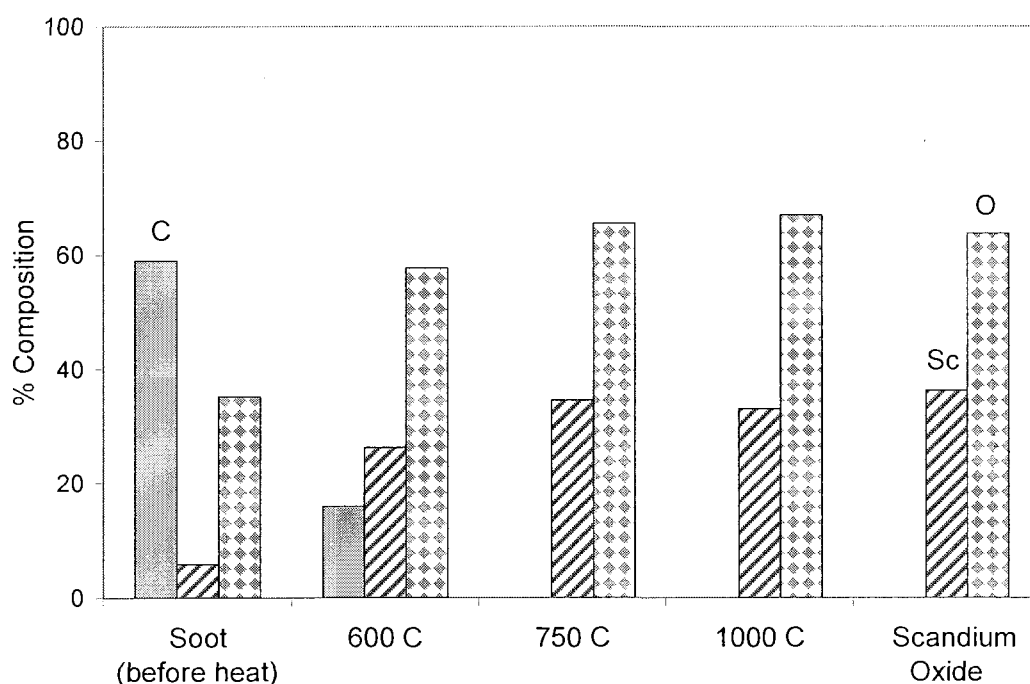
Figure 62. X-Ray Photoelectron Spectroscopy (XPS) of soot samples after 13h of thermal oxidation at various temperatures[31, 32]

This graph indicates that carbon dominates the raw soot material, leaving only a small portion to consist of scandium and oxygen. As thermal oxidation is applied, the composition loses carbon and the remaining ratios of scandium to oxygen resemble that of the commercial source of Sc_2O_3. This is consistent with our hypothesis that carbon in waste soot is oxidized to form carbon dioxide and can readily exit the reaction mixture. This is achieved at 750°C in our study. The carbon is completely consumed and the remaining ratio of scandium to oxygen is almost identical to the commercial material. This may seem to be inconsistent with the TGA data, which indicates a significant percent weight loss at 750°C. However, the consistency of the powder after thermal oxidation at 750°C is mostly white with only traces of metallic particulates (Figure 63).

| Untreated Soot | 600 °C | 750 °C | 1000 °C |
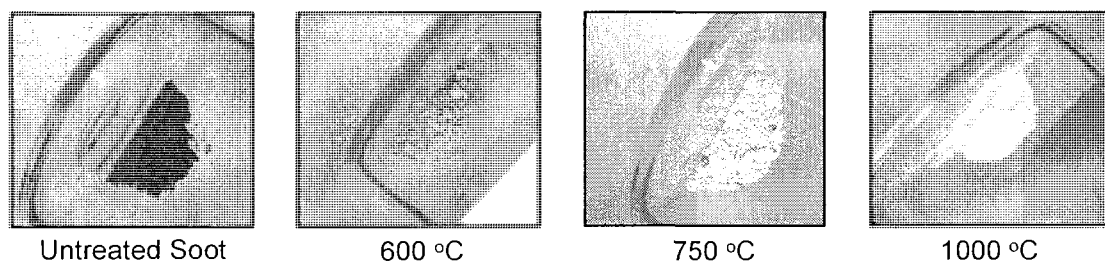
Figure 63. Photographs of various stages of thermal oxidation for Sc-based soot[31, 32]

This metallic residue is believed to be scandium $[Sc]^0$. Although, XPS data shows the scandium and oxygen to be at a similar ratio as the commercial Sc_2O_3, it is only an average of the sample and may not reflect the inclusion of these traces of metallic particulates. Therefore, the TGA responds to the density changes that the denser scandium metal undergoes to produce the less dense scandium oxide. Thus, the TGA, XPS, and powder consistency all agree that 1000°C thermal oxidation temperature is the optimum temperature to recycle the soot into reusable Sc_2O_3. However, 750°C is a sufficient compromise between practical and efficiency (i.e. 750°C displays purity close

to that of virgin Sc_2O_3 (Figure 62), with the exception of traces of scandium metal

particles). Therefore, we choose 750 °C to perform or recycling technique for subsequent

use to increase the lifetime of our oven and decrease cool down times to obtain our

recycled material.

After recycling several batches of waste soot, the new 2nd generation Sc_2O_3 was

packed into cored graphite rods (identical to the 1st generation rods) and placed in the arc

reactor under identical conditions to determine if the recycling material could reproduce

the fullerene product distribution obtained from the use of virgin Sc_2O_3 material. The

extracts from both experiments were analyzed via HPLC to determine product

distribution. Their chromatograms are shown in Figure 64 and have a comparable product

distribution. This also suggests that the recycled material is very similar in chemical

composition to the virgin material.
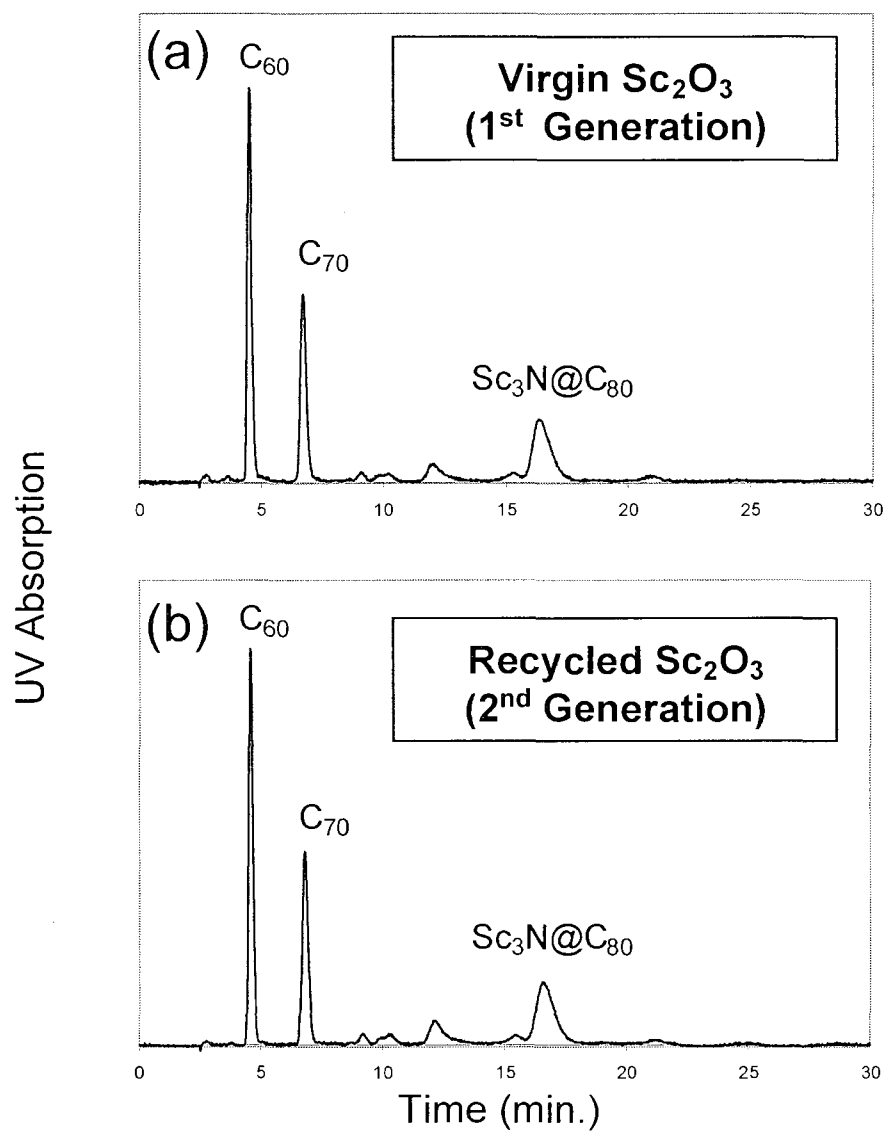
Figure 64. HPLC of fullerene extract using (a) virgin Sc$_2$O$_3$ and (b) recycled Sc$_2$O$_3$[31, 32]
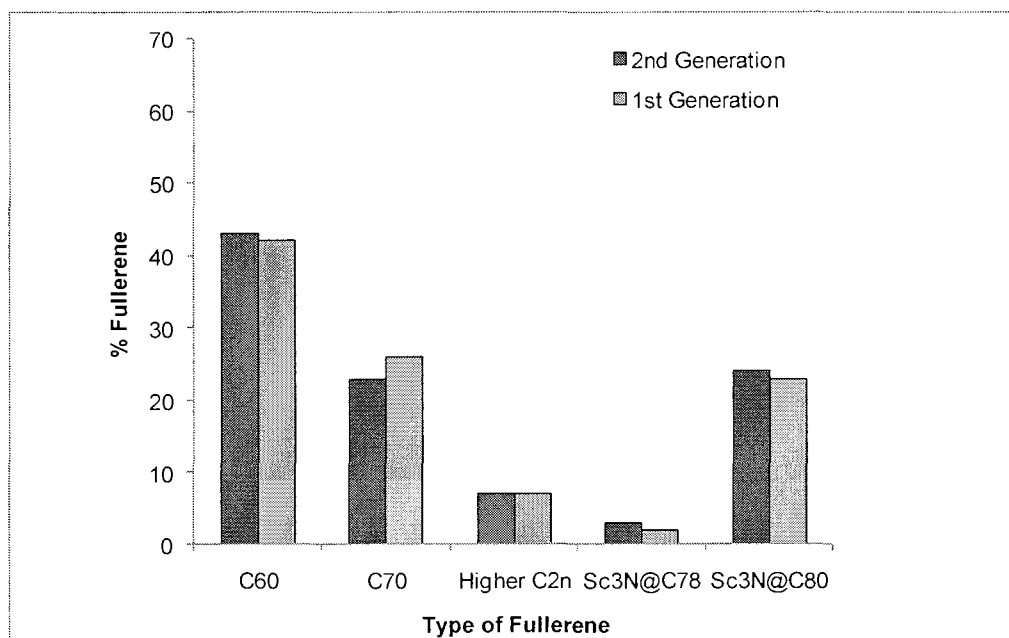
Figure 65. Bar graph of fullerene type versus % fullerene for virgin Sc$_2$O$_3$ (right) and recycled Sc$_2$O$_3$ (left)[119]

Using standard integration software, a bar graph was generated (Figure 65) for closer comparison of the fullerene peaks. As shown in the graph, the differences in fullerene percentages are small (<5%) and could be the result of determinate error in integration, extraction, or HPLC detector elution. Nevertheless, the product distribution was similar for all five types of fullerenes shown in the graph.

A graph was also generated from peak integration and mass quantities of the extracts (Figure 66).
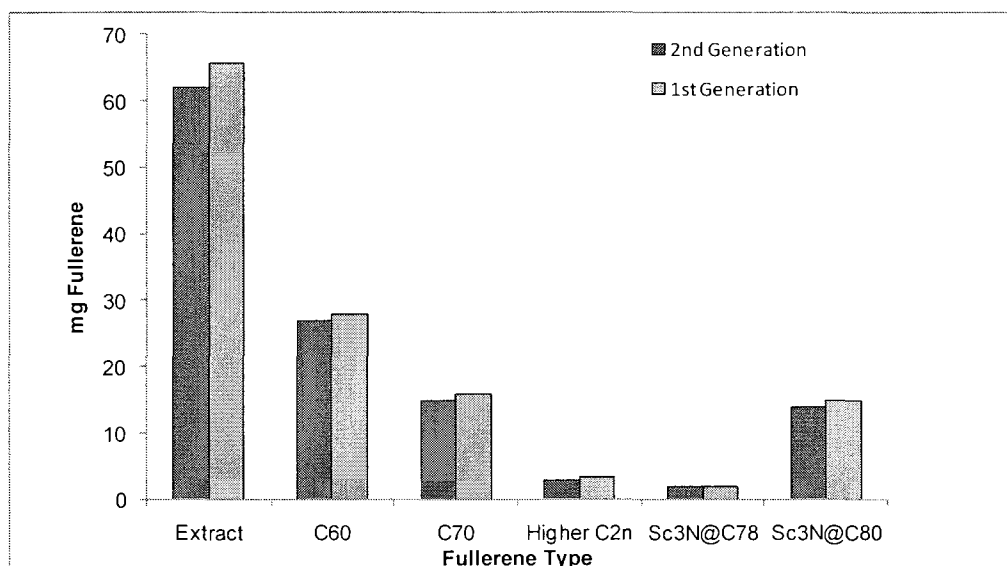
Figure 66. Bar graph of fullerene type versus mg fullerene for virgin Sc_2O_3 (right) and recycled Sc_2O_3 (left)[119]

This data shows the difference in mass for each type of fullerene produced from the 1st and 2nd generation metal oxide material. The agreement between the masses is within 5% and thus within reasonable error. The 1st generation masses are slightly higher than the 2nd generation (for C_{60}, C_{70}, higher C_{2n}, and $Sc_3N@C_{80}$). This could simply be the result of a systemic error.

Thermal Oxidation Process for Recycling Er_2O_3

The process for recycling Sc_2O_3 was repeated using Er_2O_3 to determine whether this method would be successful with a rare earth metal.[119] In the Sc_2O_3 study, 30-50 g samples of the soot were heated to 750°C for 13 hr to obtain the desired results. However, Er_2O_3 has a higher density than Sc_2O_3 (8.64 and 3.86g/mL respectively). Thus, the sample for this study was larger (100 g) than the Sc-soot samples in order to roughly a similar same surface area. At this time, the XPS data has not been generated for this study. However, the HPLC chromatograms from the virgin 1st generation and recycled

2nd generation (Figure 67 below) show a strong resemblance, much like the Sc-based recycled material (Figure 64). The chromatograms suggest that the recycled Er-based material is similar to the virgin material. If there were contaminants present in the recycled material, the product distribution should change as established in Chapter 5: Effect of Additives to the Plasma. Therefore, XPS results of the recycled Er-based soot should contain only erbium and oxygen in a ratio close to that of the virgin Er_2O_3. To further analyze the HPLC data, a bar graph was generated (Figure 68) using HPLC peak integration of different fullerene types, and the results are discussed below.
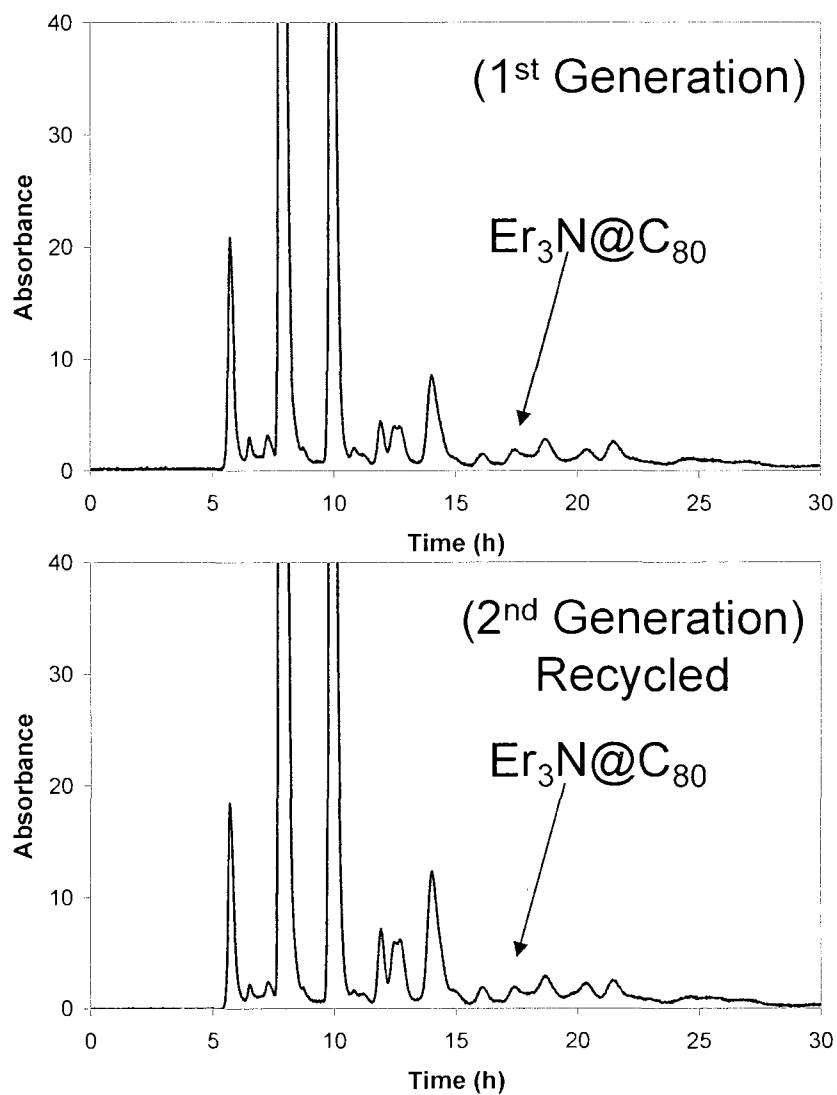
Figure 67. Chromatograms of fullerene extract from virgin Er_2O_3 (top) and recycled Er-based soot

(bottom)[79]
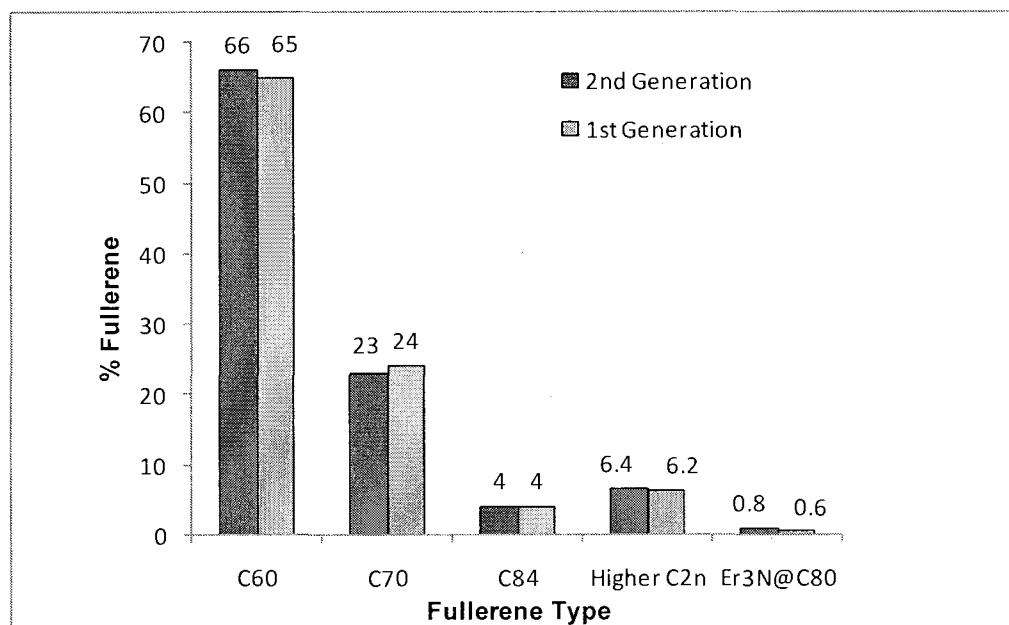
Figure 68. Bar graph of fullerene type versus % fullerene of virgin Er_2O_3 (right) and recycled Er-based soot (left)[119]

As shown in the graph, the types of fullerenes have similar percentages. As determined via their respective HPLC peak areas. The agreement in percentages of fullerene type suggests little error, and this graph is consistent with related experimental data (e.g. Sc_2O_3 data).

Following HPLC analysis, the Er fullerene extract of both samples was dried using reduced pressure and heat to obtain mg masses of the fullerenes. After washing the solid material with diethyl ether and/or acetone, the mass of $Er_3N@C_{80}$ for the 1st generation extract yield was 2.7 mg and the 2nd generation extract yielded was 2.8 mg.[119] Therefore, our recovery process is useful for our rare earth erbium MNF as well as the scandium MNFsyntheses.

Our final conclusion is that this method is both efficient and reliable for recycling Er-soot for use in subsequent experiments. Also, this method should also be successful for recycling other metal oxides (i.e. Lu_2O_3, Gd_2O_3, etc.).

CHAPTER IX

CONCLUSIONS

Effect of Plasma Additives

We have obtained fullerene data showing the effect of additives to the electric arc plasma. Copper metal has proven to be an excellent additive to increase the yield of fullerene extract as well as the overall yield of MNFs. The CAPTEAR method of introducing a highly reactive and oxidizing atmosphere to the plasma represents a new paradigm for metallofullerene synthesis and has enabled our lab to produce very selective extracts that are particularly favorable to an array of metallofullerenes (e.g. MNFs, MNAFs, and OMFs). Our CAPTEAR method shows selectivity of MNFs extracts up to 99% MNF purity without significant loss of yield. Our improved MNF selectivity has mitigated, and in some cases, obviated the need for HPLC as a separation tool. Previous literature had shown that reactive gases could greatly improve the quality of the extract (i.e. 95-99% MNF), but resulted in a significant loss in yield. CAPTEAR provides the best of both quality and quantity. Through the CAPTEAR approach, our reactor R&D has led to the discovery of OMFs (e.g. $Sc_4O_2@C_{80}$, $Sc_4O_3@C_{80}$) and MNAFs (e.g. $Sc_3N@C_{79}N$, $La_3N@C_{79}N$).

New Endohedral Fullerenes

During the course of our MNF research, two other classes of fullerenes have been discovered, Metallic Nitride Azafullerenes (MNAFs) and Oxo-Metallic Fullerenes (OMFs). Although the yield of these new compounds is generally lower than MNFs, current research to selectively synthesize these new classes of endohedral fullerenes show promise. With our results and sample distribution to the scientific community, other

researchers have become enabled to investigate these molecules as well. These scientists will be able to study physical and chemical properties and determine applications for these molecules. Another significant achievement is our synthesis of metallofullerenes with encapsulated oxygen. Our ability to entrap oxygen represents the first demonstration of encapsulating a Group VIA element. Scientists had believed that five encapsulated atoms (due to spatial constraints) would represent the maximum number of atoms inside the C_{80} cage. However, the $Sc_4O_3@C_{80}$ crystal structure has proven that at least seven atoms can fit inside the C_{80} cage.

Design, Fabrication, and Evaluation of a New Electric-Arc Reactor

Experience with our traditional Krätschmer-Huffman (KH-Type) reactor has shown flaws in traditional designs, as described in CHAPTER VII. These drawbacks represent our motivation for a novel design and subsequent fabrication of our new KH-Type reactor with advantages over the old design. New features include ergonomic and scale-up advantages to improve user ability and to increase productivity in fullerene synthesis. Success of the new reactor is demonstrated via our ability to produce several MNFs, MNAFs, and OMFs. Thus, our new design has proven to be advantageous to our research.

Green Chemistry and Recycling of Nano Soot Waste

Despite advancements in fullerene yield and MNF selectivity, the overall fullerene yield represents only a fraction of the stoichiometrically predicted amounts based on amounts of starting materials. With most of the metal content remaining in waste soot, the need for recycling soot waste represents a significant achievement. Our lab has successfully achieved the recovery of expensive metal oxide starting material

(e.g. Sc_2O_3) for reuse in subsequent experiments. As described in CHAPTER VIII, the thermal recovery method for Sc_2O_3 and Er_2O_3 represents an inexpensive, facile, and effective method for recycling the spent soot waste. Our recovered metal oxides produce similar fullerene extract compositions relative to extract obtained from virgin metal oxides.

Summary

Our lab first explored the hypothesis that plasma additives would increase the yield and selectivity of MNFs. Other fullerene researchers used an inert (e.g. He and N_2) or reducing (e.g. He and NH_3) atmosphere for fullerene production, but we were fortunate to serendipitously pave a new road with our reactor R&D. In this dissertation, we have developed effective fullerene syntheses in oxidizing atmospheres. This oxidizing atmosphere, obtained via our CAPTEAR approach, resulted in our discovery of two new classes of endohedral fullerenes (oxometallic fullerenes and metallic nitride azafullerenes). Evidence suggests that these new fullerenes actually require such an oxidizing atmosphere for their synthesis. During these studies, we not only demonstrated that scaling up a reactor was possible, but also necessary to improve the production of these highly selective fullerene extracts as well as our new endohedral fullerenes. Implementation of the new reactor design accomplished this goal of increased productivity, but also increased the cost of materials and quantity of waste material. Our recycling method for waste soot resolved issues of cost effectiveness and waste reduction. This dissertation exemplifies the significance of reactor R&D and demonstrates the tremendous impact of our research to the field of fullerene science.[15, 18, 31-34]

REFERENCES

1.   Stevenson, S.; Rice, G.; Glass, T.; Harich, K.; Cromer, F.; Jordan, M. R.; Craft, J.; Hadju, E.; Bible, R.; Olmstead, M. M.; Maitra, K.; Fisher, A. J.; Balch, A. L.; Dorn, H. C., Small-bandgap endohedral metallofullerenes in high yield and purity. *Nature* **1999,** 401, (6748), 55-57.

2.   Dorn, H. C.; S., S.; Craft, J.; Cromer, F.; Duchamp, J. C.; Rice, G.; Glass, T.; Harich, K.; Fowler, P. W.; Heine, T.; Hadju, E.; Bible, R.; Olmstead, M. H.; Maitra, K.; Fisher, A. J.; Balch, A. L., The encapsulation of trimetallic nitride clusters in fullerene cages. *Proceedings - AIP Conference, Electronic Properties of Novel Materials - Molecular Nanostructures, ed. Kuzmany H. et al* **2000,** 544, 135-141.

3.   Olmstead, M. M.; de Bettencourt-Dias, A.; Duchamp, J. C.; Stevenson, S.; Dorn, H. C.; Balch, A. L., Isolation and crystallographic characterization of $ErSc_2N@C-80$: an endohedral fullerene which crystallizes with remarkable internal order. *Journal of the American Chemical Society* **2000,** 122, (49), 12220-12226.

4.   Olmstead, M. H.; de Bettencourt-Dias, A.; Duchamp, J. C.; Stevenson, S.; Marciu, D.; Dorn, H. C.; Balch, A. L., Isolation and structural characterization of the endohedral fullerene $Sc_3N@C78$. *Angewandte Chemie-International Edition* **2001,** 40, (7), 1223-1225.

5.   Campanera, J. M.; Bo, C.; Olmstead, M. M.; Balch, A. L.; Poblet, J. M., Bonding within the endohedral fullerenes $Sc_3N@C-78$ and $Sc_3N@C-80$ as determined by density functional calculations and reexamination of the crystal structure of {$Sc_3N@C-78$}center dot $Co(OEP)$center dot $1.5(C6H6)$center dot $0.3(CHCl3)$. *Journal of Physical Chemistry A* **2002,** 106, (51), 12356-12364.

6.   Iezzi, E. B.; Duchamp, J. C.; Harich, K.; Glass, T. E.; Lee, H. M.; Olmstead, M. M.; Balch, A. L.; Dorn, H. C., A symmetric derivative of the trimetallic nitride endohedral metallofullerene, $Sc_3N@C-80$. *Journal of the American Chemical Society* **2002,** 124, (4), 524-525.

7.   Stevenson, S.; Lee, H. M.; Olmstead, M. M.; Kozikowski, C.; Stevenson, P.; Balch, A. L., Preparation and crystallographic characterization of a new endohedral, $Lu_3N@C-80$ center dot 5(o-xylene), and comparison with $Sc_3N@C(80)5$ center dot(o-xylene). *Chemistry--A European Journal* **2002,** 8, (19), 4528-4535.

8.   Olmstead, M. M.; Lee, H. M.; Duchamp, J. C.; Stevenson, S.; Marciu, D.; Dorn, H. C.; Balch, A. L., $Sc_3N@C-68$: Folded pentalene coordination in an endohedral fullerene that does not obey the isolated pentagon rule. *Angewandte Chemie-International Edition* **2003,** 42, (8), 900-+.

9.   Cai, T.; Xu, L. S.; Anderson, M. R.; Ge, Z. X.; Zuo, T. M.; Wang, X. L.; Olmstead, M. M.; Balch, A. L.; Gibson, H. W.; Dorn, H. C., Structure and enhanced reactivity rates of the D-5h $Sc_3N@C-80$ and $Lu_3N@$ C-80 metallofullerene isomers: The importance of the pyracylene motif. *Journal of the American Chemical Society* **2006,** 128, (26), 8581-8589.

10.   Stevenson, S.; Chancellor, C. J.; Lee, H. M.; Olmstead, M. M.; Balch, A. L., Internal and external factors in the structural organization in cocrystals of the mixed-metal endohedrals ($GdSc_2N@I-h-C-80$, $Gd_2ScN@I-h-C-80$, and $TbSc_2N@I-h-C-80$) and nickel(II) octaethylporphyrin. *Inorganic Chemistry* **2008,** 47, (5), 1420-1427.

11.   Zuo, T. M.; Olmstead, M. M.; Beavers, C. M.; Balch, A. L.; Wang, G. B.; Yee, G. T.; Shu, C. Y.; Xu, L. S.; Elliott, B.; Echegoyen, L.; Duchamp, J. C.; Dorn, H. C., Preparation and structural characterization of the I-h and the D-5h isomers of the endohedral fullerenes Tm3N@C-80: Icosahedral C-80 cage encapsulation of a trimetallic nitride magnetic cluster with three uncoupled Tm3+ ions. *Inorganic Chemistry* **2008**, 47, (12), 5234-5244.

12.   Stevenson, S.; Harich, K.; Yu, H.; Stephen, R. R.; Heaps, D.; Coumbe, C.; Phillips, J. P., Nonchromatographic "stir and filter approach" (SAFA) for isolating Sc3N@C-80 metallofullerenes. *Journal of the American Chemical Society* **2006**, 128, (27), 8829-8835.

13.   Shustova, N. B.; Popov, A. A.; Mackey, M. A.; Coumbe, C. E.; Phillips, J. P.; Stevenson, S.; Strauss, S. H.; Boltalina, O. V., Radical trifluoromethylation of Sc3N@C-80. *Journal of the American Chemical Society* **2007**, 129, (38), 11676-+.

14.   Stevenson, S.; Mackey, M. A.; Coumbe, C. E.; Phillips, J. P.; Elliott, B.; Echegoyen, L., Rapid removal of D-5h isomer using the "stir and filter approach" and isolation of large quantities of isomerically pure Sc3N@C-80 metallic nitride fullerenes. *Journal of the American Chemical Society* **2007**, 129, (19), 6072-6073.

15.   Stevenson, S.; Mackey, M. A.; Thompson, M. C.; Coumbe, H. L.; Madasu, P. K.; Coumbe, C. E.; Phillips, J. P., Effect of copper metal on the yield of Sc3N@C-80 metallofullerenes. *Chemical Communications* **2007**, (41), 4263-4265.

16.   Stevenson, S.; Thompson, M. C.; Coumbe, H. L.; Mackey, M. A.; Coumbe, C. E.; Phillips, J. P., Chemically adjusting plasma temperature, energy, and reactivity (CAPTEAR) method using NOx and combustion for selective synthesis of Sc3N@C80 metallic nitride fullerenes. *Journal of the American Chemical Society* **2007**, 129, (51), 16257-16262.

17.   McCluskey, D. M.; Smith, T. N.; Madasu, P. K.; Coumbe, C. E.; Mackey, M. A.; Fulmer, P. A.; Wynne, J. H.; Stevenson, S.; Phillips, J. P., Evidence for Singlet-Oxygen Generation and Biocidal Activity in Photoresponsive Metallic Nitride Fullerene-Polymer Adhesive Films. *Acs Applied Materials & Interfaces* **2009**, 1, (4), 882-887.

18.   Stevenson, S.; Coumbe, C. E.; Mackey, M. A.; Confait, B. S.; Phillips, J. P. D., H.C; Ling, Y.; Zhang, Y, Preferential Encapsulation and Stability of La3N Cluster in 80 Atom Cages: Experimental Synthesis and Computational Investigation of La3N@C79N. *Journal of American Chemical Society* **2009**, Under Review.

19.   Gan, L. H.; Yuan, R., Influence of cluster size on the structures and stability of trimetallic nitride fullerenes M3N@C-80. *Chemphyschem* **2006**, 7, (6), 1306-1310.

20.   Echegoyen, L.; Chancellor, C. J.; Cardona, C. M.; Elliott, B.; Rivera, J.; Olmstead, M. M.; Balch, A. L., X-Ray crystallographic and EPR spectroscopic characterization of a pyrrolidine adduct of Y3N@C-80. *Chemical Communications* **2006**, (25), 2653-2655.

21.   Winkler, K.; Balch, A. L.; Kutner, W., Electrochemically formed fullerene-based polymeric films. *Journal of Solid State Electrochemistry* **2006**, 10, (10), 761-784.

22.   Lukoyanova, O.; Cardona, C. M.; Rivera, J.; Lugo-Morales, L. Z.; Chancellor, C. J.; Olmstead, M. M.; Rodriguez-Fortea, A.; Poblet, J. M.; Balch, A. L.; Echegoyen, L., "Open rather than closed" malonate methano-fullerene derivatives. The formation of methanofulleroid adducts of Y3N@C-80. *Journal of the American Chemical Society* **2007**, 129, (34), 10423-10430.

23.   Mercado, B. Q.; Beavers, C. M.; Olmstead, M. M.; Chaur, M. N.; Walker, K.; Holloway, B. C.; Echegoyen, L.; Balch, A. L., Is the isolated pentagon rule merely a suggestion for endohedral fullerenes? The structure of a second egg-shaped endohedral fullerene-Gd3N @ C-s(39663)-C-82. *Journal of the American Chemical Society* **2008,** 130, (25), 7854-+.

24.   Beavers, C. M.; Chaur, M. N.; Olmstead, M. M.; Echegoyen, L.; Balch, A. L., Large Metal Ions in a Relatively Small Fullerene Cage: The Structure of Gd3N@C-2(22010)-C-78 Departs from the Isolated Pentagon Rule. *Journal of the American Chemical Society* **2009,** 131, (32), 11519-11524.

25.   Pinzon, J. R.; Gasca, D. C.; Sankaranarayanan, S. G.; Bottari, G.; Torres, T.; Guldi, D. M.; Echegoyen, L., Photoinduced Charge Transfer and Electrochemical Properties of Triphenylamine I-h-Sc3N@C-80 Donor-Acceptor Conjugates. *Journal of the American Chemical Society* **2009,** 131, (22), 7727-7734.

26.   Pinzon, J. R.; Cardona, C. M.; Herranz, M. A.; Plonska-Brzezinska, M. E.; Palkar, A.; Athans, A. J.; Martin, N.; Rodriguez-Fortea, A.; Poblet, J. M.; Bottari, G.; Torres, T.; Gayathri, S. S.; Guldi, D. M.; Echegoyen, L., Metal Nitride Cluster Fullerene M3N@C-80 (M = Y, Sc) Based Dyads: Synthesis, and Electrochemical, Theoretical and Photophysical Studies. *Chemistry-a European Journal* **2009,** 15, (4), 864-877.

27.   Chaur, M. N.; Valencia, R.; Rodriguez-Fortea, A.; Poblet, J. M.; Echegoyen, L., Trimetallic Nitride Endohedral Fullerenes: Experimental and Theoretical Evidence for the M3N6+@C-2n(6-) model. *Angewandte Chemie-International Edition* **2009,** 48, (8), 1425-1428.

28.   Melin, F.; Chaur, M. N.; Engmann, S.; Elliott, B.; Kumbhar, A.; Athans, A. J.; Echegoyen, L., The large Nd3N@C-2n (40 <= n <= 49) cluster fullerene family: preferential templating of a C-88 cage by a trimetallic nitride cluster. *Angewandte Chemie-International Edition* **2007,** 46, (47), 9032-9035.

29.   Yang, S. F.; Kalbac, M.; Popov, A.; Dunsch, L., Gadolinium-based mixed metal nitride clusterfullerenes GdxSC3-xN@C-80 (x=1, 2). *Chemphyschem* **2006,** 7, (9), 1990-1995.

30.   Krause, M.; Dunsch, L., Gadolinium nitride Gd3N in carbon cages: The influence of cluster size and bond strength. *Angewandte Chemie-International Edition* **2005,** 44, (10), 1557-1560.

31.   Stevenson, S.; Coumbe, C. E.; Thompson, M. C.; Coumbe, H. L.; Phillips, J. P.; Buckley, J. L.; Wynne, J. H., Conversion of nanomaterial waste soot to recycled Sc2O3 feedstock for the synthesis of metallic nitride fullerenes. *Industrial & Engineering Chemistry Research* **2008,** 47, (6), 2096-2099.

32.   Wynne, J. H.; Buckley, J. L.; Coumbe, C. E.; Phillips, J. P.; Stevenson, S., Reducing hazardous material and environmental impact through recycling of scandium nanomaterial waste. *Journal of Environmental Science and Health Part a-Toxic/Hazardous Substances & Environmental Engineering* **2008,** 43, (4), 357-360.

33.   Stevenson, S.; Thompson, M. C.; Coumbe, H. L.; Mackey, M. A.; Coumbe, C. E.; Phillips, J. P., Chemically adjusting plasma temperature, energy, and reactivity (CAPTEAR) method using NOx and combustion for selective synthesis of SC3N@C-80 metallic nitride fullerenes. *Journal of the American Chemical Society* **2007,** 129, (51), 16257-16262.

34.   Mercado, B. Q.; Olmstead, M. M.; Beavers, C. M.; Easterling, M. L.; Stevenson, S.; Mackey, M. A.; Coumbe, C. E.; Phillips, J. D.; Phillips, J. P.; Balch, A. L., A Seven Atom Cluster in a Carbon Cage, the Crystallographically Determined Structure of $Sc_4(\mu-O_3)@I_h-C_{80}$. *Journal of the American Chemical Society* **2009,** Under Review.

35.   Lu, J.; Sabirianov, R. F.; Mei, W. N.; Gao, Y.; Duan, C. G.; Zeng, X. C., Structural and magnetic properties of $Gd3N@C$-80. *Journal of Physical Chemistry B* **2006,** 110, (47), 23637-23640.

36.   Bolskar, R. D.; Alford, J. M.; Benedetto, A. F.; Huesbo, L. O.; Wilson, L. J., Development of $Gd@C$-60 based MRI contrast agents. *Abstracts Of Papers Of The American Chemical Society* **2002,** 223, U660-U661.

37.   Fatouros, P. P.; Corwin, F. D.; Chen, Z. J.; Broaddus, W. C.; Tatum, J. L.; Kettenmann, B.; Ge, Z.; Gibson, H. W.; Russ, J. L.; Leonard, A. P.; Duchamp, J. C.; Dorn, H. C., In vitro and in vivo imaging studies of a new endohedral metallofullerene nanoparticle. *Radiology* **2006,** 240, (3), 756-764.

38.   Iezzi, E. B.; Duchamp, J. C.; Fletcher, K. R.; Glass, T. E.; Dorn, H. C., Lutetium-based trimetallic nitride endohedral metallofullerenes: New contrast agents. *Nano Letters* **2002,** 2, (11), 1187-1190.

39.   McCluskey, D. M.; Smith, T. N.; Madasu, P. K.; Coumbe, C. E.; Mackey, M. A.; Fulmer, P. A.; Wynne, J. H.; Stevenson, S.; Phillips, J. P., Evidence for Singlet Oxygen Generation and Biocidal Activity In Photo-Responsive Metallic Nitride Fullerene-Polymer Adhesive Films. *American Chemical Sociesty: Applied Materials and Interfaces* **2009,** 1, (4), 882-887

40.   Thrash, T. P.; Cagle, D. W.; Alford, J. M.; Wright, K.; Ehrhardt, G. J.; Mirzadeh, S.; Wilson, L. J., Toward fullerene-based radiopharmaceuticals: high-yield neutron activation of endohedral Ho-165 metallofullerenes. *Chemical Physics Letters* **1999,** 308, (3-4), 329-336.

41.   Macfarlane, R. M.; Bethune, D. S.; Stevenson, S.; Dorn, H. C., Fluorescence spectroscopy and emission lifetimes of Er3+ in ErxSc3-xN@C-80 (x=1-3). *Chemical Physics Letters* **2001,** 343, (3-4), 229-234.

42.   Pyrolysis process for making fullerenes. *United States Patent 6083469.*

43.   Chibante, L. P. F., Solar Generation of Fullerenes. *J. Phys. Chem* **1993,** 97, 8696-8700.

44.   Kratschmer, W.; Lamb, L. D.; Fostiropoulos, K.; Huffman, D. R., Solid C-60 - A New Form Of Carbon. *Nature* **1990,** 347, (6291), 354-358.

45.   Millon, É., Laser ablation of carbonaceous materials: a method to produce fullerenes. *C. R. Acad. Sci. Paris* **1992,** t. 315 (Série II), 947-953.

46.   HEFA, Product quote: Scandium Oxide 99.9%. **2009.**

47.   Shustova, N. B.; Kareev, I. E.; Kuvychko, I. V.; Popov, A. A.; Mackey, M. A.; Coumbe, C. E.; Bubnov, V. P.; Lebedkin, S. F.; Chen, Y.; Phillips, J. P.; Stevenson, S.; Strauss, S. H.; Boltalina, O. V., $Sc_3N@(C_{80}-I_h(7))(CF_3)_{14}$ and $Sc_3N@(C_{80}-I_h(7))(CF_3)_{16}$. Endohedral Metallofullerene Derivatives with Exohedral Addends on Four and Eight Triple-Hexagon Junctions. Does the Sc_3N Cluster Control the Addition Pattern or Vice Versa? . *Journal of the American Chemical Society* **2009,** Under Review.

48.   Dunsch, L.; Krause, M.; Noack, J.; Georgi, P., Endohedral nitride cluster fullerenes - Formation and spectroscopic analysis of L3-xMxN@C-2n (0 <= x <= 3; N=39,40). *Journal of Physics and Chemistry of Solids* **2004,** 65, (2-3), 309-315.

49. Kroto, H. W.; Taylor, R.; Walton, D. R. M., The Structure And Reactivity Of C60. *Pure and Applied Chemistry* **1994**, 66, (10-11), 2091-2094.

50. Prinzbach, H.; Weller, A.; Landenberger, P.; Wahl, F.; Worth, J.; Scott, L. T.; Gelmont, M.; Olevano, D.; von Issendorff, B., Gas-phase production and photoelectron spectroscopy of the smallest fullerene, C-20. *Nature* **2000**, 407, (6800), 60-63.

51. Piskoti, C.; Yarger, J.; Zettl, A., C-36, a new carbon solid. *Nature* **1998**, 393, (6687), 771-774.

52. Achiba, Y.; Fowler, P. W.; Mitchell, D.; Zerbetto, F., Structural Predictions for the C116 Molecule. *J. Phys. Chem. A* **1998**, 102, (34), 6835–6841.

53. Kroto, H. W., The Future of Fullerenes. *Nature* **1985**, 318, 162.

54. Yamamoto, K.; Saunders, M.; Khong, A.; Cross, R. J.; Grayson, M.; Gross, M. L.; Benedetto, A. F.; Weisman, R. B., Isolation and spectral properties of Kr@C-60, a stable van der Waals molecule. *Journal of the American Chemical Society* **1999**, 121, (7), 1591-1596.

55. Saunders, M., Stable compounds of helium and neon. He@C60 and Ne@C60. *Science* **1993**, 259, 1428-1430.

56. Vazquez, R., Incorporation of helium, neon, argon, krypton, and xenon into fullerenes using high pressure *Journal of the American Chemical Society* **1994**, 116, (5), 2193-2194.

57. Pietzak, A., A New Family of Carbon Clusters. *Kluwer Academic Publishers* **2002**.

58. Shinohara, H., Endohedral metallofullerenes. *Reports on Progress in Physics* **2000**, 63, (6), 843-892.

59. Connerade, J. P.; Semaoune, R., Relativistic study of the electronic structure and 5d orbital of La confined inside a C-60 fullerene cage. *Journal Of Physics B-Atomic Molecular And Optical Physics* **2000**, 33, (5), 869-880.

60. Liu, D.; Hagelberg, F.; Park, S. S., Charge transfer and electron backdonation in metallofullerenes encapsulating NSc3. *Chemical Physics* **2006**, 330, (3), 380-386.

61. Ogawa, T.; Sugai, T.; Shinohara, H., Isolation and characterization of Er@C-60. *Journal of the American Chemical Society* **2000**, 122, (14), 3538-3539.

62. Wang, C. R.; Kai, T.; Tomiyama, T.; Yoshida, T.; Kobayashi, Y.; Nishibori, E.; Takata, M.; Sakata, M.; Shinohara, H., Materials science - C-66 fullerene encaging a scandium dimer. *Nature* **2000**, 408, (6811), 426-427.

63. Stevenson, S.; Burbank, P.; Harich, K.; Sun, Z.; Dorn, H. C.; van Loosdrecht, P. H. M.; deVries, M. S.; Salem, J. R.; Kiang, C. H.; Johnson, R. D.; Bethune, D. S., La-2@C-72: Metal-mediated stabilization of a carbon cage. *Journal of Physical Chemistry A* **1998**, 102, (17), 2833-2837.

64. Chen, Z.; Fatouros, P. P.; Corwin, F. D.; Broaddus, W. C.; Dorn, H. C., In vitro and in vivo imaging studies of a new gadolinium endohedral metallofullerene MRI contrast agent. *Neuro-Oncology* **2006**, 8, (4), 492-492.

65. Russ, J. L.; Wang, X. L.; Fatouros, P.; Corwin, F.; Tatum, J.; Chen, Z. J.; Broaddus, W. C.; Gibson, H.; Leonard, A. P.; Duchamp, J. C.; Ge, Z. X.; Dorn, H. C., MRI relaxivity studies of trimetallic nitride endohedral metallofullerenes. *Abstracts Of Papers Of The American Chemical Society* **2006**, 231.

66. Shu, C. Y.; Ma, X. Y.; Zhang, J. F.; Corwin, F. D.; Sim, J. H.; Zhang, E. Y.; Dorn, H. C.; Gibson, H. W.; Fatouros, P. P.; Wang, C. R.; Fang, X. H., Conjugation of a

water-soluble gadolinium endohedral fulleride with an antibody as a magnetic resonance imaging contrast agent. *Bioconjugate Chemistry* **2008**, 19, (3), 651-655.

67. Shu, C. Y.; Wang, C. R.; Zhang, J. F.; Gibson, H. W.; Dorn, H. C.; Corwin, F. D.; Fatouros, P. P.; Dennis, T. J. S., Organophosphonate functionalized Gd@C-82 as a magnetic resonance imaging contrast agent. *Chemistry of Materials* **2008**, 20, (6), 2106-2109.

68. Wharton, T.; Wilson, L. J., Toward fullerene-based X-ray contrast agents: design and synthesis of non-ionic, highly-iodinated derivatives of C-60. *Tetrahedron Letters* **2002**, 43, (4), 561-564.

69. Elim, H. I.; Ji, W.; Meng, G. C., Nonlinear optics and optical limiting properties of multifunctional fullerenol/polymer composite. *J. Nonlinear Opt. Phys. Mater.* **2003**, 12, (2), 175-186.

70. Xia, X. R.; Monteiro-Riviere, N. A.; Riviere, J. E., Trace analysis of fullerenes in biological samples by simplified liquid-liquid extraction and high-performance liquid chromatography. *Journal of Chromatography A* **2006**, 1129, (2), 216-222.

71. Krause, M.; Dunsch, L., Isolation and characterisation of two Sc3N@C-80 isomers. *Chemphyschem* **2004**, 5, (9), 1445-1449.

72. Elliott, B.; Yu, L.; Echegoyen, L., A simple isomeric separation of D-5h and I-h Sc3N@C-80 by selective chemical oxidation. *Journal of the American Chemical Society* **2005**, 127, (31), 10885-10888.

73. Cai, T.; Slebodnick, C.; Xu, L.; Harich, K.; Glass, T. E.; Chancellor, C.; Fettinger, J. C.; Olmstead, M. M.; Balch, A. L.; Gibson, H. W.; Dorn, H. C., A pirouette on a metallofullerene sphere: Interconversion of isomers of N-tritylpyrrolidino I-h Sc3N@C-80. *Journal of the American Chemical Society* **2006**, 128, (19), 6486-6492.

74. Fowler, P. W., *An Atlas of Fullerenes*. Oxford Univ. Press: Oxford, 1995.

75. Duchamp, J. C.; Demortier, A.; Fletcher, K. R.; Dorn, D.; Iezzi, E. B.; Glass, T.; Dorn, H. C., An isomer of the endohedral metallofullerene Sc3N@C-80 with D-5h symmetry. *Chemical Physics Letters* **2003**, 375, (5-6), 655-659.

76. Yang, S. F.; Dunsch, L., Expanding the number of stable isomeric structures of the C-80 cage: A new fullerene DY3N@C-80. *Chemistry-A European Journal* **2005**, 12, (2), 413-419.

77. Stevenson, S.; Phillips, J. P.; Reid, J. E.; Olmstead, M. M.; Rath, S. P.; Balch, A. L., Pyramidalization of Gd3N inside a C-80 cage. The synthesis and structure of Gd3N@C-80. *Chemical Communications* **2004**, (24), 2814-2815.

78. Bolskar, R. D.; Benedetto, A. F.; Husebo, L. O.; Price, R. E.; Jackson, E. F.; Wallace, S.; Wilson, L. J.; Alford, J. M., First soluble M@C-60 derivatives provide enhanced access to metallofullerenes and permit in vivo evaluation of Gd@C-60[C(COOH)(2)](10) as a MRI contrast agent. *Journal of the American Chemical Society* **2003**, 125, (18), 5471-5478.

79. Unpublished Results, *Stevenson Lab, University of Southern Mississippi*.

80. Dorn, H. C.; Rice, G.; Burbank, P.; Craft, J.; Sun, Z.; Glass, T.; Harich, K.; Cromer, F.; Jordan, M. R.; Hadju, E.; Bible, R.; Anderson, M.; Stevenson, S., ScxEr3-xN@C-80: A new family of trimetallic nitride clusters encapsulated in icosahedron cages. *Abstracts Of Papers Of The American Chemical Society* **1999**, 218, U726-U726.

81.   Chen, N.; Zhang, E. Y.; Wang, C. R., C-80 encaging four different atoms: The synthesis, isolation, and characterizations of ScYErN@C-80. *Journal of Physical Chemistry B* **2006**, 110, (27), 13322-13325.

82.   Chibante, L. P. F.; Thess, A.; Alford, J. M.; Diener, M. D.; Smalley, R. E., Solar generation of the fullerenes. *Journal of Physical Chemistry* **1993**, 97, (34), 8696-8700.

83.   Dubrovsky, R., Enhanced Approach to Synthesize Carbon Allotropes By Arc Plasma. *Rev. Adv. Mater. Sci.* **2003**, 5, 420-424.

84.   Scott, L. T., A Rational Chemical Synthesis of C_{60} *Science* **2002**, 295, (5559), 1500.

85.   Ajie, H.; Alvarez, M. M.; Anz, S. J.; Beck, R. D.; Diederich, F.; Fostiropoulos, K.; Huffman, D. R.; Kratschmer, W.; Rubin, Y.; Schriver, K. E.; Sensharma, D.; Whetten, R. L., Characterization Of The Soluble All-Carbon Molecules C60 And C70. *Journal of Physical Chemistry* **1990**, 94, (24), 8630-8633.

86.   Bulina, N. V.; Petrakovskaya, E. A.; Marachevsky, A. V.; Lityaeva, I. S.; Osipova, I. V.; Glushchenko, G. A.; Kratschmer, W.; Churilov, G. N., Synthesis and investigation of iron fullerene clusters. *Physics Of The Solid State* **2006**, 48, (5), 1012-1015.

87.   Kratschmer, W.; Dunsch, L., Fullerenes - New on the inside and the outside. *Nachrichten Aus Der Chemie* **2000**, 48, (4), 448-+.

88.   Kratschmer, W.; Fostiropoulos, K.; Huffman, D. R., The infrared and uvltraviolet absorption spectra of laboratory-produced carbon dust: evidence for the presence of the C60 molecule. *Chemical Physics Letters* **1990**, 170, 167-170.

89.   Lebedkin, S.; Ballenweg, S.; Gross, J.; Taylor, R.; Kratschmer, W., Synthesis of C120O: a new dimeric [60]fullerene derivative. *Tetrahedron Letters* **1995**, 36, 4971-4974.

90.   Authors, M., Plasma Physics. *http://en.wikipedia.org/wiki/Plasma_(physics)* **2009**.

91.   Grassie, A. D. C. e. a., Contemporary Physics. *University of Sussex and Nuffield Physics Project* **1965**.

92.   Dubrovsky, R.; Bezmelnitsyn, V.; Sokolov, Y., Reduction of cathode carbon deposit by buffer gas outflow. *Carbon* **2005**, 43, (4), 796-802.

93.   Smyaglikov, I. P.; Shimanovich, V. D.; Zolotovsky, A. I., Characterizations of the carbon arc at fullerene synthesis. *High Temperature Material Processes* **2004**, 8, (2), 221-231.

94.   Smyaglikov, I. P.; Shimanovich, V. D.; Zolotovsky, A. I., Characterizations of the carbon arc for fullerene synthesis. *High Temperature Material Processes* **2005**, 9, (3), 453-462.

95.   Churilov, G. N.; Fedorov, A. S.; Novikov, P. V., Influence of electron concentration and temperature on fullerene formation in a carbon plasma. *Carbon* **2003**, 41, (1), 173-178.

96.   Fedorov, A. S.; Novikov, P. V.; Churilov, G. N., Influence of electron concentration and temperature on endohedral metallofullerene Me@C-84 formation in a carbon plasma. *Chemical Physics* **2003**, 293, (2), 253-261.

97.   Stepanov, K. L.; Stankevich, Y. A.; Stanchits, L. K.; Churilov, G. N.; Fedorov, A. S.; Novikov, P. V., The effect of electron density on the kinetics of fullerene formation in carbon plasma. *Technical Physics Letters* **2003**, 29, (11), 927-929.

98.   Abanades, S.; Badie, J. M.; Flamant, G., On-line temperature measurement in a plasma reactor for fullerene synthesis. *High Temperature Material Processes* **2003**, 7, (1), 43-49.

99.   Saidane, K.; Razafinimanana, M.; Lange, H.; Huczko, A.; Baltas, M.; Gleizes, A.; Meunier, J. L., Fullerene synthesis in the graphite electrode arc process: local plasma characteristics and correlation with yield. *Journal Of Physics D-Applied Physics* **2004**, 37, (2), 232-239.

100.   Lange, H.; Saidane, K.; Razafinimanana, M.; Gleizes, A., Temperatures and C-2 column densities in a carbon arc plasma. *Journal Of Physics D-Applied Physics* **1999**, 32, (9), 1024-1030.

101.   Saidane, K.; Lange, H.; Razafinimanana, M.; Huczko, A.; Zedde, C.; Baltas, M., Characteristics of a carbon arc discharge. *High Temperature Material Processes* **2001**, 5, (2), 243-252.

102.   Afanas'ev, D. V.; Dyuzhev, G. A.; Kruglikov, A. A., Effect of gas flows on fullerene formation process. *Technical Physics* **2001**, 46, (7), 923-925.

103.   Alekseev, N. I.; Dyuzhev, G. A., Analysis of an arc-formed gas-plasma jet in the arc method of fullerene production. *Technical Physics* **2005**, 50, (11), 1423-1430.

104.   Markovic, Z.; Todorovic-Markovic, B.; Marinkovic, M.; Nenadovic, T., Temperature measurement of carbon arc plasma in helium. *Carbon* **2003**, 41, (2), 369-371.

105.   Markovic, Z.; Todorovic-Markovic, B.; Mohai, I.; Karoly, Z.; Szepvolgyi, J.; Farkas, Z.; Nikolic, Z., Optical emission study of RF thermal plasma during fullerene synthesis. *Fullerenes Nanotubes And Carbon Nanostructures* **2005**, 13, (3), 215-226.

106.   Todorovic-Markovic, B.; Markovic, Z.; Marinkovic, M.; Nenadovic, T., Experimental study of physical parameters significant in fullerene synthesis. *Journal of the Serbian Chemical Society* **2003**, 68, (7), 543-547.

107.   Todorovic-Markovic, B.; Markovic, Z.; Mohai, I.; Szepvolgyi, J., Optical diagnostics of carbon arc and induction plasmas. In *Progress In Advanced Materials And Processes*, 2004; Vol. 453-454, pp 277-281.

108.   Farhat, S.; Scott, C. D., Review of the arc process modeling for fullerene and nanotube production. *Journal Of Nanoscience And Nanotechnology* **2006**, 6, (5), 1189-1210.

109.   Churilov, G. N.; Novikov, P. V.; Lopatin, V. A.; Vnukova, N. G.; Bulina, N. V.; Bachilo, S. M.; Tsyboulski, D.; Weisman, R. B., Electron density as the main parameter influencing the formation of fullerenes in a carbon plasma. *Physics Of The Solid State* **2002**, 44, (3), 419-423.

110.   Churilov, G. N.; Novikov, P. V.; Tarabanko, V. E.; Lopatin, V. A.; Vnukova, N. G.; Bulina, N. V., On the mechanism of fullerene formation in a carbon plasma. *Carbon* **2002**, 40, (6), 891-896.

111.   Bilodeau, J. F.; Pousse, J.; Gleizes, A., A mathematical model of the carbon arc reactor for fullerene synthesis. *Plasma Chemistry and Plasma Processing* **1998**, 18, (2), 285-303.

112.   Takikawa, H.; Imamura, M.; Kouchi, M.; Sakakibara, T., Decrease in fullerene productivity due to air leakage in carbon arc method. *Fullerene Science and Technology* **1998**, 6, (2), 339-349.

113.   Geldard, L.; Keegan, J. T.; Young, B. R.; Wilson, M. A., Pathways of polycyclic hydrocarbon formation during plasma arcing of carbonaceous materials. *Fuel* **1998**, 77, (1-2), 15-18.

114.   Muthakarn, P.; Sano, N.; Charinpanitkul, T.; Tanthapanichakoon, W.; Kanki, T., Characteristics of carbon nanoparticles synthesized by a submerged arc in alcohols, alkanes, and aromatics. *Journal of Physical Chemistry B* **2006**, 110, (37), 18299-18306.

115.   Gao, F.; Xie, S. Y.; Huang, R. B.; Zheng, L. S., Significant promotional effect of CCl4 on fullerene yield in the graphite arc-discharge reaction. *Chemical Communications* **2003**, (21), 2676-2677.

116.   Gao, F.; Xie, S. Y.; Ma, Z. J.; Feng, Y. Q.; Huang, R. B.; Zheng, L. S., The graphite arc-discharge in the presence of CCl4: Chlorinated carbon clusters in relation with fullerenes formation. *Carbon* **2004**, 42, (10), 1959-1963.

117.   Churilov, G. N.; Weisman, R. B.; Bulina, N. V.; Vnukova, N. G.; Puzir, A. P.; Solovyov, L. A.; Bachilo, S. M.; Tsyboulski, D. A.; Glushenko, G. A., The influence of Ir and Pt addition on the synthesis of fullerenes at atmospheric pressure. *Fullerenes Nanotubes And Carbon Nanostructures* **2003**, 11, (4), 371-382.

118.   Lityaeva, I. S.; Bulina, N. V.; Petrakovskaya, E. A.; Marachevsky, A. V.; Zharkov, S. M.; Gedanken, A.; Churilov, G. N., Iron-fullerene clusters. *Fullerenes Nanotubes And Carbon Nanostructures* **2006**, 14, (2-3), 499-502.

119.   Coumbe, C., Unpublished Results. *University of Southern Mississippi*.

120.   Stevenson, S.; Mackey, M. A.; Stuart, M. A.; Phillips, J. P.; Easterling, M. L.; Chancellor, C. J.; Olmstead, M. M.; Balch, A. L., A distorted tetrahedral metal oxide cluster inside an Icosahedral carbon cage. Synthesis, isolation, and structural characterization of Sc-4(mu(3)-O)(2)@I-h-C-80. *Journal of the American Chemical Society* **2008**, 130, (36), 11844-11845.

121.   Brown, C. M.; Cristofolini, L.; Kordatos, K.; Prassides, K.; Bellavia, C.; Gonzalez, R.; KeshavarzK, M.; Wudl, F.; Cheetham, A. K.; Zhang, J. P.; Andreoni, W.; Curioni, A.; Fitch, A. N.; Pattison, P., On the crystal structure of azafullerene (C59N)(2). *Chemistry of Materials* **1996**, 8, (11), 2548-&.

122.   Le Strat, G.; Noiret, N.; Roucoux, A.; Patin, H., The solubility of some azafullerene derivatives. *Fullerene Science and Technology* **1999**, 7, (5), 757-768.

123.   Manaa, M. R.; Sprehn, D. W.; Ichord, H. A., High-energy structures of azafullerene C48N12. *Chemical Physics Letters* **2003**, 374, (3-4), 405-409.

124.   Mattay, J.; Torres-Garcia, G.; Averdung, J.; Wolff, C.; Schlachter, I.; Luftmann, H.; Siedschlag, C.; Luger, P.; Ramm, M., Progress in fullerene chemistry: Exohedral functionalization of first and second generation and a new approach to aza-heterofullerenes. *Journal of Physics and Chemistry of Solids* **1997**, 58, (11), 1929-1937.

125.   Prassides, K.; Keshavarz, M.; Beer, E.; Bellavia, C.; Gonzalez, R.; Murata, Y.; Wudl, F.; Cheetham, A. K.; Zhang, J. P., Spheres of spheres of azafullerene in the solid state. *Chemistry of Materials* **1996**, 8, (10), 2405-&.

126.   Kumashiro, R.; Tanigaki, K.; Ohashi, H.; Tagmatarchis, N.; Kato, H.; Shinohara, H.; Akasaka, T.; Kato, K.; Aoyagi, S.; Kimura, S.; Takata, M., Azafullerene (C59N)(2) thin-film field-effect transistors. *Applied Physics Letters* **2004**, 84, (12), 2154-2156.

127.   Stevenson, S.; Dorn, H.; Zuo, T., United States Patent US 2009/0250661 A1. **2009**.

128. Zuo, T. M.; Xu, L. S.; Beavers, C. M.; Olmstead, M. M.; Fu, W. J.; Crawford, D.; Balch, A. L.; Dorn, H. C., M-2@C79N (M = Y, Tb): Isolation and characterization of stable endohedral metallofullerenes exhibiting M-M bonding interactions inside aza[80]fullerene cages. *Journal of the American Chemical Society* **2008**, 130, (39), 12992-12997.

129. Stevenson, S.; Coumbe, C. E.; Mackey, M. A.; Confait, B. S.; Phillips, J. P. D., H.C; Ling, Y.; Zhang, Y, Preferential Encapsulation and Stability of La_3N Cluster in 80 Atom Cages: Experimental Synthesis and Computational Investigation of $La_3N@C_{79}N$. *Journal of the American Chemical Society* **2009,** Under Review.

130. Stevenson, S.; Dorn, H.; Zuo, T., Trimetallic Nitride Clusters Entrapped within CnN Heteroatom Cages and Method for Making Same using Oxidizing Gases and Combustion. *Joint Disclosure between 2 Universities (Southern Miss, Virginia Tech)* **2008**, 1-12.

131. Chaur, M. N.; Athans, A. J.; Echegoyen, L., Metallic nitride endohedral fullerenes: synthesis and electrochemical properties. *Tetrahedron* **2008,** 64, (50), 11387-11393.

132. Dunsch, L.; Yang, S., Metal Nitride Cluster Fullerenes: Their Current State and Future Prospects. *Small* **2007,** 3, (8), 1298-1320.

133. Dunsch, L.; Yang, S. F., Endohedral clusterfullerenes - playing with cluster and cage sizes. *Physical Chemistry Chemical Physics* **2007,** 9, (24), 3067-3081.

134. Stevenson, S.; Dorn, H.; Zuo, T., United States Patent DM_US:21770597_1. **2008**.

135. Stevenson, S.; Harich, K.; Yu, H.; Stephen, R. R.; Heaps, D.; Coumbe, C.; Phillips, J. P., Nonchromatographic "stir and filter approach" (SAFA) for isolating Sc3N@C80 metallofullerenes. *Journal of the American Chemical Society* **2006,** 128, (27), 8829-8835.

136. Coumbe, C., Reactor R&D. *USM Prospectus* **2007**, 1-33.

137. Stuart, M. A., Unpublished Results. *University of Southern Mississippi.*

138. BP-Oil, Statistical Review of World Energy. **2009**.

139. EIA, Official energy statistics from the U.S. Government. *http://www.eia.doe.gov* **2009**.

140. Wynne, J. H.; Buckley, J. L., X-ray Photoelectron Spectroscopy. *Navy Research Labs (NRL)* **2007**.